INTEGRATED 3-D FINITE ELEMENT SIMULATION OF THE EDREMIT GEOTHERMAL SYSTEM

A THESIS SUBMITTED TO
THE GRADUATE SCHOOL OF NATURAL AND APPLIED SCIENCES
OF
MIDDLE EAST TECHNICAL UNIVERSITY

BY

ALP YOĞURTÇUOĞLU

IN PARTIAL FULFILLMENT OF THE REQUIREMENTS
FOR
THE DEGREE OF MASTER OF SCIENCE
IN
GEOLOGICAL ENGINEERING

MAY 2016

Approval of the thesis:

INTEGRATED 3-D FINITE ELEMENT SIMULATION OF THE EDREMIT GEOTHERMAL SYSTEM

submitted by **ALP YOĞURTÇUOĞLU** in partial fulfillment of the requirements for the degree of **Master of Science in Geological Engineering Department, Middle East Technical University** by,

Prof. Dr. M. Gülbin Dural Ünver _____
Dean, Graduate School of **Natural and Applied Sciences**

Prof. Dr. Erdin Bozkurt _____
Head of Department, **Geological Engineering**

Prof. Dr. Nurkan Karahanoğlu _____
Supervisor, **Geological Engineering Department, METU**

Examining Committee Members:

Prof. Dr. Serhat Akın _____
Petroleum and Natural Gas Engineering Department, METU

Prof. Dr. Nurkan Karahanoğlu _____
Geological Engineering Department, METU

Prof. Dr. M. Zeki Çamur _____
Geological Engineering Department, METU

Assoc. Prof. Dr. Koray K. Yılmaz _____
Geological Engineering Department, METU

Assist. Prof. Dr. Türker Kurttaş _____
Geological Engineering Department, Hacettepe University

Date: 02/05/2016

I hereby declare that all information in this document has been obtained and presented in accordance with academic rules and ethical conduct. I also declare that, as required by these rules and conduct, I have fully cited and referenced all material and results that are not original to this work.

Name, Last name : Alp YOĞURTÇUOĞLU

Signature :

ABSTRACT

INTEGRATED 3-D FINITE ELEMENT SIMULATION OF THE EDREMIT GEOTHERMAL SYSTEM

Yoğurtçuoğlu, Alp

M.S., Department of Geological Engineering

Supervisor : Prof. Dr. Nurkan Karahanoğlu

May 2016, 146 pages

The Edremit Geothermal system consists of a shallow cold aquifer and a hot reservoir layer at depth. A 3-Dimensional Finite element model with 65596 nodes is used to simulate this system by an integrated algorithm in a 3 km by 3 km with 300 meters of depth study area consisting of currently operating geothermal field deep water wells. To determine the permeability values and hydraulic gradient values in the study area, a 2-Dimensional simulation was performed with 27664 nodes for the entire Edremit Basin, and its results are integrated into the 3-Dimensional model of the study area which was calibrated with 2 different evolutionary scenarios. The thermally calibrated 3-Dimensional model was used in simulations for numerical applications including effects of hypothetical production rates which revealed temperature drops between 6 and 16º C that didn't reach steady state; moreover the simulated model can reach pre-production state naturally in between 200 and 400 years. The modelled reservoir response of the study area to hypothetical reinjection scenario was found to be minimal, thus with the hypothetical production rates, the production is found to be unsustainable in the long term.

Keywords: Geothermal, Finite Element Method, Simulation, Numerical Applications

ÖZ

EDREMİT JEOTERMAL SİSTEMİNİN SONLU ELEMANLAR YÖNTEMİ İLE ENTEGRE OLARAK 3 BOYUTLU SİMULASYONU

Yoğurtçuoğlu, Alp

Yüksek Lisans, Jeoloji Mühendisliği Bölümü

Tez Yöneticisi : Prof. Dr. Nurkan Karahanoğlu

Mayıs 2016, 146 sayfa

Edremit jeotermal sistemi üstte soğuk su akiferi ve bunun altında bulunan sıcak su rezervuarından oluşmaktadır. 65596 noktadan oluşan 3 Boyutlu sonlu elemanlar modeli kullanılarak, mevcut jeotermal derin kuyuları içeren 3 km ye 3 kilometre alanlı ve 300 metre derinlikli çalışma alanında bu sistemin entegre simulasyonu yapılmıştır. Çalışma alanındaki geçirgenlik ve hidrolik gradyan değerlerini bulabilmek için öncelikle Edremit Baseninin tamamı için 27664 noktalı 2 boyutlu bir simulasyon çalıştırılarak, bulunan sonuçlar 3 Boyutlu çalışma alanına entegre edilmiştir. 2 farklı oluşum evrimine göre termal olarak günümüz koşullarında kalibre edilen 3 boyutlu modelin nümerik uygulamalarındaki hipotetik üretim koşullarında modelde 6 ila 16º C sıcaklık düşüşü oluşmuş ve denge durumu oluşmamıştır. Bu üretim koşullarından sonra simulasyon modelinin kendisini 200 ila 400 yıl arasında yenileyebileceği bulunmuştur. Sanal reenjeksiyon simulasyonuna modelin tepkisi de çok az olarak bulunmuştur, bu yüzden belirtilen sanal üretim koşullarında üretim uzun vadede sürdürebilir gözükmemektedir.

Anahtar Kelimeler: Jeotermal, Sonlu Elemanlar Yöntemi, Simulasyon, Nümerik Uygulamalar

To my family & Mustafa Kemal KURDAŞ,

ACKNOWLEDGEMENTS

I would like to thank Prof. Dr. Nurkan Karahanoğlu for his support, guidance, advice and patience during the period of this thesis.

I would like to thank United States Geological Survey for making hydrogeology software available and free of charge.

I would also like to thank the members of the jury for their valuable criticisms, corrections and comments.

TABLE OF CONTENTS

LIST OF TABLES

LIST OF FIGURES

CHAPTER 1

INTRODUCTION

1.1 Purpose and Scope

Turkey has Europe's first and world's fifth geothermal potential because of neogene geological processes that resulted in volcanism and active tectonics. Around 227 geothermal fields have been identified and around 1200 wells drilled with temperatures varying from 20 to 287 °C (Figure 1). The geothermal fields are utilized for thermal tourism (420 MWt), greenhouse heating (612 MWt), district heating, (805 MWt) balneological use (1005 MWt), heat pump applications (428 MWt), electricity production (400MWe) and lately, liquid carbon-dioxide and dry ice production. (Mertoğlu and others, 2015)

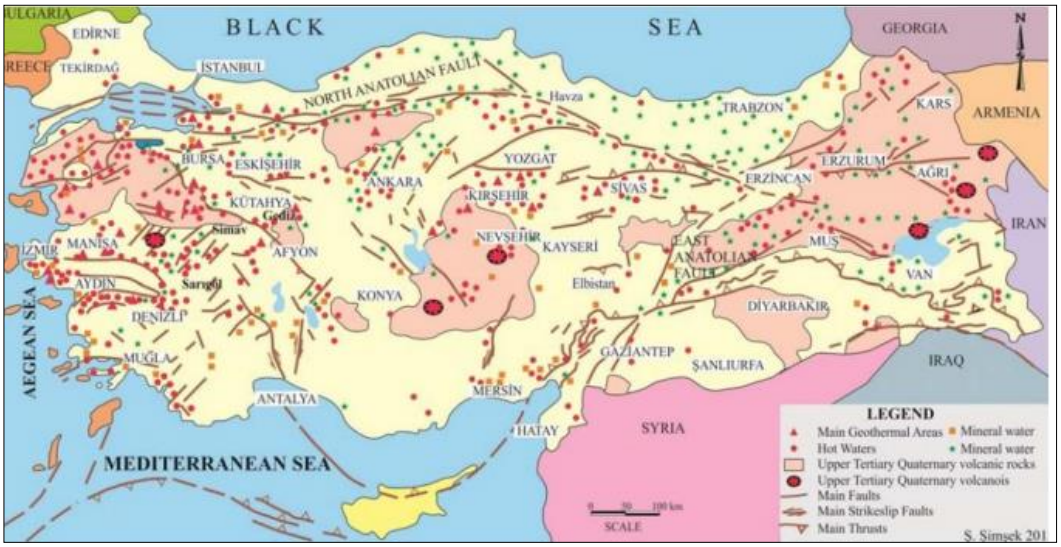

Figure 1.1: Active Hot Springs and main neotectonic lines (MTA 2016)

These geothermal fields are more abundant and also utilized more in the western part of Turkey, where horst-graben structures are dominant (Figure 1.2). Moreover, only the fields in western Anatolia have the geothermal potential to produce electricity (MTA 2015).

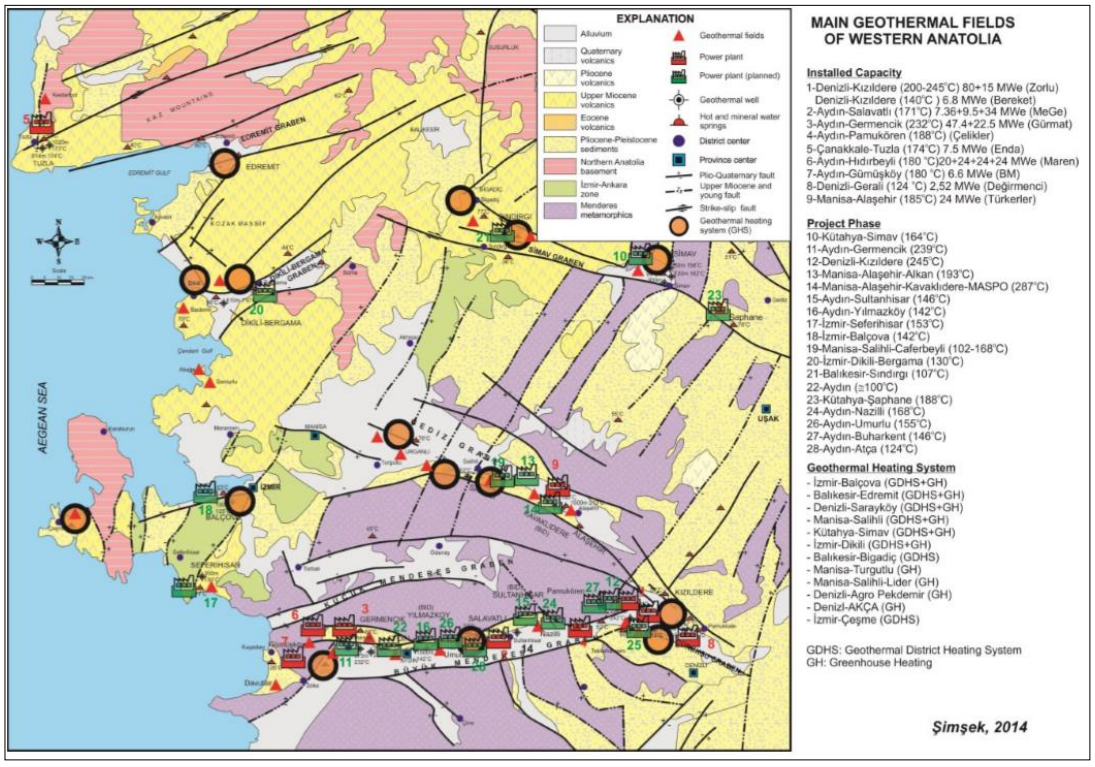

Figure 1.2: Geothermal fields in Western Anatolia. (Şimsek 2014)

The purpose of this study is to perform a 3-dimensional simulation of the study area and to carry out numerical analyses for the Edremit Geothermal Field which is located in the northwestern part of Anatolia. Although numerous studies of its potential were carried out before (Avşar 2011), and the field is currently operated by a private firm for district heating (planned as maximum7500 residences, 5400 as of 2015), the field has not been investigated for its sustainable development yet. It is aimed to describe in 3 dimensions, the characteristics of the geothermal field and to provide a basis to perform numerical simulations and to study the response of the geothermal system for different production and reinjection scenarios.

1.2 Geographic Setting

The study area is located in the Edremit Plain in the NW of Anatolia, which is SW to Edremit Town of Balıkesir Province. (Figure 1.3) The Edremit Plain is surrounded by Kazdağ Mountain in the north, by Madra Mountain in the SW and Eybekdağ to the NE. The Edremit Plain is a depression plain formed by tectonic processes, formed by Edremit Fault which is dextral strike-slip branch of North Anatolian Fault Zone to the North, and sinistral strike-slip Havran-Balıkesir Fault Zone to the south.

The study area is located at the intersection of E87 and D230 highways, thus accessible throughout the year.

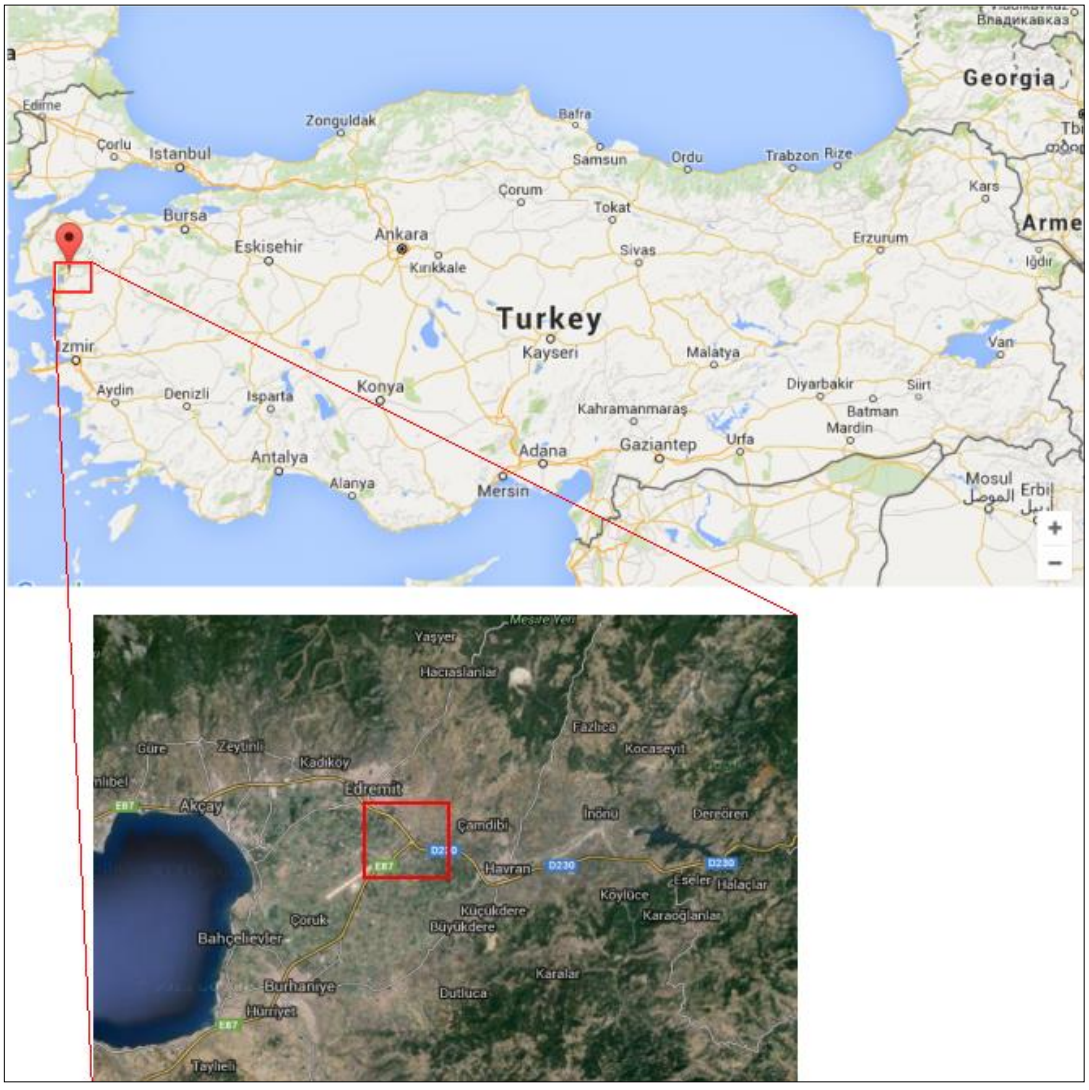

Figure 1.3: The study area.

1.3 Previous Studies

The area was first studied by General Directorate of State Hydraulic Works (DSİ, 1977). The studies were to describe the potential of Edremit Basin for irrigation studies. Water Wells were drilled to produce water from the upper aquifer.

Ural (1978) used the data from DSİ studies, and performed a numerical study by finite difference method, and determined the potentiometric levels of the Edremit Basin.

Three new wells were drilled in the area in 2001 by the General Directorate of Mineral Research and Exploration (MTA, abbreviated for Maden Tetkik Arama in Turkish) with depths varying from 195 to 495 meters and drilled down to the hot basement rocks.

Coşkun (2007) in his master's thesis, studied energetic and exergetic analyses of the Balıkesir Geothermal district heating systems including Edremit town.

In 2007, General Directorate of Bank of Provinces (İB, abbreviated for İller Bankası in Turkish) drilled 6 other wells to the hot aquifer.

Mutlu (2007) studied the origin of Balikesir Thermal waters, and found by isotope studies that the geothermal waters in Balikesir are meteoric in origin.

Avşar (2011) extensively studied the geochemical evaluation and conceptual modeling of the Edremit Geothermal Field and found that geothermal waters, during their ascent to the surface, invaded the two superimposed cold and hot aquifers. He also made resource assessments with statistical analysis and found an accessible resource about 3.45x1013 kJ and 9.1 MWt recoverable heat energy for Edremit geothermal field with 90% probability. In his work, along with the stratigraphy; the important structural formation in the form of two intersecting and buried faults near Derman spa was defined with their location and strike/dip measurements.

Günay (2012) performed a finite element numerical modeling of the Edremit Geothermal Field and studied the geothermal potential, sustainability and reinjection possibilities of the Edremit Geothermal Field with 2-dimensional cross sectional model consisting of a cold water aquifer superimposed on a hot water aquifer. In his numerical applications, three alternative scenarios were performed and the response of the reservoir was documented.

1.4 Layout of the Thesis

The thesis consists of 6 chapters.

In Chapter 1, the purpose and scope is given with introduction and previous studies.

In Chapter 2, the geological setting is explained with regional geology, local geology and hydrogeological setting.

In Chapter 3, numerical modeling is given with 2-dimensional and 3-dimensional simulations along with their respective calibration studies. Also conceptual studies in 3-dimensions are given.

In Chapter 4, numerical applications done for the geothermal field is presented.

In Chapter 5, results and discussions are presented.

In Chapter 6, conclusions and recommendations are presented.

1.5 Technologies Used

The technologies used during this study are as follows:

SUTRA: A Finite-Element Simulation Model for Saturated Unsaturated Fluid-Density-Dependent Groundwater Flow with Energy Transport or Chemically Reactive Single Species Solute Transport, in 2 or 3 dimensions.

Sutra Prep: A data preparation tool for SUTRA. Also gives wire mesh VRML output of model.

GW Chart: Hydrograph generating software from SUTRA and other USGS hydrogeology software result files.

Model Muse: Pre-processing, post-processing software for SUTRA and other USGS hydrogeology software products for 2-dimensional and quasi 3 dimensional models. Can produce finite element or finite difference meshes, record initial and boundary conditions, run related software and show results.

Model Viewer: Post-processing tool for SUTRA and other USGS software result files that can show model and results in 3-dimensions.

MapInfo & Discover: Commercial GIS tool; for geocoding, image rectification and spatial analyses.

CHAPTER 2

GEOLOGICAL SETTING

2.1 Regional Geology

The geology of Turkey is complex, because it is formed by bits and pieces of two mega continents Laurasia and Gondwana-Land. Those bits and pieces were formed by closure of Palaeo-Tethys Ocean first, then collision of Arabian Plate with the Eurasian Plate, during the Alpine -Himalayan orogeny process, where the Neo-Tethys Ocean also closed (Figure 2.1).

After collision of the two plates in the Miocene Period, The western part of Anatolia began first to compress, then started thinning to form the current horst-graben structures visible today. There are different tectonic models proposed for these tectonic events; back-arc spreading model (J. Jackson, D. McKenzie, 1988), (McKenzie, 1978), (X. LePichon, J. Angelier, 1979,1981),(C. Kissel, C. Laj, 1988), (J. E. Meulenkamp, et al, 1988),(S.N. Thomson, B. Stöckhert, M.R. Brix, 1988) ; tectonic escape model (J.F. Dewey, A.M.C. Şengör, 1979) (also Şengör, 1979, 1982, 1987),(Şengör, et al. 1985) ; orogenic collapse model; Dewey (1988), Seyitoğlu & Scott (1992) and Seyitoğlu et al. (1992); episodic, two stage extension model (Koçyiğit et al, 1999) . Some recent studies support this extension model of Koçyiğit et al. (Koçyiğit et al., 2000; Koçyiğit and Özacar, 2003; Koçyiğit, 2005; Bozkurt and Rojay, 2005; Emre and Sözbilir, 2007; Kaya et al., 2007), while some studies oppose this model. (Seyitoğlu, 1999; Seyitoğlu et al., 2000; 2002; 2009; Seyitoğlu and Işık, 2009; Şengör and Bozkurt, 2013, Kaya et al.2014)

The formation of the geothermal fields is related to the tensional earth structures that shaped the current Western part of Anatolia, which were formed by the thinning of the continental crust because of the N~S extension from the result of the aforementioned tectonic processes. (Figure 2.2)

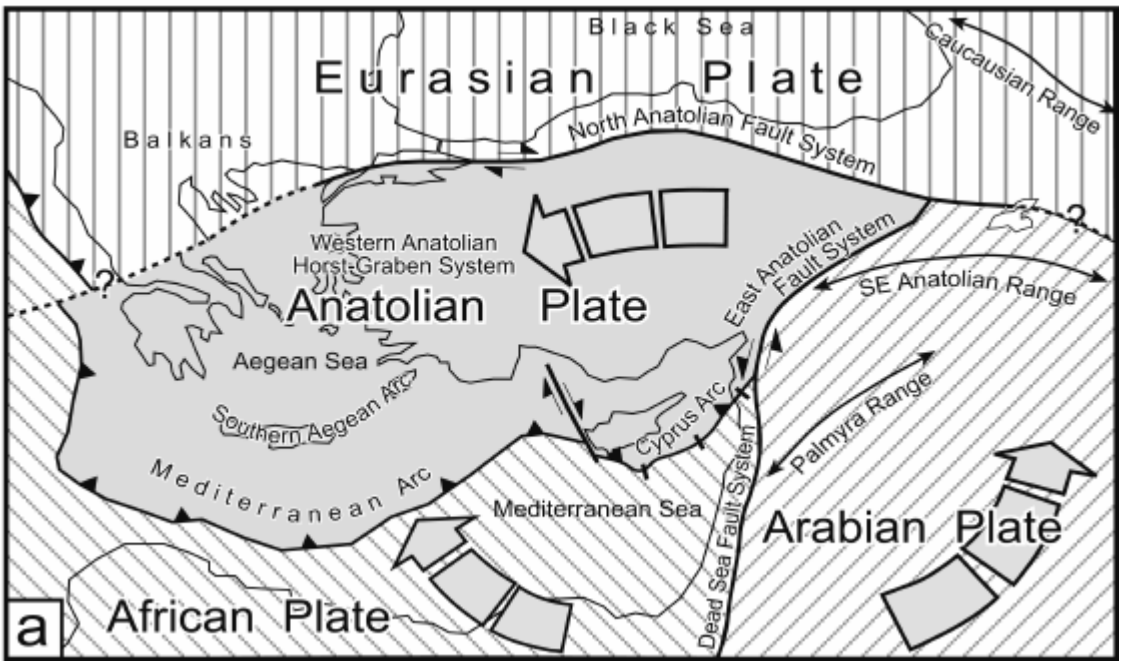

Figure 2.1: Current tectonic events in Turkey. (Bozkurt - Rojay 2005)

This horst graben system, which was formed by the thinning of the crust present in Western Anatolia, was reported to show little magmatism. The dominant geothermal activity is found to be hydrothermal fluids which are originally meteoric waters carried downwards by deep faults in the region. Also, this horst graben system was considered similar to western Great Basin of USA, which also shows continental extension. (Faulds et al., 2009)

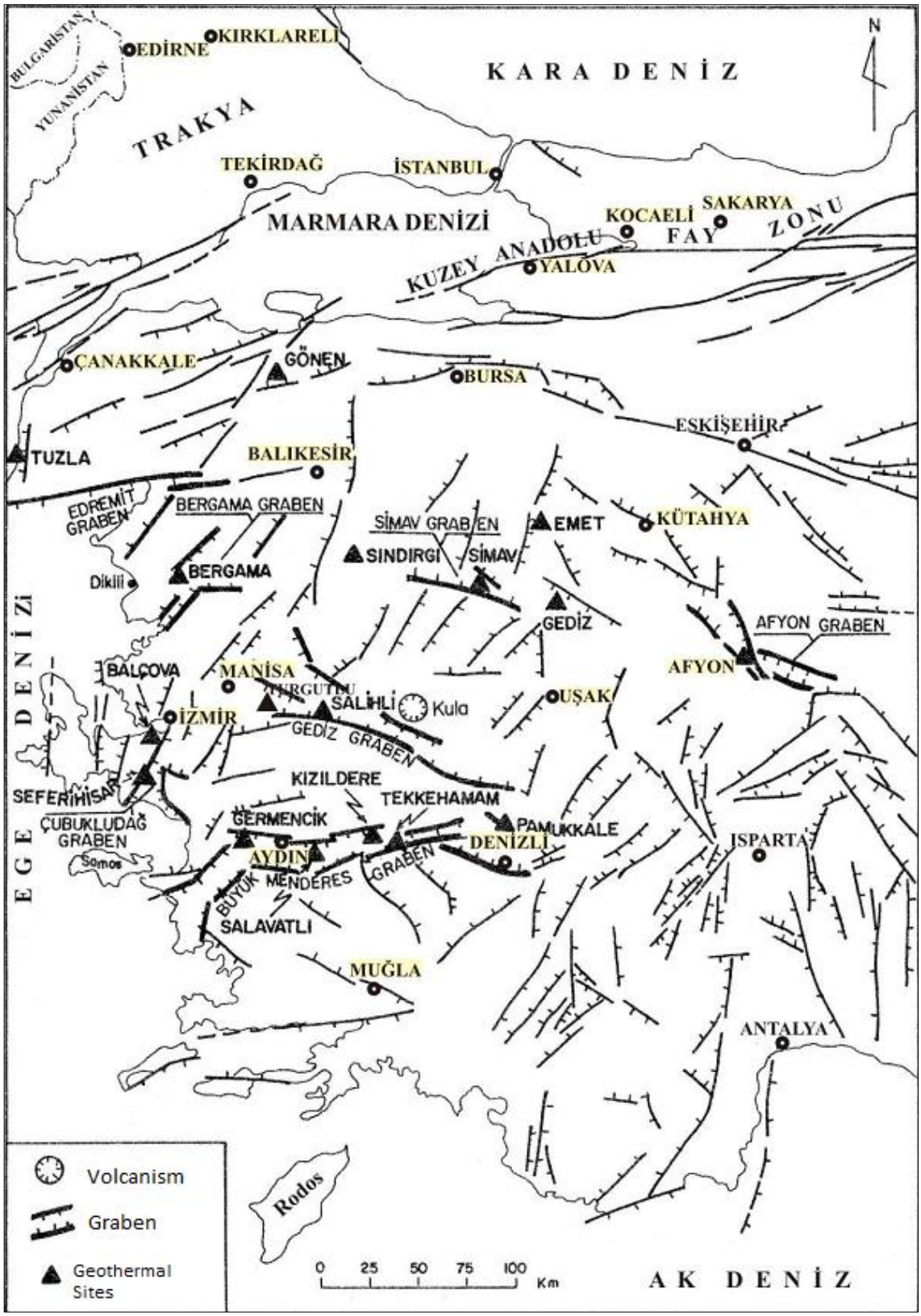

Figure 2.2: Structural geological map of Western Anatolia showing horst - graben structures in a tensional regime. (Modified after Şimşek Ş., Güleç N., 1994)

2.2 Local Geology

The formations in the study area are; Kazdağ Metamorphics, Karakaya Formation, Bilecik Limestone, Hallaçlar Volcanics, Eybek Granodiorite, Ballıca Formation and Plio-Quartenary deposits, from old to young units respectively. (Figure 2.3 & Figure 2.4)

Kazdağ Metamorphics are Paleozoic in origin. They are formed of schists, amphibolites, marbles, gneisses, granitic gneisses, amphibolite-gneisses, sillimanite-gneisses, metadunites, metagabbros, orthoamphibolites and migmatites. This unit is noted as impervious to semipervious.

Karakaya Formation, which is Lower Triassic in age, consists of spilitic basalts, mudstones, radiolarites; and sandstone with feldspar, quartzite, conglomerate and siltstones, accompanied with limestone blocks. This formation has a tectonic lower boundary with Kazdağ metamorphics. This formation is noted as semipervious.

Uncomformably overlain over Karakaya Formation is the Bilecik Formation, which is Upper Jurassic to Lower Cretaceous in age. It is composed of limestone and noted as impervious.

Eybek Granodiorite intrudes these three formations, which is Oligocene in age.

Eybek Granodiorite and Bilecik Formation is overlain by Hallaçlar Formation, which is Late Oligocene to Early Miogene in age. It contains andesite, dacite, tuff and agglomerate. This formation is noted as highly pervious.

Ballıca Formation, which uncomformably overlies Hallaçlar Formation is Middle to Upper Miocene in age, and consists of alternation of siltstone, marl,conglomerate, sandstone and clayey limestones. This formation is noted as impervious.

Lastly, uncomformably overlain on Ballıca Formation is the Pliocene - Quartenary deposits, consisting of alluvium, loosely cemented conglomerate, sandstone and mudstones. These deposits are noted as pervious.

Also, two buried and intersecting faults are described in the region with their measurements and types. (Avşar, 2011)

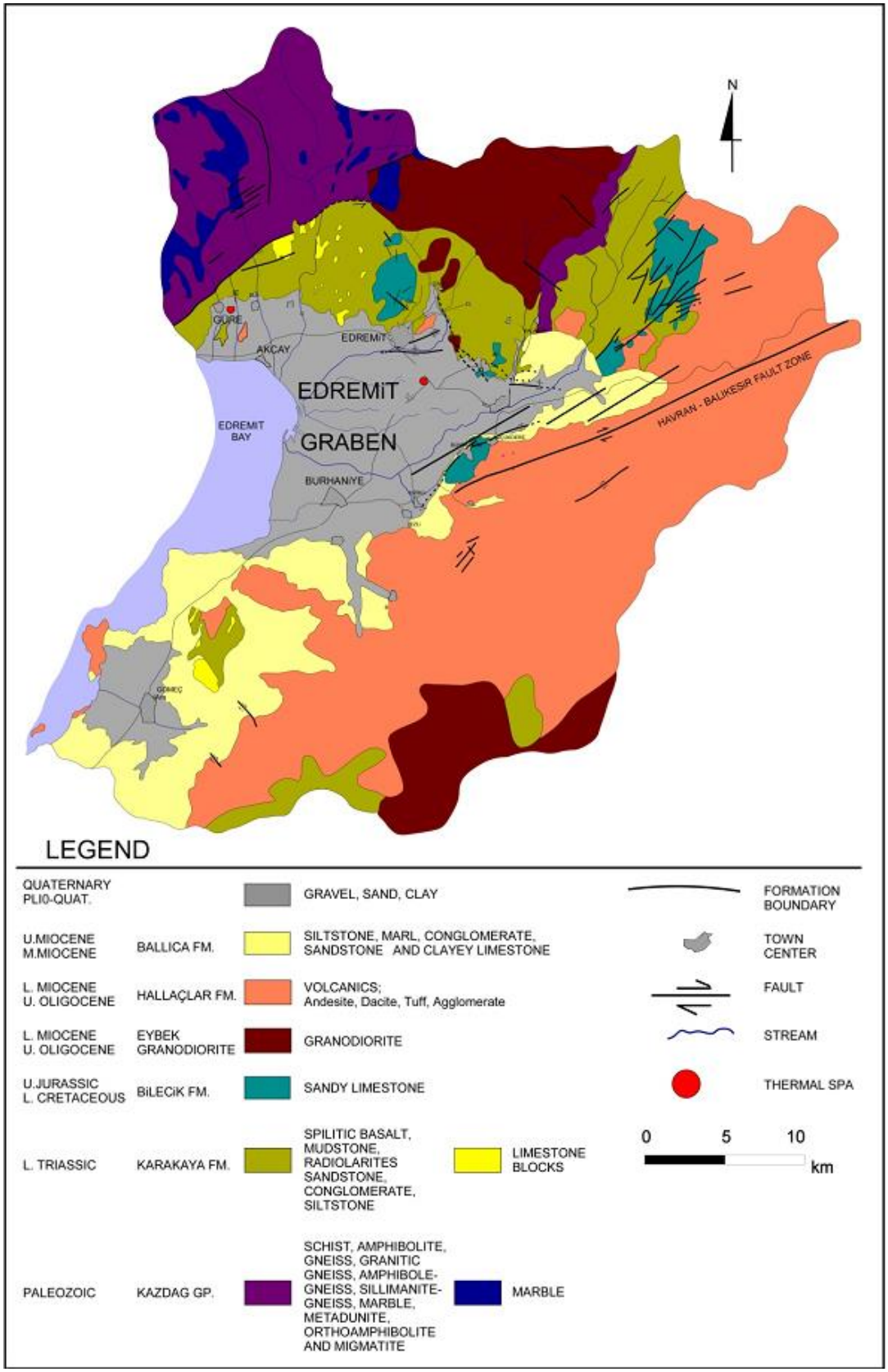

Figure 2.3: Geological Map of Edremit Region (DSİ, 1977; Sarp et al., 1998; MTA, 2007; Bingöl et al., 1973; Duru et al. 2004, compiled by Avşar, 2011)

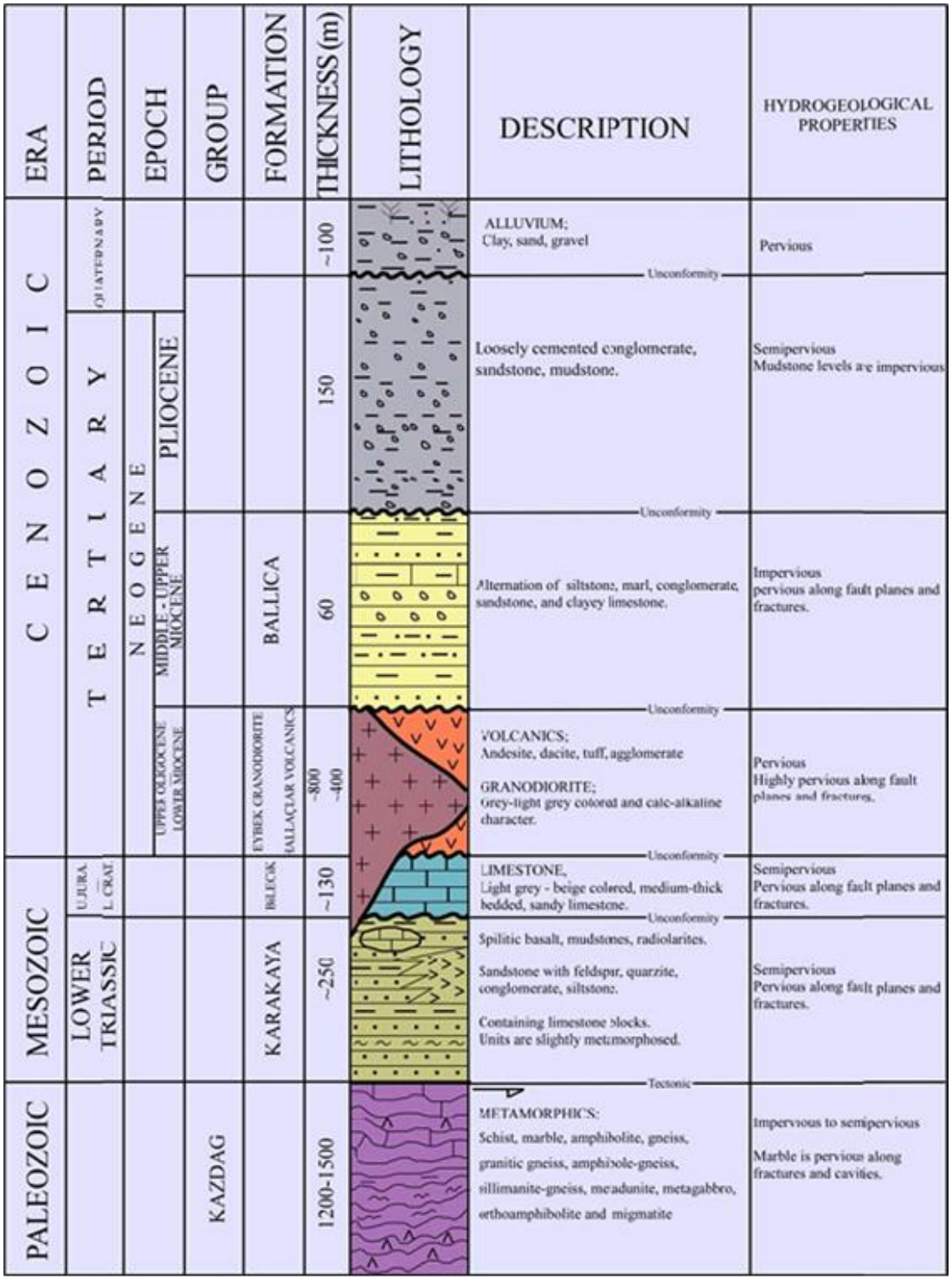

Figure 2.4: Generalized columnar section of Edremit Region (Sarp et al., 1998; Bingöl et al., 1973; DSİ, 1977, compiled by Avşar, 2011, modified after Avşar, 2011)

2.3 Hydrogeological Setting

From the borehole data obtained from the studies of MTA (2007) and İB (2011), three hydrogeological units can be defined from bottom to top:

- Karakaya and Hallaçlar Formations: Permeable units, which forms the lower confined hot aquifer, overlying Kazdağ Metamorphics and Eybek Granodiorite.
- Ballıca Formation: Geothermal Trap Formation. Aquiclude.
- Plio-Quartenary Deposits: Permable units, which forms the upper unconfined cold aquifer.

A generalized hydrogeological cross section of the study area with units and faulting can be seen in figure 2.5.

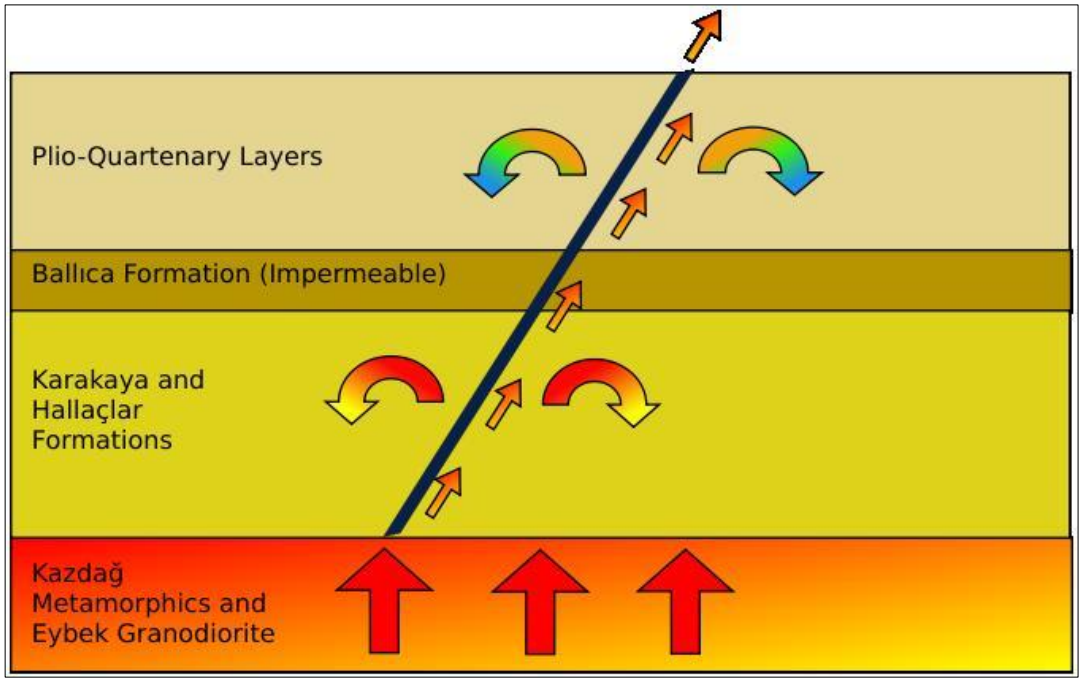

Figure 2.5: Generalized hydrogeological cross section with faults.

As of current available well data; DSİ, MTA and İB had drilled wells in the region. DSİ wells are older and drilled for irrigation purposes and drilled in the upper cold aquifer; while MTA and İB have deep wells which penetrate the lower hot aquifer and drilled down to Kazdağ Metamorphics and Eybek Granodiorite.

Table 2.1: Wells with available data (From Avşar 2011)

Aquifer	Name	Driller	E	N	Elevation	Depth (m)	Temp (°C)
Lower	ED-3	M.T.A	503639	4380394	22	495	62
Lower	ED-1	M.T.A	503718	4380329	22	189	62
Lower	EDJ-3	I.B.	503634	4380252	21	266	59
Lower	EDJ-2	I.B.	503916	4380049	24	300	58
Lower	EDJ-5	I.B.	504054	4380273	23	216	55
Upper	DERMAN	M.	503731	4380197	22	100	53
Upper	ENTUR	M.	503743	4380178	22	90	51
Lower	EDJ-7	I.B.	503968	4380402	23	246	51
Lower	EDJ-4	I.B.	503458	4380136	19	296	50
Lower	ED-2	M.T.A	504014	4380293	23	496	47
Lower	EDJ-8	I.B.	503815	4380491	23	250	43
Upper	YAGCI	M.	503729	4380591	23	100	42
Upper	DSI-6	D.S.I.	503753	4379919	24	95	39
Upper	DOGANDER	M.	503753	4379919	24	30	32
Upper	DSI-9	D.S.I.	502958	4380668	20	122	32
Upper	HASTANE	D.S.I.	504099	4381130	28	90	31
Upper	DSI-5	D.S.I.	503949	4380066	24	91	30
Upper	DSI-7	D.S.I.	504088	4379653	22	132	21
Upper	DSI-8	D.S.I.	505195	4380605	26	83	18
Upper	EMINDSI	D.S.I.	502824	4382144	24	100	12

From the geographical distribution of well, temperature and the fault data in the region, it can be seen that hot water rises from the lower hot aquifer to the upper colder aquifer through faults. Hotter temperatures can be observed in the wells drilled to the upper aquifer and, in the upper aquifer wells that; DSI7, DSI-8, EMINDSI and EMINKUYU wells have temperatures around 20 ^{o}C; DSI-9, HASTANE, DSI-6 and DSI-5 are warm wells with temperatures around 30 ^{o}C, and the rest of the wells in the upper aquifer have temperatures around 45 ^{o}C averaged.

The distribution of well temperatures show that the aquifer intermixing is centered at the faults' intersection, and gradually decreases to the edges. (Figure 2.5)

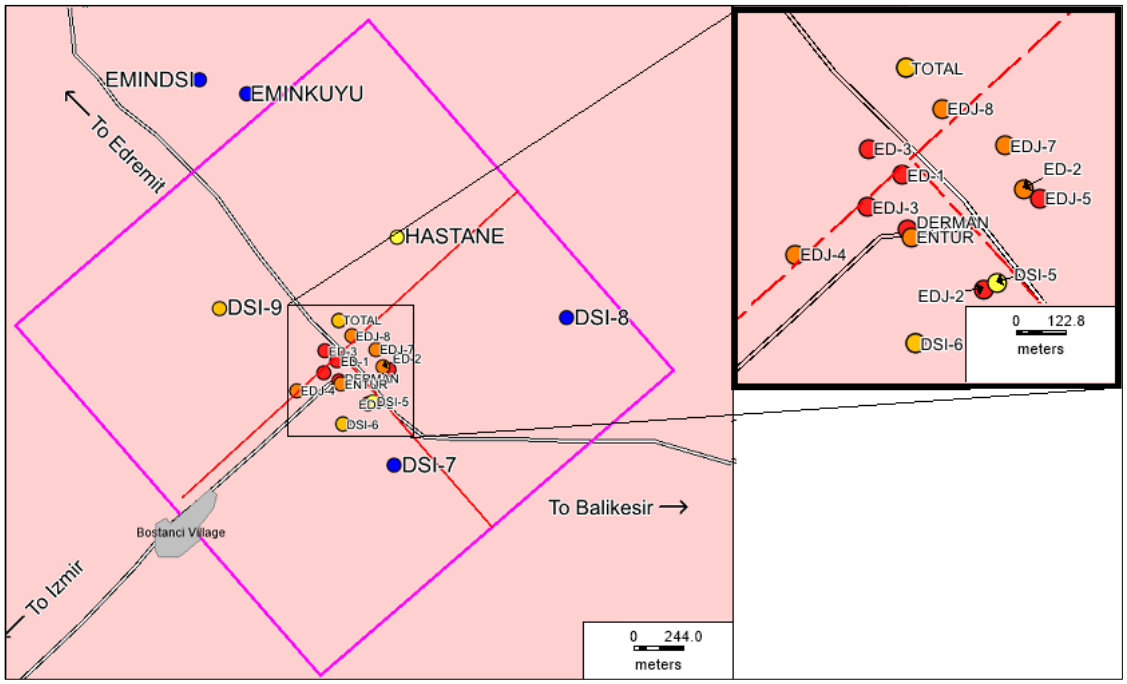

Figure 2.6: Location of faults, wells and their temperatures in the study area. Red dots are hot water wells, yellow and orange dots are warm water wells, and blue dots are cold water wells.

Currently, the Edremit Geothermal System is operated by a private firm, and operating the wells ED-1, ED-3, EDJ-2, EDJ-3, EDJ-4 (Assigned to Adramis Termal Hotel and greenhouses), EDJ-5, EDJ-6, EDJ-7, EDJ-8, EDJ-10 and EDJ-11. The well production is average 463 lt/s flow rate with 51.46 ^{o}C temperature. It is reported that ED-2 and EDJ-9 are not operated due to low temperature and pressures.

In 2007, 6 wells (ED-1, ED-3, EDJ-3, EDJ-4, EDJ-5 and EDJ-7) were operated with average wellhead production temperature of 60 ^{o}C, with flow rates varying from 18 and 86 kg/s. (Coşkun, 2007)

CHAPTER 3

NUMERICAL MODELING

3.1 Introduction

Edremit Geothermal system consists of a deep hot aquifer overlain by a cold shallower aquifer. Considering a hydrodynamic relation between these two aquifers, a finite element simulation study is accomplished.

It is important to note that, without adequate amount of data, a model of the real system cannot be done correctly. However, using observation data from previous field studies, a preliminary or equivalent model can be simulated.

In the numerical modeling, Saturated Unsaturated Transport software, also known as SUTRA finite element modeling software is used.

The Edremit Basin has nearly 100 square kilometers of area and 300 meters of depth to study. However, the 3-dimensional study area had to be minimized to a 3x3 km area and 300 meters of depth, because the data for the thickness of two aquifers are known from the deep wells and deep wells were only drilled in the study area. There were two unknowns for the study area; which were the permeability values and hydraulic gradient since for both aquifers those values are not known. As permeability and hydraulic gradient values were needed, another approach was taken. The Edremit Basin was studied by Ural (1978) to perform a numerical simulation of the water levels by finite difference method. Using that study as a reference, a 2-dimensional steady-state simulation was performed to find the permeability values and hydraulic gradient for the entire basin in which the results could also be used in the study area. (Figure 3.1)

By matching the head values from Ural's study and the 2-Dimensional simulations, the needed permeability and hydraulic gradient values were obtained to be used in 3-Dimensional simulation.

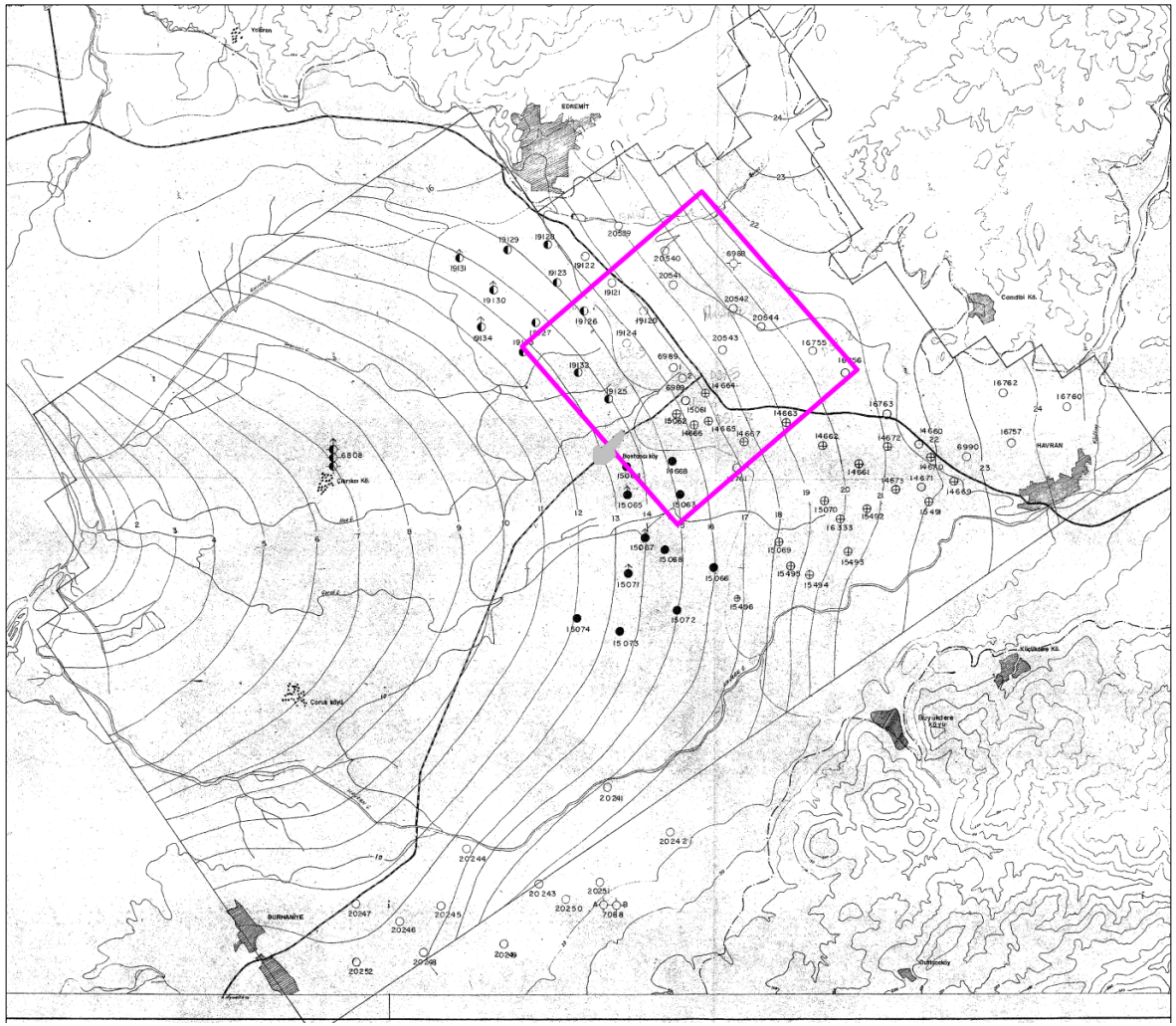

Figure 3.1: Map of the Edremit Basin, from Ural (1978). The study area is denoted in purple color.

3.2 2-Dimensional Simulation

The study area of the Edremit Basin by Ural (1978) was scanned and its computer image is rectified with MapInfo Discover's image rectification tool. After that, the map of the area is head-on digitized using MapInfo software. Lastly, the boundary of the study area was exported to ModelMuse.

Using ModelMuse, the study area was divided into finite element mesh of 100 meters, utilizing Irregular Mesh Generation, using Cuthill and McKee renumbering method with default program values. (Figure 3.2)

For the 2-dimensional simulation, is assumed that the thermal phenomenon is local and also the two aquifers are intermixed, thus any pressure differences between two aquifers had already reached a steady state. Therefore, the 2-dimensional simulation was prepared for a single aquifer with the full vertical thickness of the study area, which is 300 meters; resulting in 27664 nodes and 13577 elements.

The 2-dimensional finite element simulation was performed with pressure only in steady state condition, using different boundary conditions.

It might have been better if the hydrogeological data from DSI that were used in Ural's study were available; however those data could not have been accessed. Moreover, deep well data became available only after 2001, and the existence of a bottom hot aquifer was not known 40 years ago.

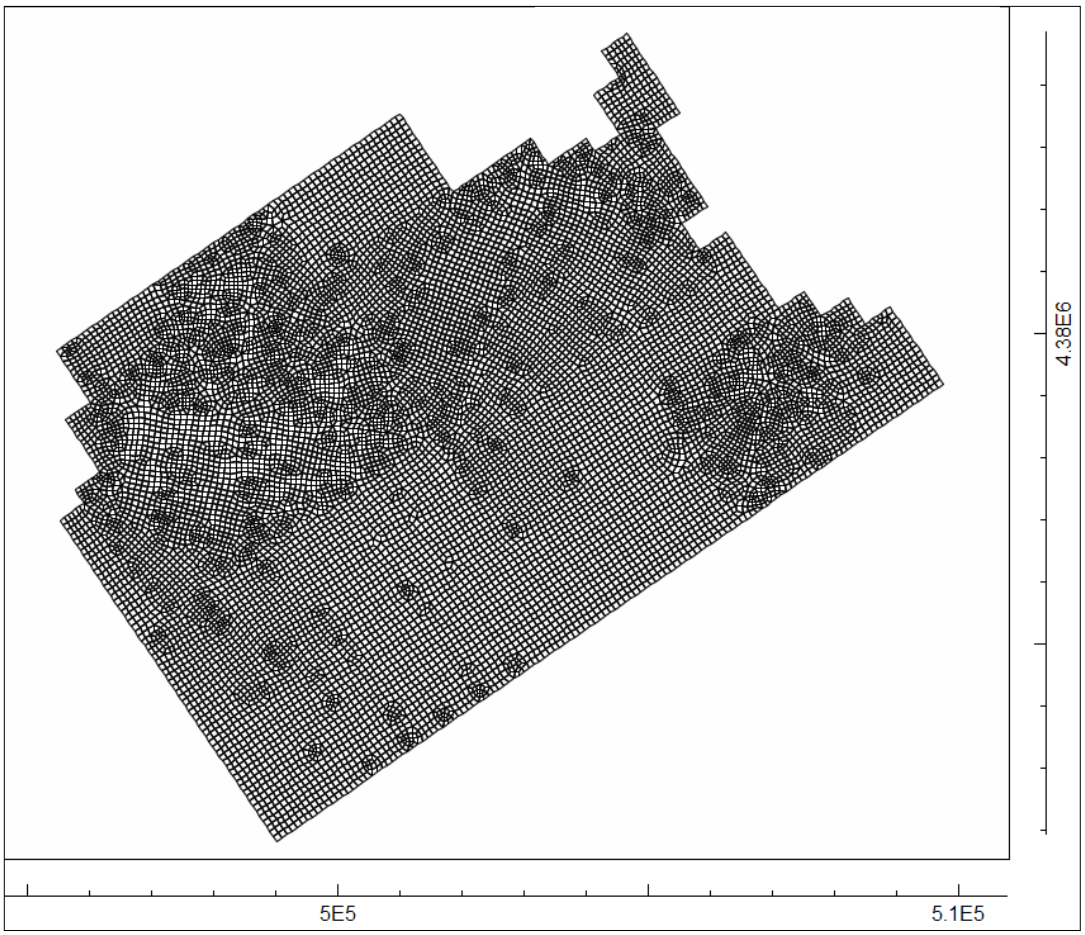

Figure 3.2: Geocoded Finite Element Mesh generated for 2-dimensional simulation.

3.2.1 Physical Properties and Boundary Conditions

As the porosity and permeability values are unknown from previous studies, assumptions were made for the Edremit Basin for a single aquifer having a thickness of 300 meters.

The upper unconfined aquifer consists of Plio-Quartenary deposits having alluvium, loosely cemented conglomerate, sand, silt and clay. Since consolidated rocks' permeability values start with a value of 10^{-11} m^2, a value of 10^{-10} m^2 was assumed. (Bear, 1988)

The 2-dimensional simulation was performed for steady-state condition, using the following geological parameters:

- initial head of 12 meters,
- 0.1 porosity,
- Isotropic permeability of 10^{-10} m^2.

For calibration studies, different boundary conditions were assigned as follows:

- Constant Heads
- Flow and Constant Heads
- Flow and Constant Heads with Varying Permeability

3.2.2 Calibration Studies

Different boundary conditions, with the same geological parameters were run in the software and calibration studies were performed.

3.2.2.1 Constant Heads

In the constant head boundary simulation, the head contour points at the edge of the study area were exported to ModelMuse from MapInfo with 66 points.

Adding to these points, 6 constant head areal borders were added. 2 of those have 25 meters of head at the valley borders to the east, which are the main inflows to the region. One constant head area of 16 meters was added south of Edremit Town, another constant head area was added to the south of the simulation area with a head value of 18 meters, lastly another area with 14 meters of head was added to the southwest of the basin. These interpretations can be made from the convex potentiometric lines near the map's borders that can be seen in Figure 3.1.

Lastly, 0 meters of potentiometric head was added at the elements adjacent to Gulf of Edremit. (Figure 3.3)

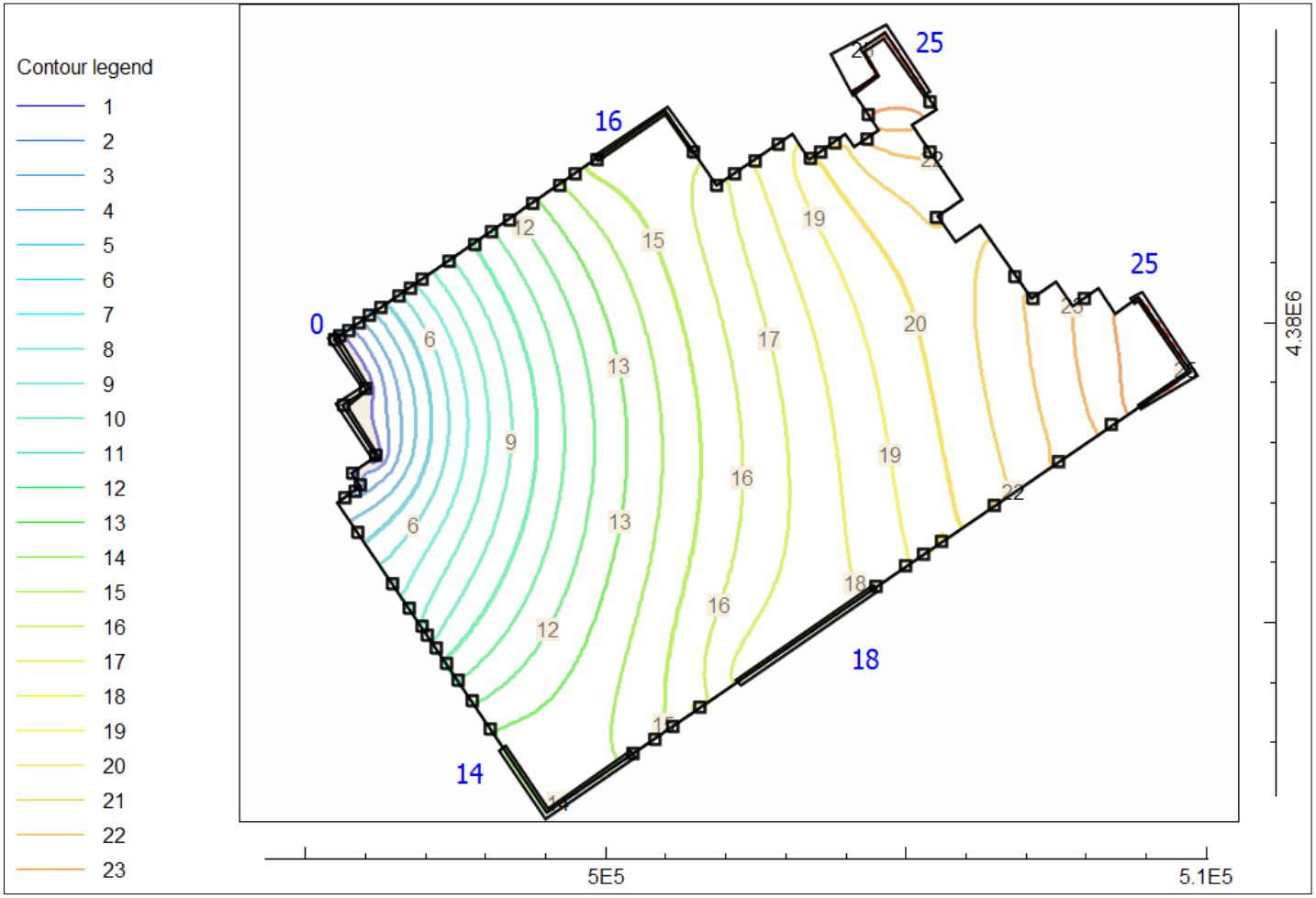

Figure 3.3: Constant Heads Steady-State Simulation with 5 areal borders and 66 constant head points. Assigned head values are denoted in black color.

3.2.2.2 Flow with Constant Heads

Recharge / inflow type boundary conditions are applied to be more realistic. The constant head values of the previous constant head simulation at the eastern part of the mesh were removed, and 5 boundaries were used with various fluid flux values, which were placed at the valley borders of the study area.

Constant head of zero meters are assigned to the nodes adjacent to Gulf of Edremit. The remaining 38 constant head nodes from the constant head simulation were kept in place. (Figure 3.4)

3.2.2.3 Flow and Constant Heads with Varying Permeability

In the varying permeability simulation, it is assumed that the permeability in the middle of the valley is more because of alluvial deposition from the 4 streams in the area. Thus a different value was used at the valley floor near the seashore.

An arbitrary cone shaped area was selected which had its edges at the seashore 0 meter head areal border and widening towards east and north-southwards. The area was closed where a sharp angle in potentiometric head levels were beginning to form near the middle of the Edremit Basin. (Figure 3.5)

The simulation with varying permeability is done with permeability values of $3x10^{-10}$ m^2 in the valley floor, and 10^{-10} m^2 at the rest of the area.

In the simulation with varying permeability, the higher permeability zone acted like a “magnifying glass” on the potentiometric head contours in the valley bottom, thus the contours were more like the head contours of Ural’s study area. Also, the higher permeability area “squeezed” the higher potentiometric contours to the east of the higher permeability area between itself and the eastern flow boundaries. (Figure 3.6)

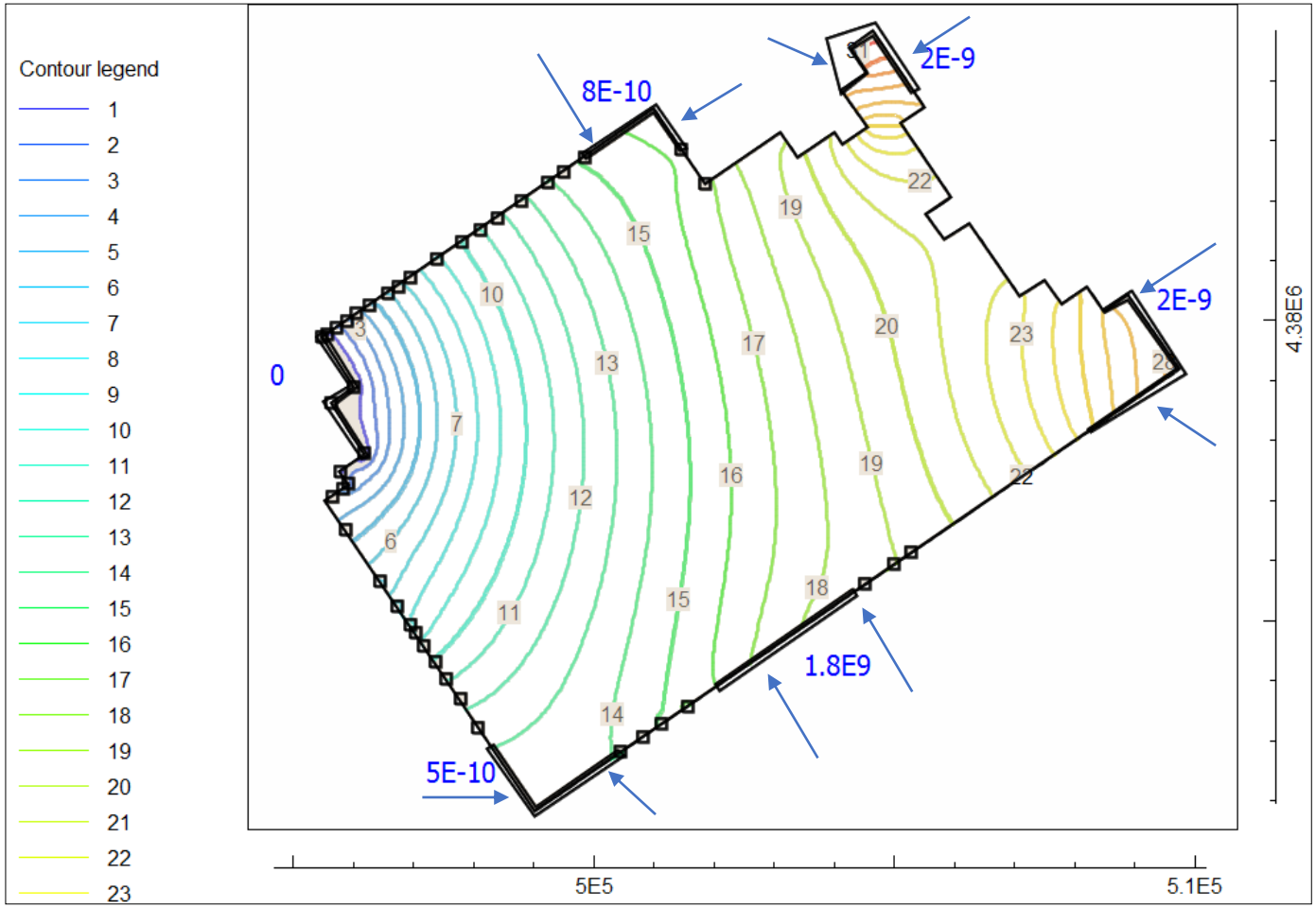

Figure 3.4: Flow with Constant Head Steady-State Simulation with 6 areal borders and 38 constant head points denoted in black color. Assigned flux values are in m^3/s and denoted in blue color.

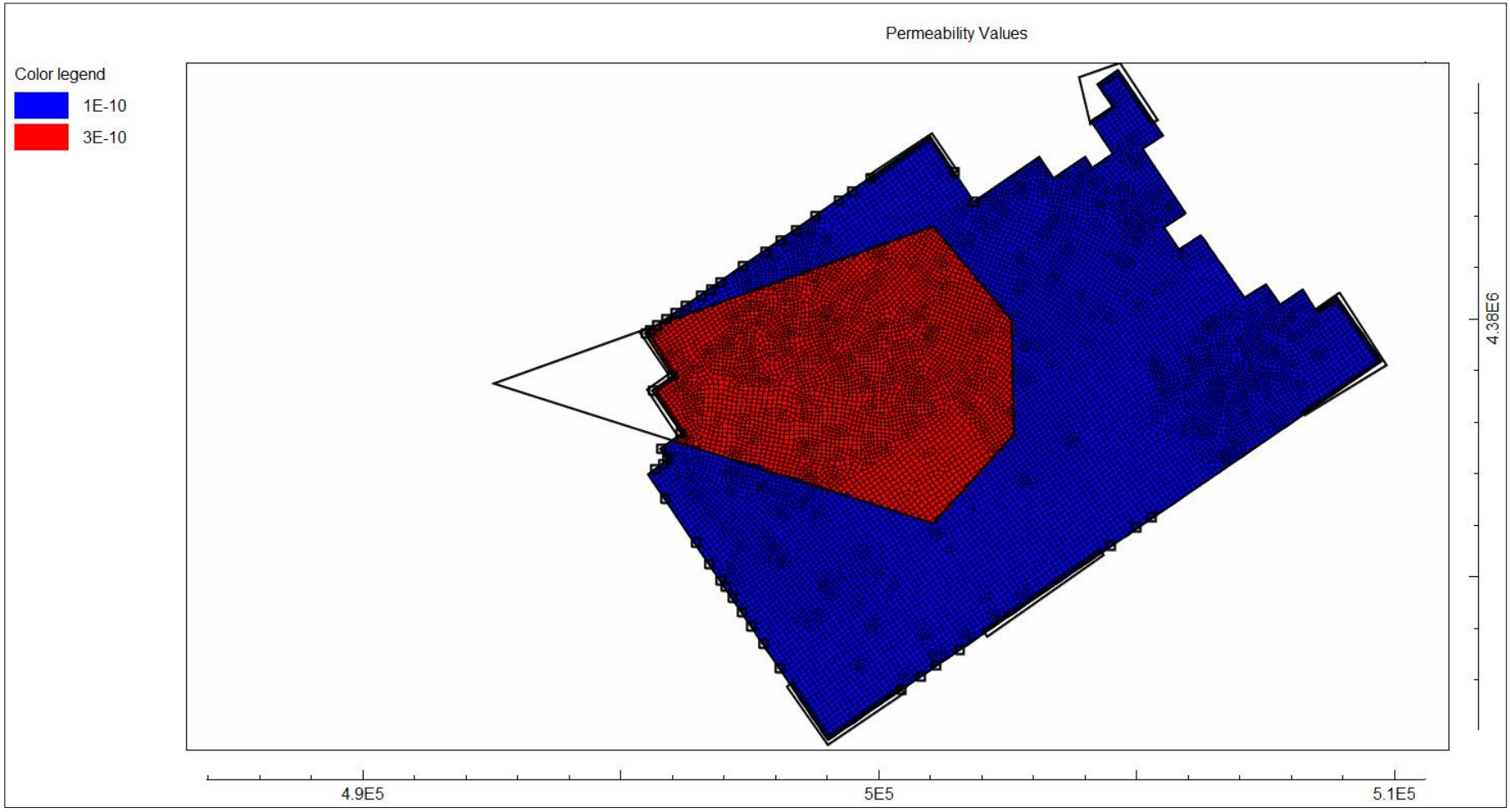

Figure 3.5: Different permeability values assigned at the valley floor because of assumed alluvial deposition effect.

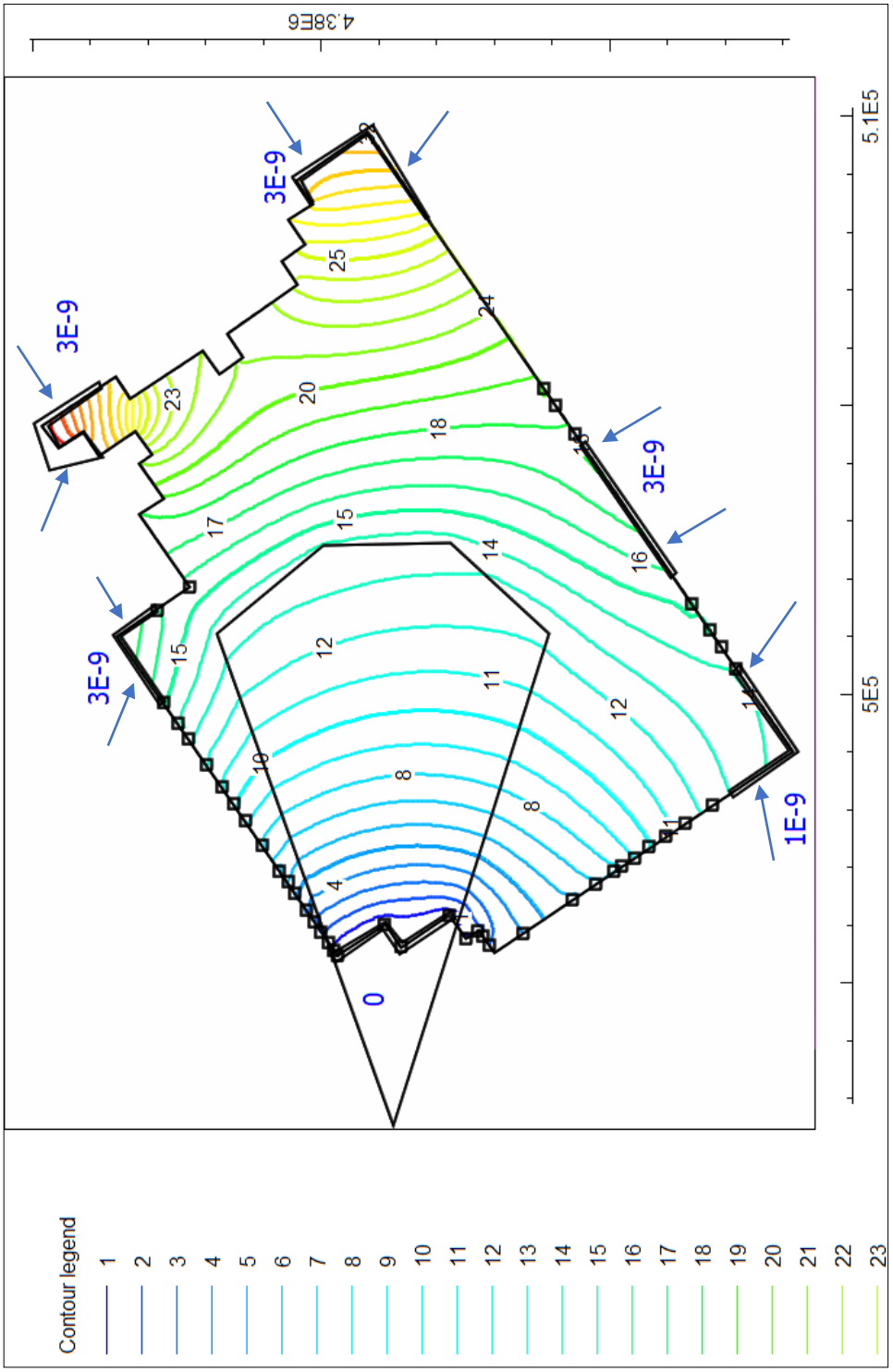

Figure 3.6: Flow with Constant Head using varying permeability steady-state simulation with 6 areal borders and 38 constant head points denoted in black color Assigned flux values are in m^3/s and denoted in blue color. Difference in permeability is shown as a black area overlain on the potentiometric contour map.

The calibration studies were performed for 2-dimensional simulation with 55 distributed points in the simulation area of which the head values are known from Ural (1978). The error calculations were made using the mean square error of the computed heads from the finite element simulations and observed head values of the control points of the study area.

Since the finite element mesh consists of 13832 nodes, the matching was done with geographical information system buffering methodology. Buffer circles with a radius of 100 meters were constructed with the control points as their centers. The buffer distance was chosen to be equal to the finite element mesh size.

Secondly, the finite element node points with their computed head values were exported from ModelMuse as CSV file and then imported into MapInfo software. The node points were geocoded with their x and y values. (Figure 3.7)

Thirdly, the averages of head values of the computed nodes which are inside a control point buffer zone were computed using geographic intersection aggregation method.

Fourthly, the square of the differences between observed and computed head values were computed in MapInfo software as a separate column.

Lastly, the mean square error was computed using the formula below:

$$MSE = \sqrt{\frac{\sum(observed - computed)^2}{nb.of\ control\ points}}$$

The mean square error results for the steady-state simulations are as follows:

Table 3.1: 2-Dimensional Model Error calculations for different simulations.

Simulation Type	**MSE of Ural's Study Area**	**MSE of Avşar's Study Area**
Constant Head	2.52	1.41
Flow with Constant Head	2.45	1.45
Flow with Varying Permeability	1.35	0.5

From these results, the flow with varying permeability 2-Dimensional simulation is more adequate to be used to determine the permeability and hydraulic gradient for the 3-Dimensional simulation.

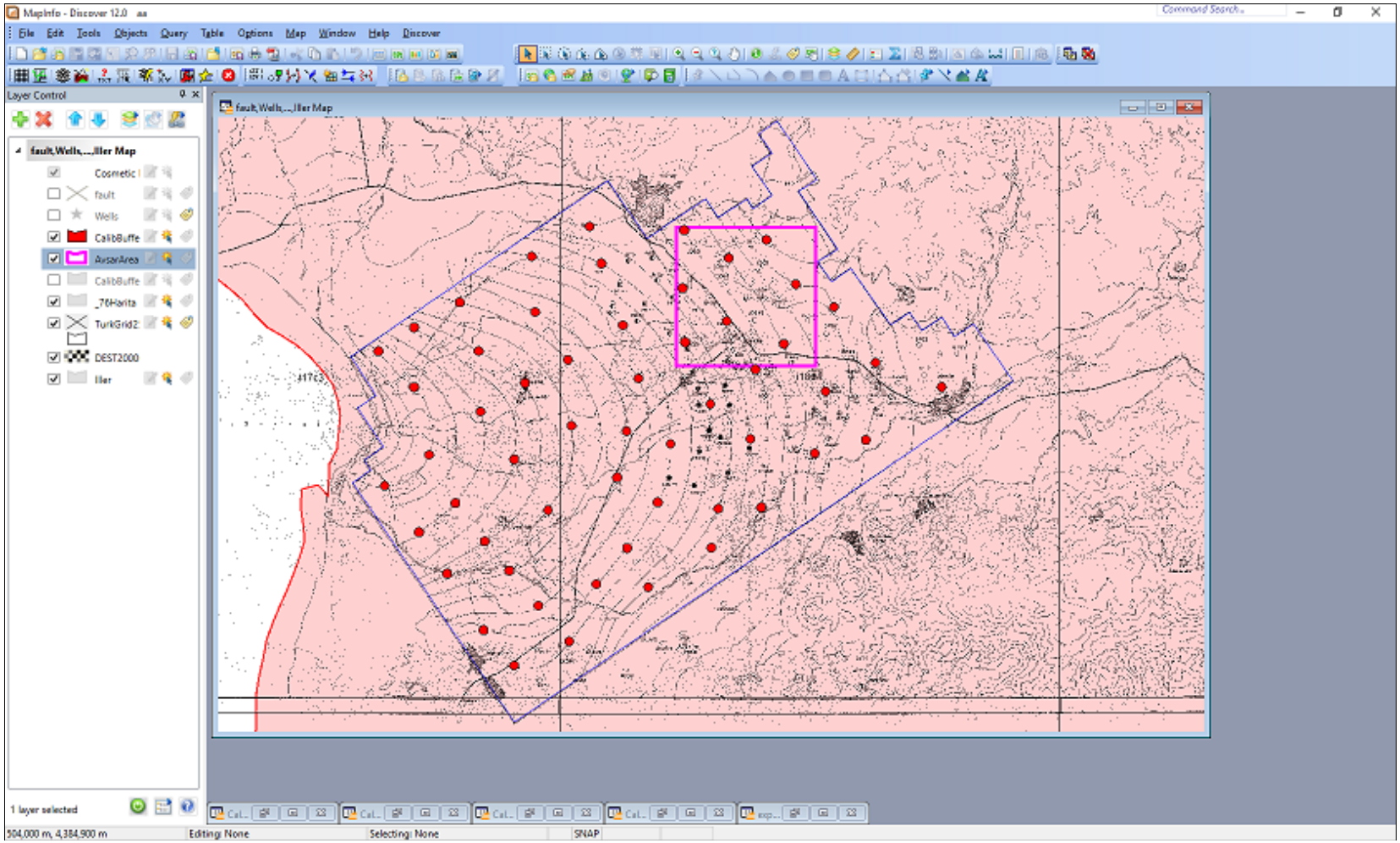

Figure 3.7: Control Points with their 100 m buffers used in calibration studies. The purple area is the study area of Avşar (2011).

3.2 3-Dimensional Simulation

3.2.1 Conceptual Studies

In 3-dimensional studies, it may be different in terms of perception to describe a phenomenon that a user observes after finite element processing. To have a better understanding, heat transfer patterns in geological processes that were studied prior to 3-dimensional simulations of the study are added to this chapter.

In a saturated porous medium, where the bottom is heated, and is cooler at the top, a temperature difference will occur. If the temperature difference is too low, then there would be no motion, heat is transferred through conduction only, and there would be no fluid flow between two plates. (Oosthuizen and Naylor, 1999)

If the temperature difference is high, then a fluctuation in the fluid would occur. The fluid particle would be hotter than the neighboring particles and as its density would be lower than the upper particles, it would experience buoyancy and will start to rise, and would increase thermal fluctuations, forming convection flow.

The convection flow is resisted by the fluid's viscosity and the thermal diffusion which would reduce temperature fluctuations. These opposing forces are parameterized by Rayleigh's Number. When Rayleigh's number is above a critical value, convection will occur and if it is high, will form clockwise/counter clockwise “convection rolls”, which will form Rayleigh-Bénard Convection Cells in the medium. (UC San Diego Library, 2005)

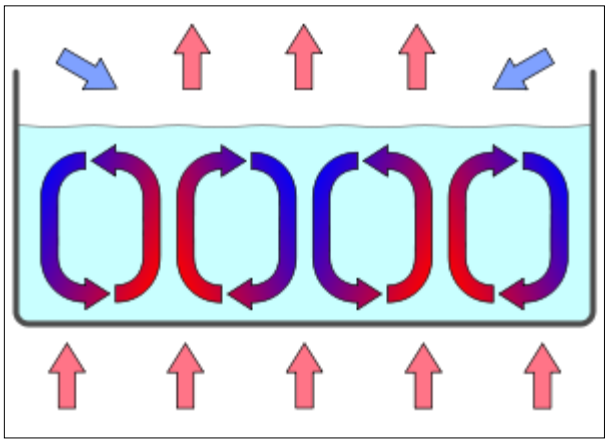

Figure 3.8: Convection cells in a gravity field.

In a simple simulation, a cube with dimensions 100m x 100m x 100m was studied. The initial temperature of fluid is 20 °C, and heated from below with a heat source of 80°C. All the boundaries, except lowermost of the cube are impervious to heat and pressure. In this condition, the convection current formation and movement can be observed. The middle part, as it is colder is denser; and can be seen sinking to the bottom, while the edges are hotter and less dense since hotter fluids are rising from below.

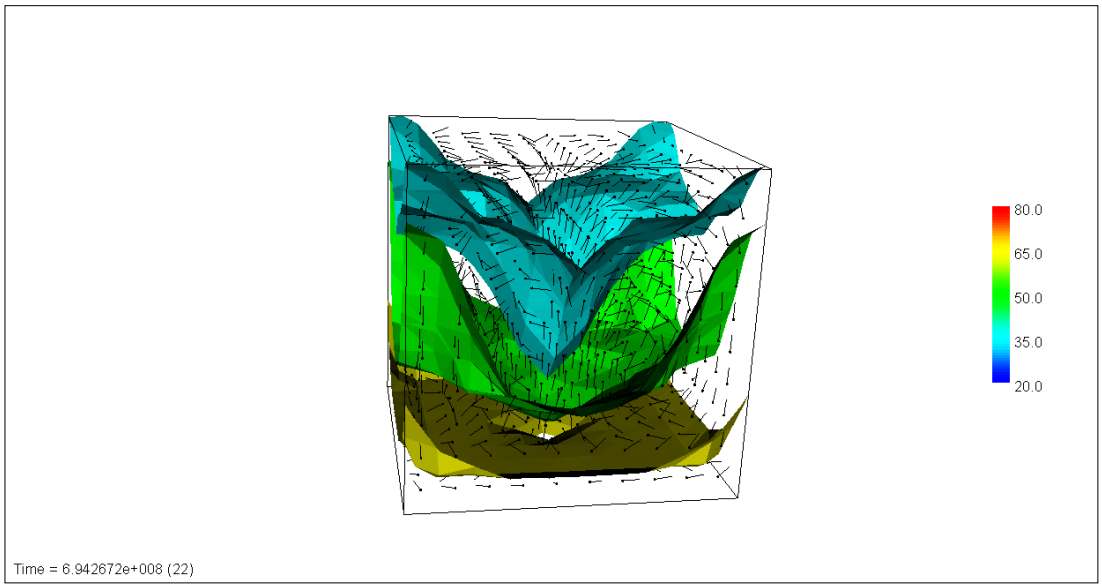

Figure 3.9: Rayleigh-Benard Convection cells. The line segments denote fluid velocity vectors. Temperatures are shown as isosurfaces. Color legend shows the temperatures in °C.

Considering the study area, a series of conceptual simulations were carried out, using the geological settings of the well ED-2 in the study area, with the borehole and simulation data defined by Günay (2012); where the borehole data consists of 3 geological units. The uppermost part is the permeable Plio-Quartenary alluvium, from the surface to 170 m of depth; the Ballıca Formation (Neogene Lacustrine Sediments) as an impervious layer with a thickness of 20 meters, and lastly, agglomerate (Hallaçlar) and conglomerate (Karakaya) formations with 110 meters of thickness which are also permeable.

During conceptual simulations, a 1000 m x 1000 m area with 300 m of depth was studied with 25 m x 25 m x 10 m elements in x, y and z axes respectively. The uppermost layer defining alluvium was given $5x10^{-10}$; and the lowermost layer was given $5x10^{-11}$ m^2 permeability. The middle layer was studied with differing

permeability values of $5x10^{-15}$ (impervious), $5x10^{-14}$ and $5x10^{-13}$ m^2 (semi-pervious).

The boundary conditions were defined as follows:

- The top part is impervious to temperature and flow
- The bottom part is heated with 80^o C constant temperature without flow
- The x and y side-planes are divided into 3 parts. Flux with hydrostatic pressure is applied to 4 sides with varying temperatures. The temperature is constant as 20 ^{o}C from surface, down to 170 m of depth; and 60^o C from 190 m to the bottom, representing the cold and hot aquifers respectively. The impervious layer sides, defined between 170 m to 190 meters of depth has no fluid flux, and defined as impervious to heat and flow.

The initial conditions were; all the water in the system is in hydrostatic pressure, with a temperature of 20^o C.

The simulations were run for different time lengths, until steady state conditions were met in the lower aquifer. (Observation point coordinates are at 500, 500, -250 m)

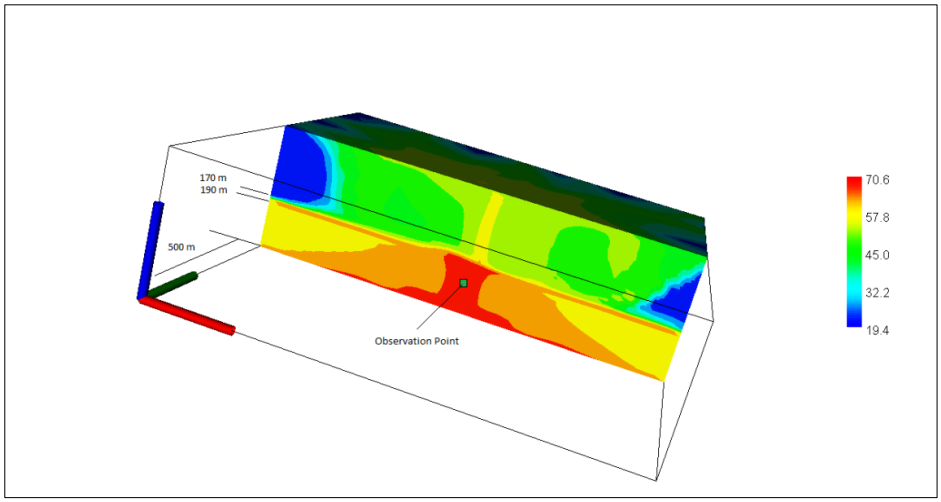

Figure 3.10: Y-axis half cut-away view of simulation with semi-pervious middle layer having a permeability of $5x10^{-13}$ m^2 after 200 years. Color legend shows the temperatures in ^oC.

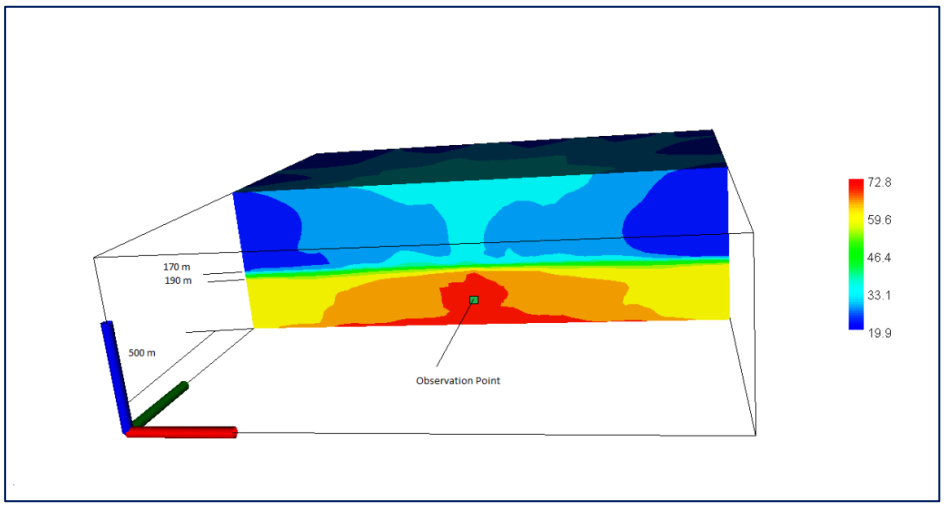

Figure 3.11: Y-axis half cut-away view of simulation with semi-pervious middle layer having a permeability of $5x10^{-14}$ m^2 after 400 years. Color legend shows the temperatures in ^oC.

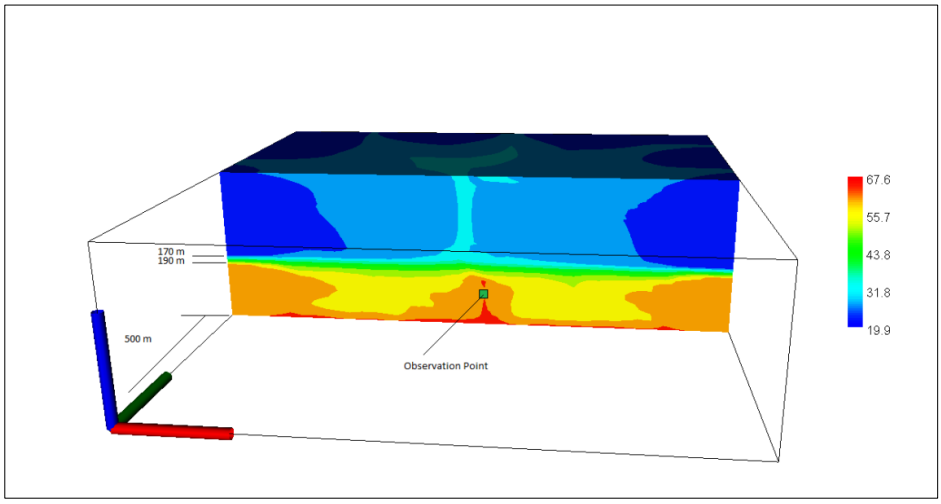

Figure 3.12: Y-axis half cut-away view of simulation with impervious middle layer having a permeability of $5x10^{-15}$ m^2 after 1000 years. Color legend shows the temperatures in ^oC.

From these simulations, it can be seen that the middle part's permeability is very important. If the permeability is high enough to be semi-permeable, heat plumes can form, however with an impervious middle layer, definite heat plumes like in semi-pervious middle layer simulations cannot be observed. In fact, in the impervious scenario, a steady state condition was not reached, even after 1000 years.

After these simulations, since the study area consists of faults, the same scenario with a 25 meter wide opening in the middle of the impervious layer was studied, with the same boundary and initial conditions. The only difference is that, the "opening" was defined with elements having a permeability value of $5x10^{-12}$ m^2 in the middle of the impervious layer which has a permeability value of 5x10-15 m^2.

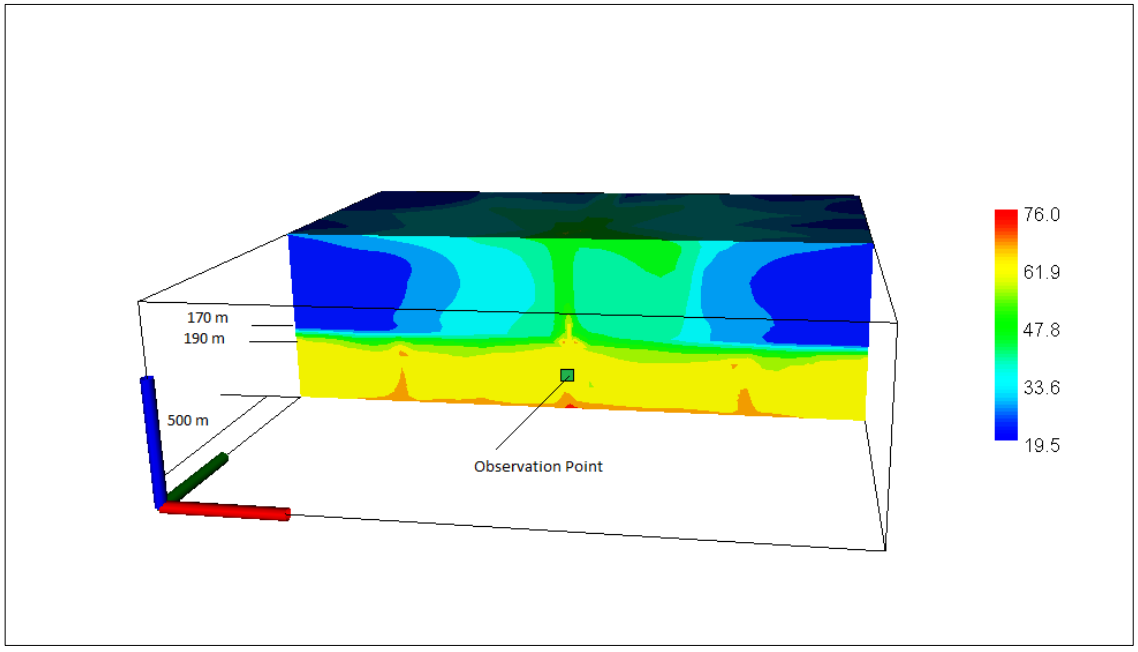

Figure 3.13: Cut-away view of simulation with opening in the impervious middle layer having a permeability of $5x10^{-15}$ m^2 after 400 years. Color legend shows the temperatures in ^oC.

3.2.2 3 Dimensional Modeling Details

3.2.2.1 Model and Study Area

The boundary conditions for the 3-dimensional simulation were determined from the 2-dimensional results. For modeling, 3 km x 3 km part of the study area which includes both upper and lower aquifer wells and has deep well data was selected.

From the 2-dimensional area studies, a square area which is more or less perpendicular to the flow direction and containing nearly all the wells and faults was selected. (Figure 3.14) Also, for ease of modeling, the area was rotated and moved, so that the two faults defined in Avşar (2011) intersect in the middle the study area, while the study area square edges are parallel or perpendicular to the faults (Figure 3.15). It is also assumed that the hydraulic gradient did not change in 40 years, since current water level data is not available.

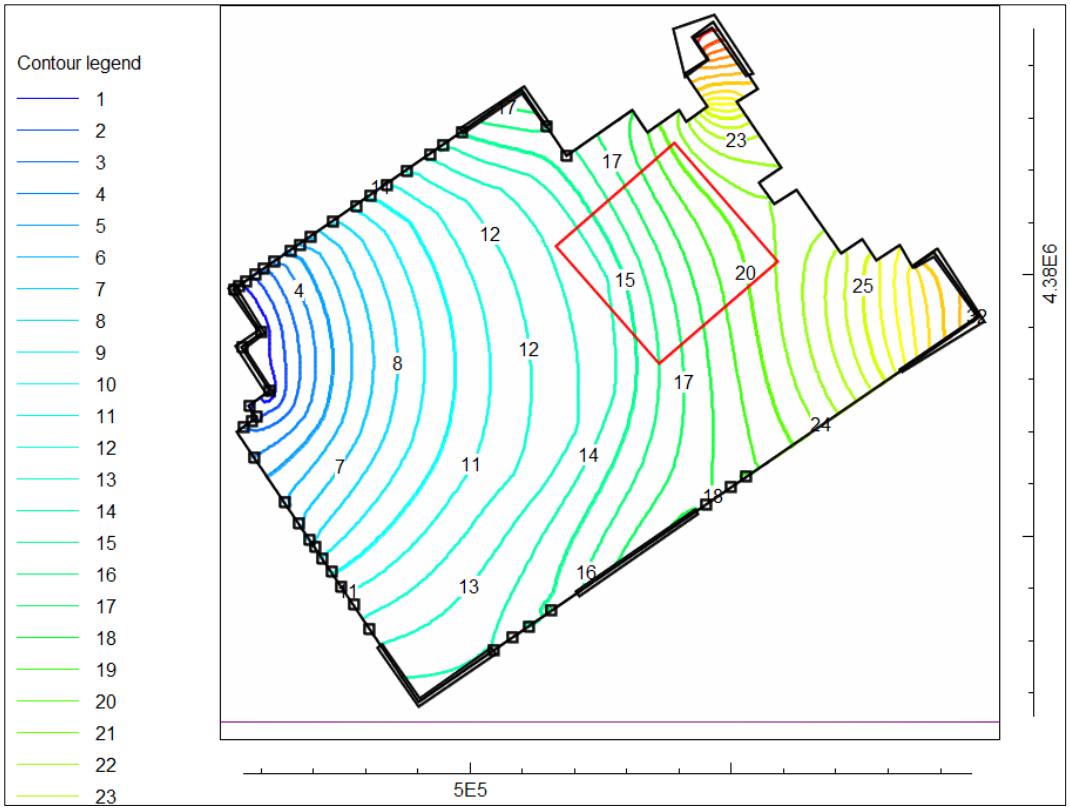

Figure 3.14: The study area overlain as a red square over 2-dimensional simulation.

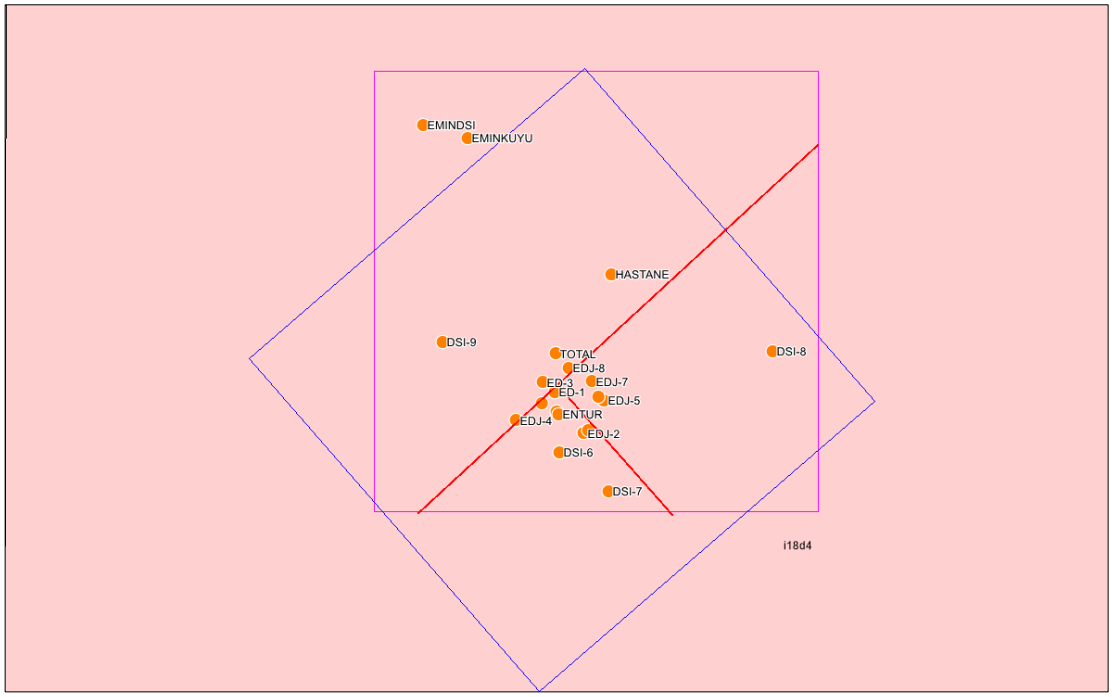

Figure 3.15: Wells and faults overlain on the study area which is denoted in Blue Square. The red lines are the buried faults and the pink square is the study area of Avşar (2011).

With the rotation of the study area to the hydraulic gradient, and by the location of the faults, the y-planes of the model was placed nearly perpendicular to the flow direction, and parallel to the long fault and perpendicular to the short fault in the study area. (Figure 3.16)

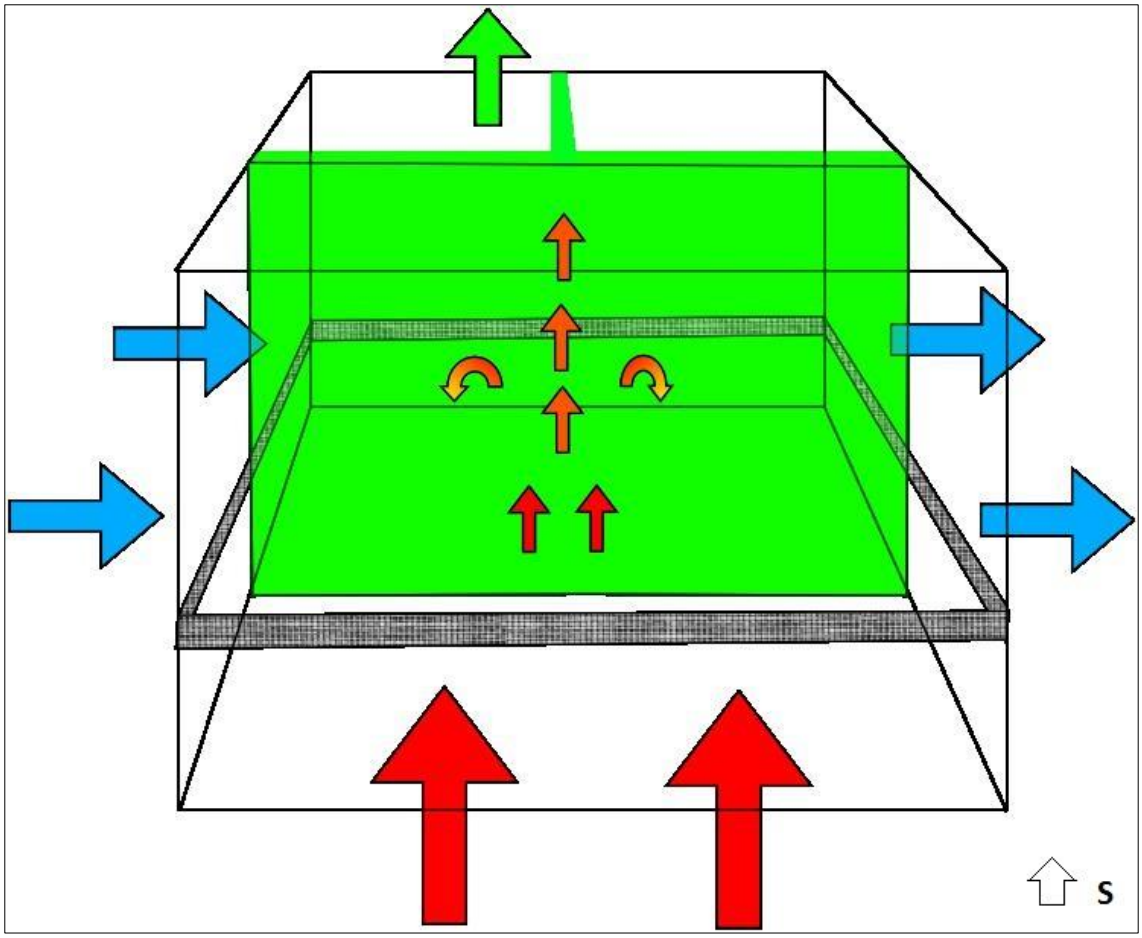

Figure 3.16: Conceptual model of the study area from north. Red arrows indicate the heat source from below. Blue arrows indicate the groundwater flow. Green arrow indicates the discharge from the faults that are denoted as green planes. The upward movements of hot water through faults are denoted as orange arrows. Grey parts indicate the impervious Ballıca Formation. (Not to scale)

3.2.2.2. Model Parts

The borehole data obtained from the studies of MTA (2007) and İB (2011) are used in the model. The two borehole data from the two government agencies differ much in terms of formation classifications.(See Appendix-A) İB borehole data is more detailed in terms of formations that were defined in the regional geology chapter; especially in the geothermal trapping impermeable neogene lacustrine sediment layer (Ballıca Formation), which was not defined in MTA borehole data. However, using the fault lines and formation thicknesses in the study area as "structural borders", and thus dividing the study area into four different parts, borehole data matching was accomplished. (Figure 3.16)

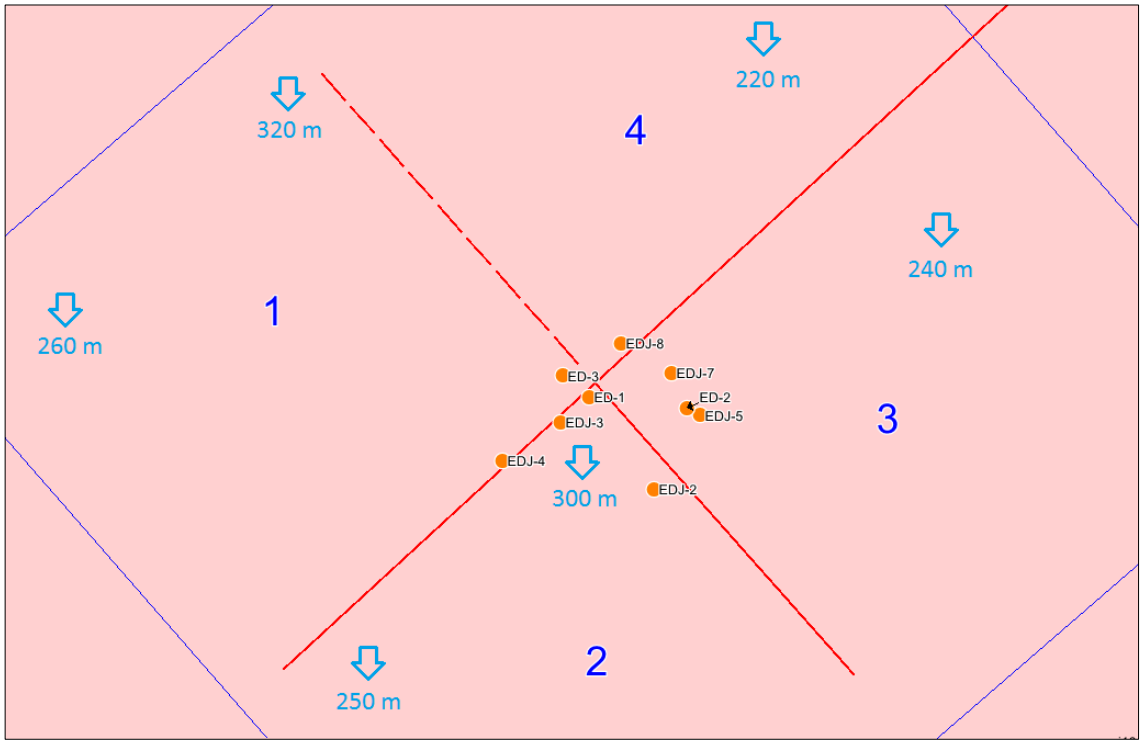

Figure 3.17: Study area divided into 4 parts, using faults as borders. Red dashed line is not a fault, but a "formational" border. The variable depths of parts are shown with blue arrows.

In this partition, part 4 was created even if there is not a fault defined between EDJ-8 and ED-3 in previous studies. At borehole EDJ-8, the lower aquifer depth is only 60 meters, whereas in ED-3, the lower aquifer depth is around 170 meters, and these two wells are relatively close to each other.

Considering this partition, part 1 has boreholes EDJ-4 and ED3; part 2 has EDJ-3, ED-1 and EDJ-2, part 3 has EDJ-7, ED-2 and EDJ-5, and lastly part 4 has EDJ-8 borehole only.

3.2.2.2.1 Part 1

Part 1 consists of EDJ-4 and ED-3 boreholes. Neogene lacustrine sediments in EDJ-4, is matched with a formation consisting alternation of sand and clay defined in ED-3 between 98 m and 132 meters of depth. A generalized columnar section is defined to be used in 3 dimensional modeling, with a depth varying from 260 m to 320 meters. (Figure 3.17)

3.2.2.2.2 Part 2

Part 2 consists of boreholes ED-1, EDJ-3 and EDJ-2. Neogene lacustrine sediments of EDJ-3 and EDJ-2 are matched with clayey and sandy formations marked in ED-1 borehole between 85 m and 107 meters of depth. A generalized columnar section has been defined, with a depth varying from 250 m to 300 meters. (Figure 3.18)

3.2.2.2.3 Part 3

Part 3 consists of EDJ-7, ED-2 and EDJ-5 boreholes. Neogene lacustrine sediments of EDJ-7 and EDJ-5 are matched with a clayey formation defined in ED-2 between 100 m and 110 meters of depth. A generalized columnar section has been defined with a depth of 240 meters. (Figure 3.19)

3.2.2.2.4 Part 4

Part 4 consists of borehole EDJ-8 only. The neogene lacustrine sediment formation is 60 meters thick. This part has a depth of 220 meters.

3.2.2.3 Model Production

3-dimensional modelling of parts was done with SutraPrep software. The input data file contents can be found in Appendix 3. Model block sections that re produced are shown in Figure 3.20. The model consists of 65596 nodes, and 60750

elements which are made up of 45 nodes in x and y dimensions and 30 nodes in the z dimension, making 74.5 m x 74.5 m x 10 m elements. The elements in the fault volume are made up of 4 m x 4 m x 10 m elements, since the fault width was reported to be 20 meters.

The 3 dimensional wire mesh output of the model from Sutra Prep software can be seen in figure 3.21.

Faults in the study area are modelled as low permeability parts between the parts aforementioned with their dip angles of 81 and 64 degrees, and can be seen in figure 3.22.

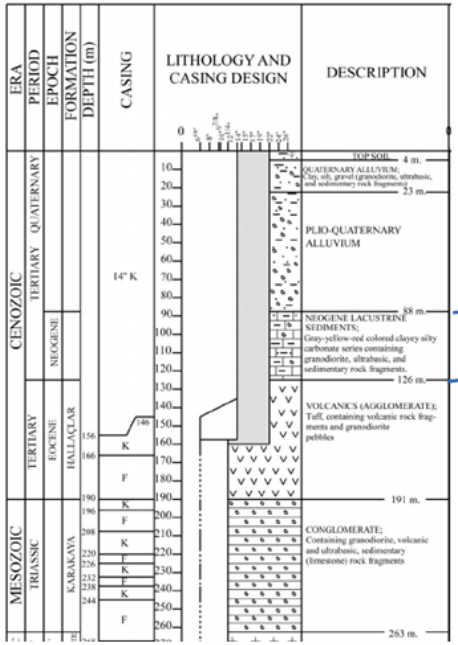

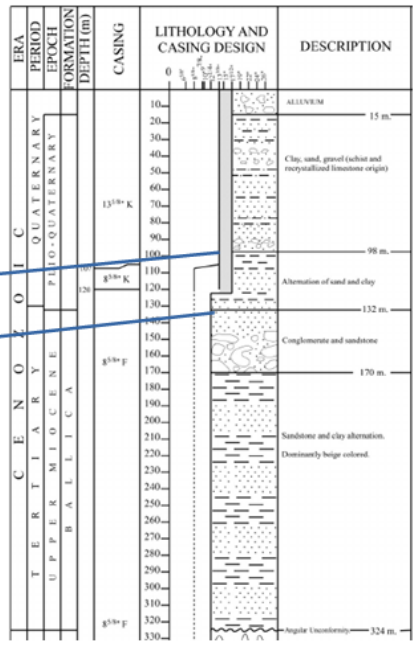

EDJ-4 (38 m)	ED-3 (34 m)
Generalized Columnar Section (SW ~ NE Direction)	0 m 90 m 130 m 260 ~ 300m

Figure 3.18: Borehole data matching and generalized columnar section for part 1.

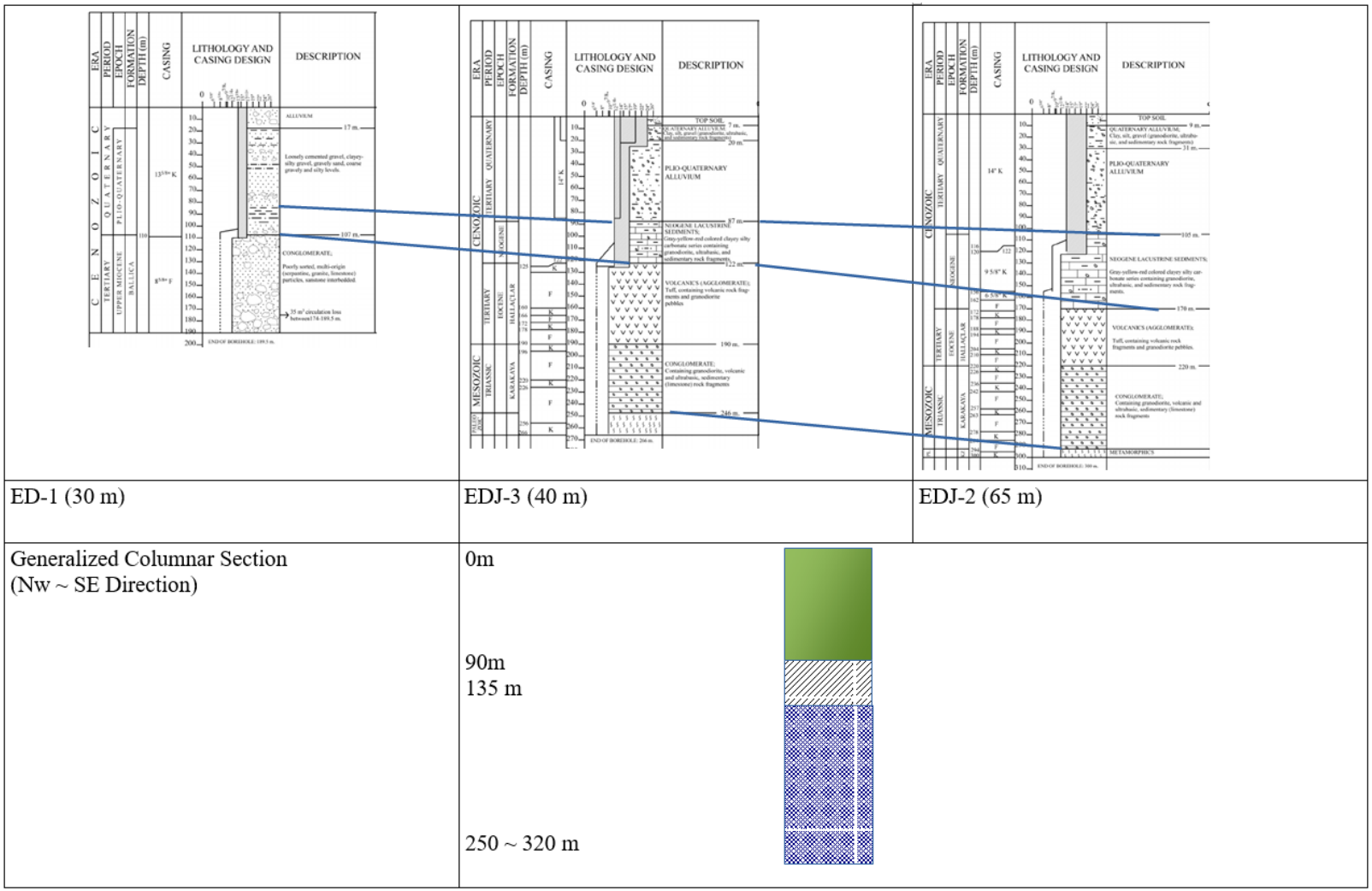

Figure 3.19: Borehole data matching and generalized columnar section for part 2.

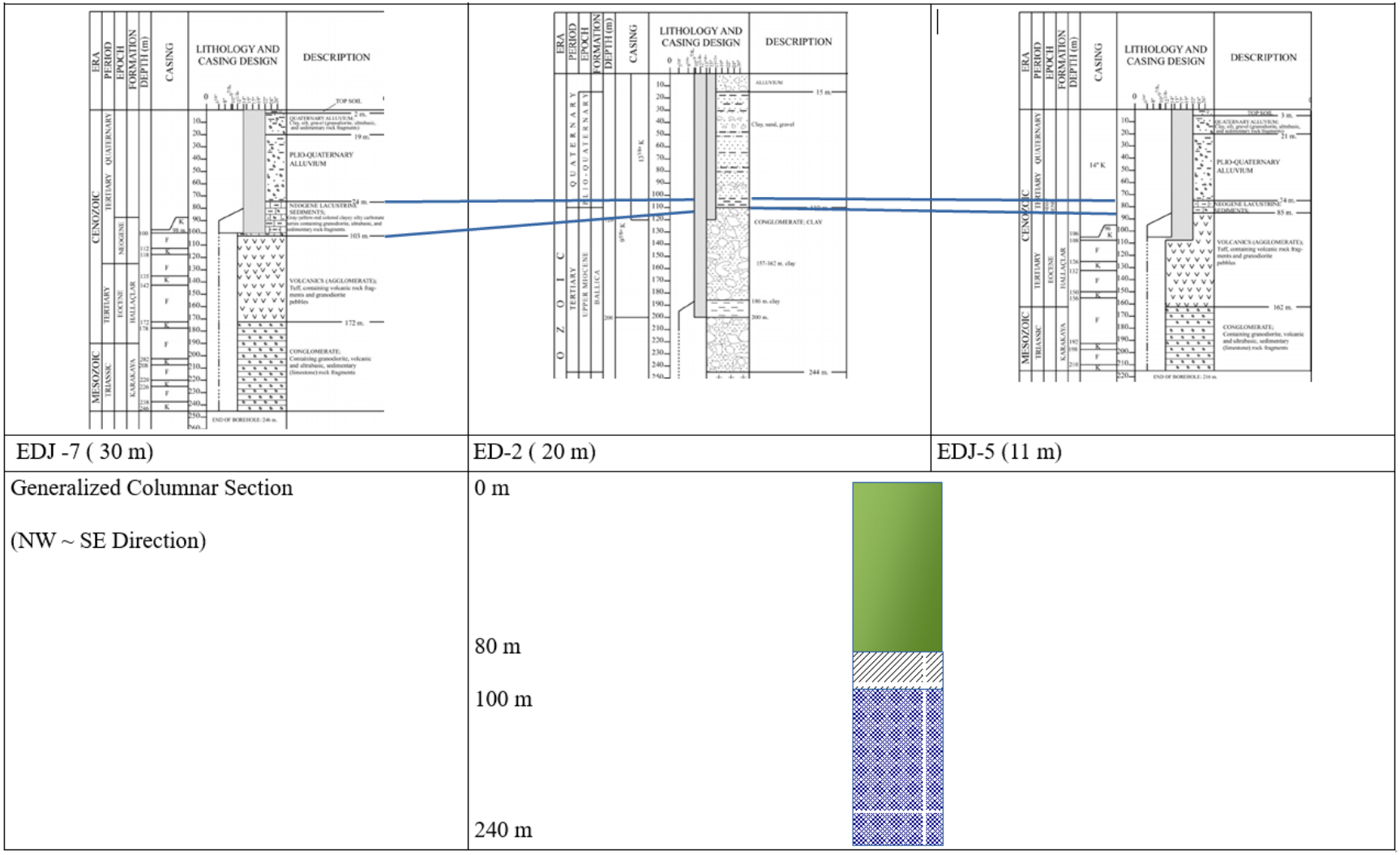

Figure 3.20: Borehole data matching and generalized columnar section for part 3.

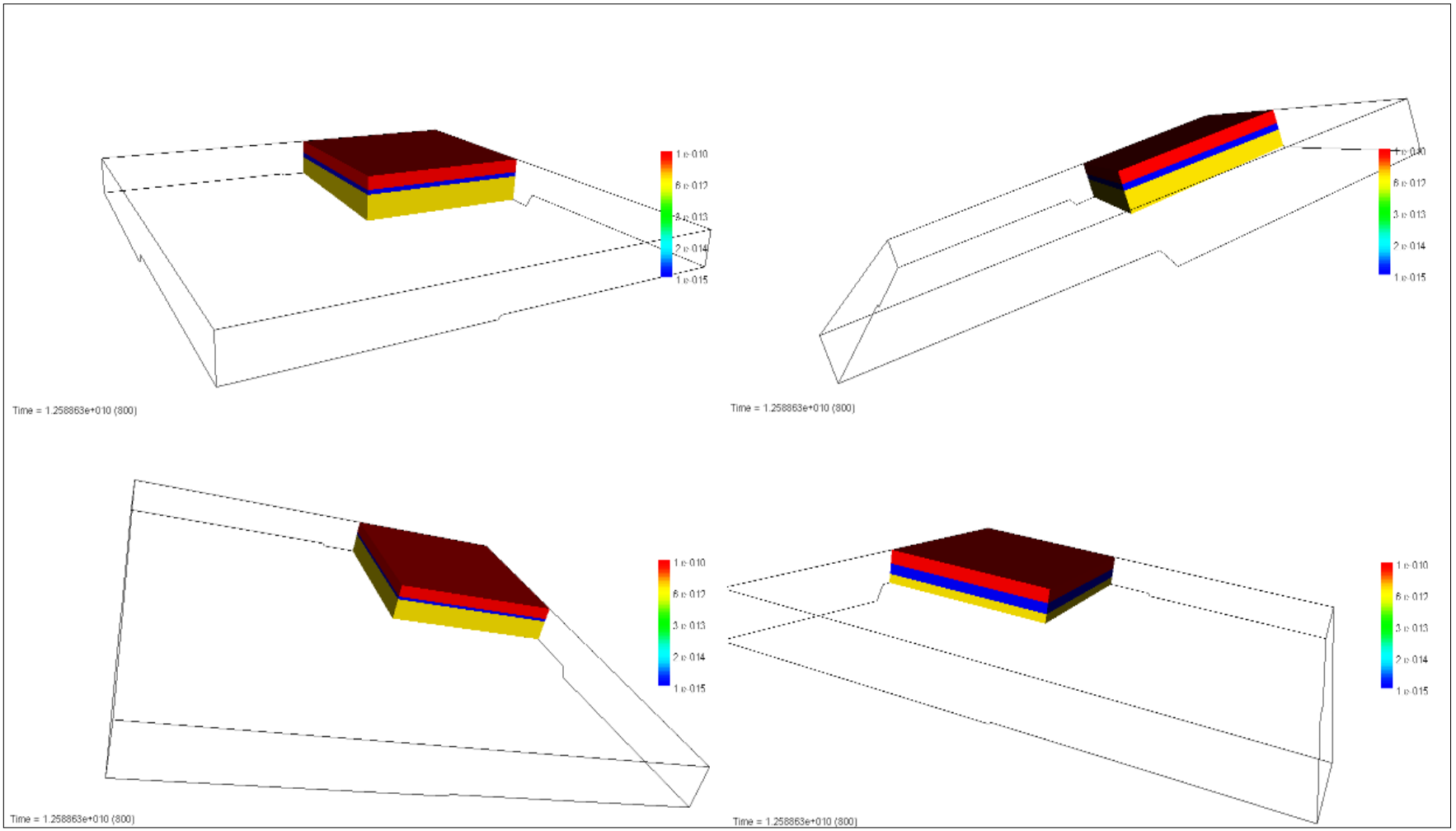

Figure 3.21: The 3-d model parts used in the simulation. Alluvium is in red, lacustrine sediments are blue, agglomerate and conglomerate are yellow in color. Sections 1 to 4 are from left to right and top to bottom. Legends show permeabilities.

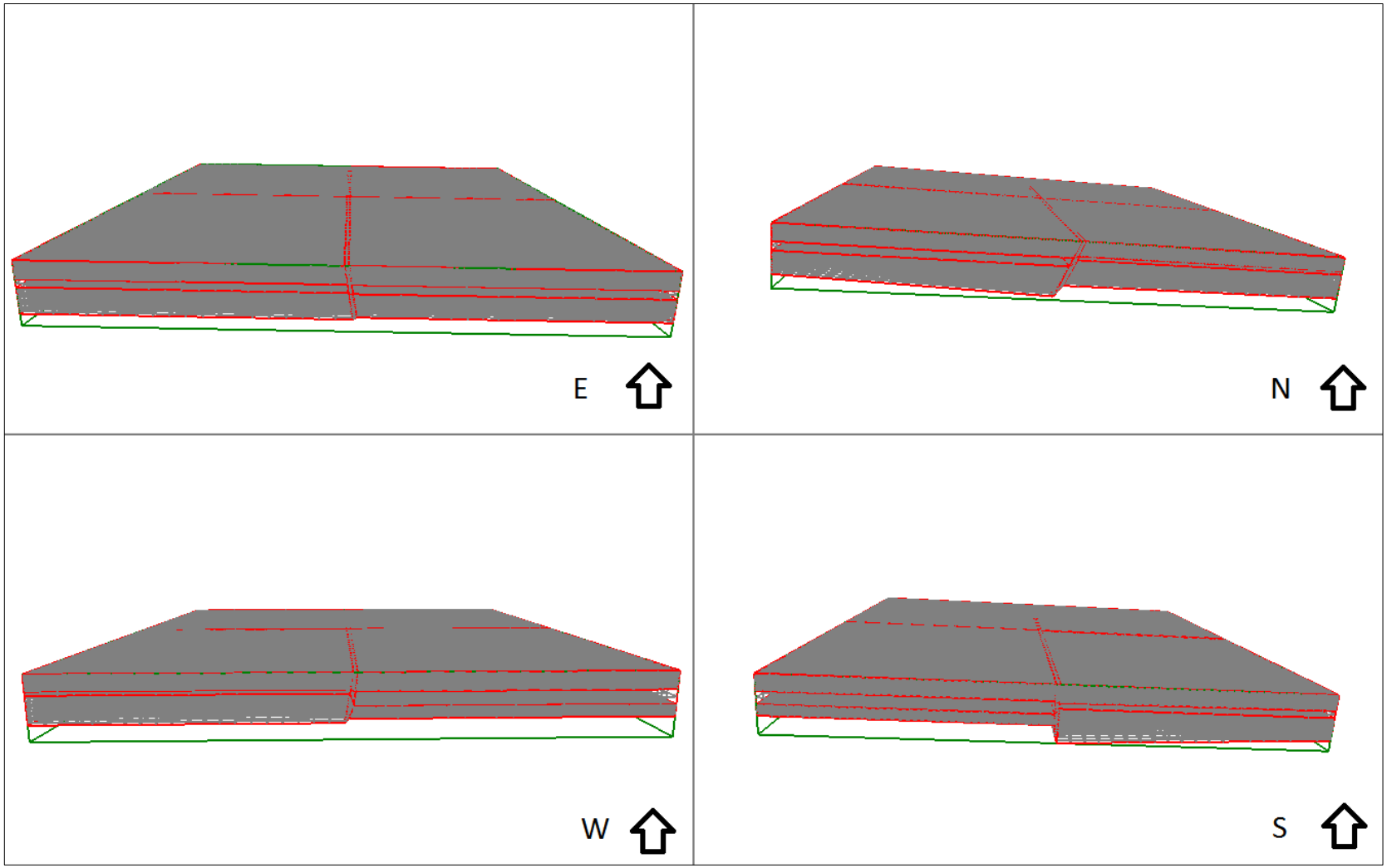

Figure 3.22: 3 dimensional wire-mesh vrml output of model area from Sutra Prep software.

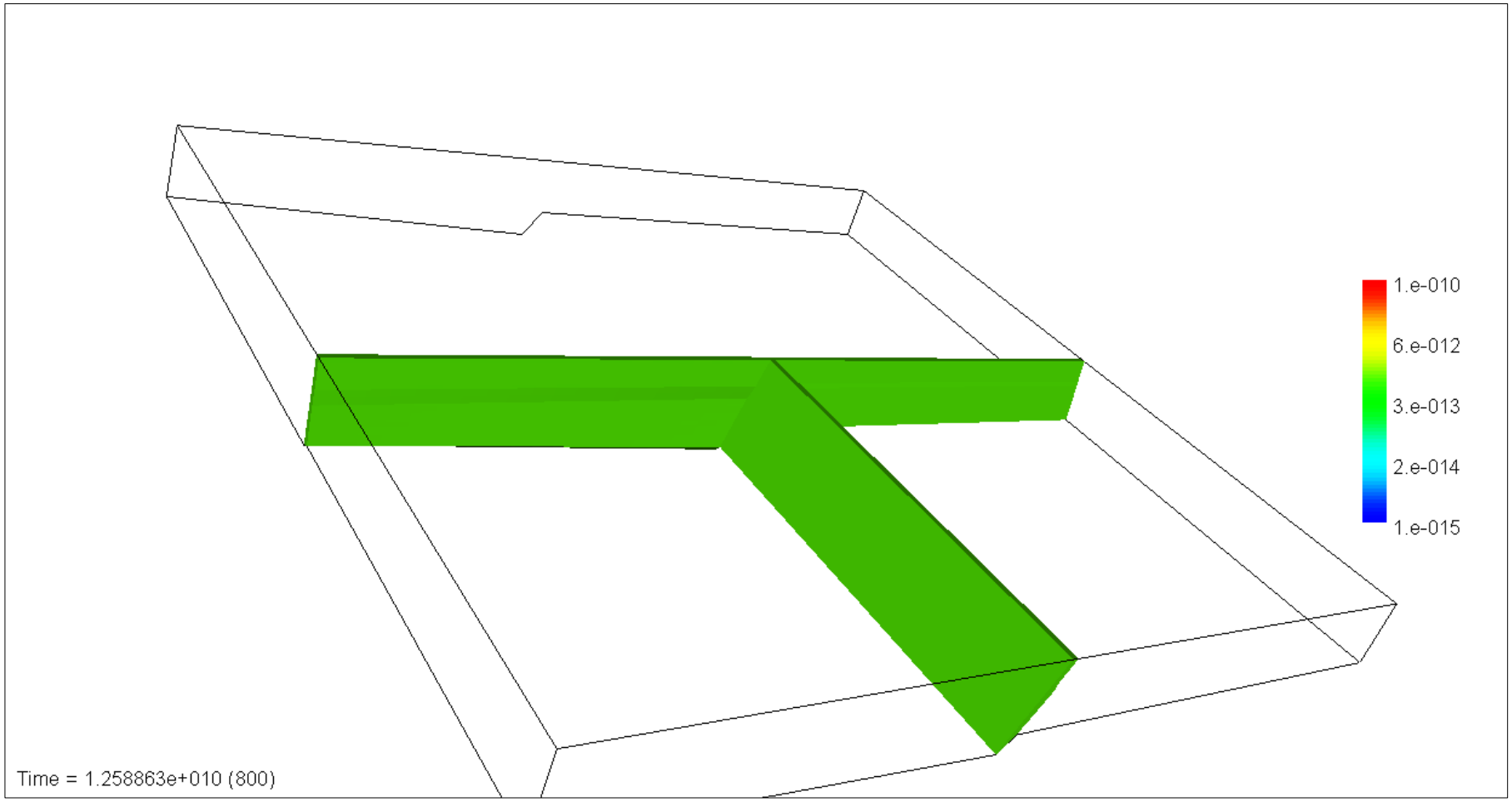

Figure 3.23: Faults in the study area modelled with their dip angles of 81 and 64 degrees. Legend shows permeability values.

3.2.3 Boundary Conditions

For the evolution of the Edremit Geothermal area, 2 different scenarios were studied because of structural geology and the intrusion phenomenon in the study area, and will have their relevant boundary and initial conditions:

1- The faulting happened with the intrusion, and the waters of both aquifers are heated from the bottom after faulting.
2- The faulting happened after the intrusion, but the lower aquifer was already heated before the formation of faults, then the waters of both aquifers began to mix with the faulting event.

3.2.3.1 Scenario 1: Heating After Faulting:

In this scenario, the piezometric head difference of 6.5 meters was applied to x-planes due to the 20.5 meters and 14 meters of heads that was computed in the 2-dimensional simulation at the x edges of the study area (Figure 3.14). Since flow lines are parallel to the study area, no flow was assigned to the model at y plane boundaries.

The boundary conditions for pressure are; hydrostatic for –x boundary, hydrostatic + 6.5 meters for +x boundary. The flux boundary is assigned as 1 kg/s at +z boundary but distributed at the faults only with 396 nodes.

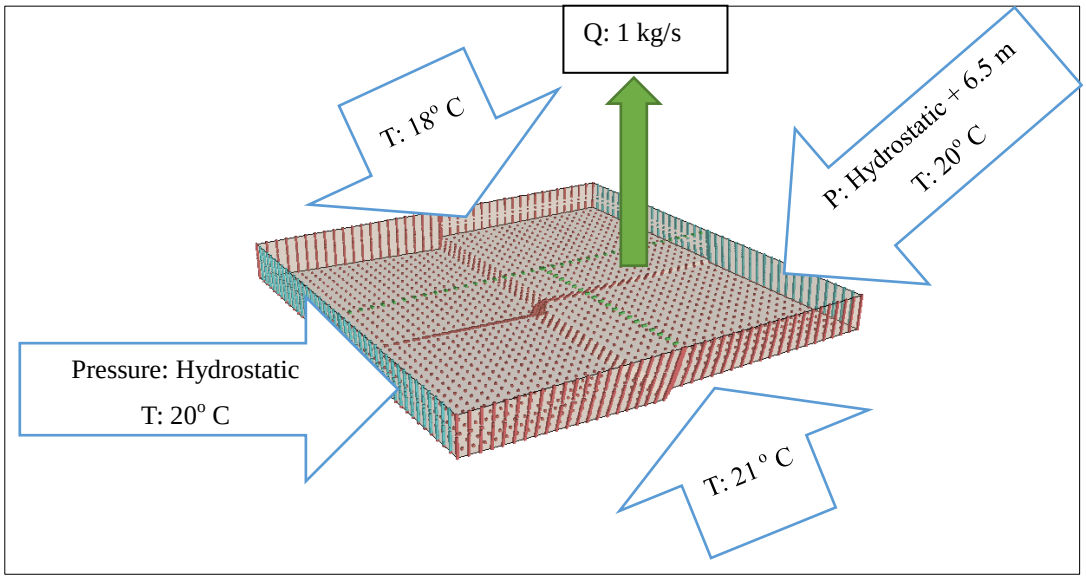

Figure 3.24: Boundary conditions for scenario 1, heating after faulting.

The initial conditions for this scenario are; hydrostatic pressure and 18º C of temperature for the whole system. This value was assigned as the average weather temperature of the region since the origin of the geothermal waters is stated as meteoric both by Mutlu (2007) and Faulds et al. (2009).

For thermal boundaries, it is assumed that both aquifers are being fed with surficial waters from the top, thus for temperature; boundaries are 18º C at +y (from EMIN well), 21º C, at -y boundary (From DSI-7 well) and 20º C at +x and –x boundaries (DSI -7 and DSI-8 wells, and average temperature.). Lastly, the system is heated at the bottom with various temperatures.

3.2.3.2 Scenario 2: Faulting After Heating:

In this scenario, the boundary conditions for pressure and flux are the same as scenario 1. For temperature; boundaries are 20º C for +x, -x, +y and –y boundaries down to 100 meters of depth, assuming that the upper aquifer is being fed with surficial waters from the top, and 60º C from 100 meters to the bottom of the system for +x, -x, +y and –y boundaries, assuming that the lower aquifer is being fed with hot waters from below. The system is heated at the bottom with various temperatures.

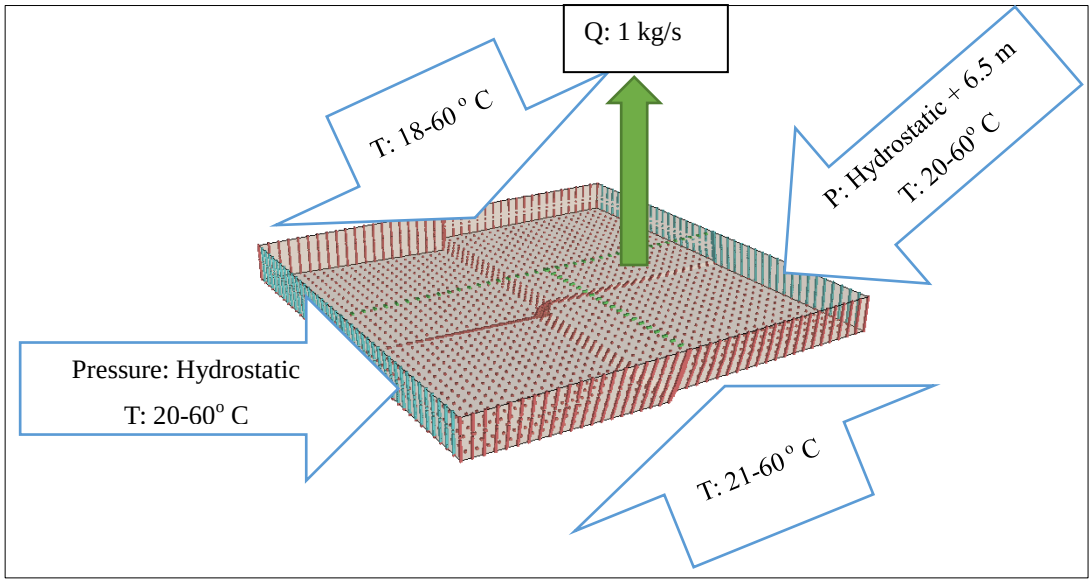

Figure 3.25: Boundary conditions for scenario 2, faulting after lower aquifer heating.

The initial conditions for this scenario are; hydrostatic pressure and 18º C of temperature down to 100 meters of depth, after which the temperature is between 40 º C to 60º C down to the bottom of the system.

It is assumed in this scenario that the bottom aquifer had already been heated to temperatures between 40º C to 60º C, and the upper aquifer is cold with a temperature of 20° C as in the study of Günay (2011). Then the faults were formed and the waters of two aquifers began to mix with each other.

3.2.4 Physical Properties

The physical properties of the model which is constant throughout the models are defined in table 3.2 below. The other physical property is the permeability which changes with the formations in the model and thus used as a variable in calibration studies, with a unit of m^2.

Table 3.2: Physical properties of the model

Symbol	Definition	Unit	Value
β_w	Water compressibility	$[\ kg / (m . s^2)\ ]^{-1}$	4.47×10^{-10}
λ_w	Water thermal conductivity	J / (kg . ºC . s)	0.6
μ	Water viscosity	kg / m . s	1 *
ρ_o	Base water density	kg / m^3	1000 at 20 ºC
$\frac{\partial \rho_w}{\partial T}$	Coefficient of water density change with temperature	$kg / (m^3 . ºC)$	-0.375
C_w	Specific heat of water	J /(kg . ºC)	4182
α_s	Solid matrix compressibility	$[\ kg/(m . s^2)\ ]^{-1}$	1×10^{-10}
C_s	Solid grain specific heat	J / (kg . ºC)	840
λ_s	Solid thermal conductivity	J / (kg . ºC . s)	3.5
ρ_s	Density of solid grains	kg / m^3	2650
n	Porosity	-	0.1

*: This value is actually viscosity scale factor. Viscosity is computed internally by the program with the following formula: $\mu(T) \cong (239.4 \times 10^{-7})\ 10^{\frac{248.37}{T+133.15}}$

3.2.5 Calibration Studies

3.2.5.1 Hydraulic Gradient Effect

The hydraulic gradient of 6.5 meters had an effect on the calibration studies. The model computed without hydraulic gradient with upper aquifer permeability of 10^{-10} m^2 and lower aquifer permeability of 10^{-11} m^2, fault zone having a permeability value of 10^{-12} m^2 , and heated below with 100 ºC is shown in figure 3.25, where the model with the same model values under the effect of hydraulic gradient can be seen in figure 3.26.

It is apparent from the figures that, the hydraulic gradient prevented the heat accumulation in both aquifers. The upper aquifer permeability value was assigned from the 2-dimensional simulation, but with this result, the permeability values had to be lowered, for the heat to accumulate in the system.

Günay (2012), in his study, had taken the upper aquifer permeability value as 10^{-11} m^2 and lower aquifer permeability value as 10^{-12} m^2. Since the previous field studies did not give specific information about permeability values, various permeability values were used in calibration studies around the values supplied by that study.

It is known from local geology information (chapter 2.2) that the upper aquifer consists of plio-quartenary alluvium, loosely cemented conglomerate, sandstone and mudstones. Using this as a resource, the upper model part permeability values were taken between 10^{-11} and 5 x 10^{-12} m^2. The lower model part permeability values were taken between 10^{-12} and 5 x 10^{-13} m^2.

3.2.5.2 Fault Zone Permeability Values

The fault zone itself was given an isotropic permeability value of 10^{-12} m^2 for it to be permeable, since the previous studies state the two aquifers are connected because of the faulting. Thus, to have another variable in calibration studies, anisotropic permeability values are assigned to the fault zone with between 10^{-12} and 10^{-14} m^2. To guarantee easier upward water flow, z-axis permeability values are kept at 10^{-12} m^2 at all times, but the x and y-axes were assigned different values. The x and y-axes permeability values were assigned equal to each other, since two faults in the study area intersect at right angles with each other.

3.2.5.3 Hydraulic Gradient and Pressure Levels

The hydraulic properties used in the simulations assume that the hydraulic gradient did not change in 40 years since the conditions found in Ural's study (1978), because data for current water levels are not available. Thus, the boundary conditions are compiled from the 2-dimensional simulation results in Chapter 3.2.2.

3.2.5.3 Permeability Values

The permeability values for the formations are not studied before. Using the conceptual studies in chapter 3.2.1 and the results from 2-dimensional simulations, various permability values are assigned to the formations based on the lithologies.

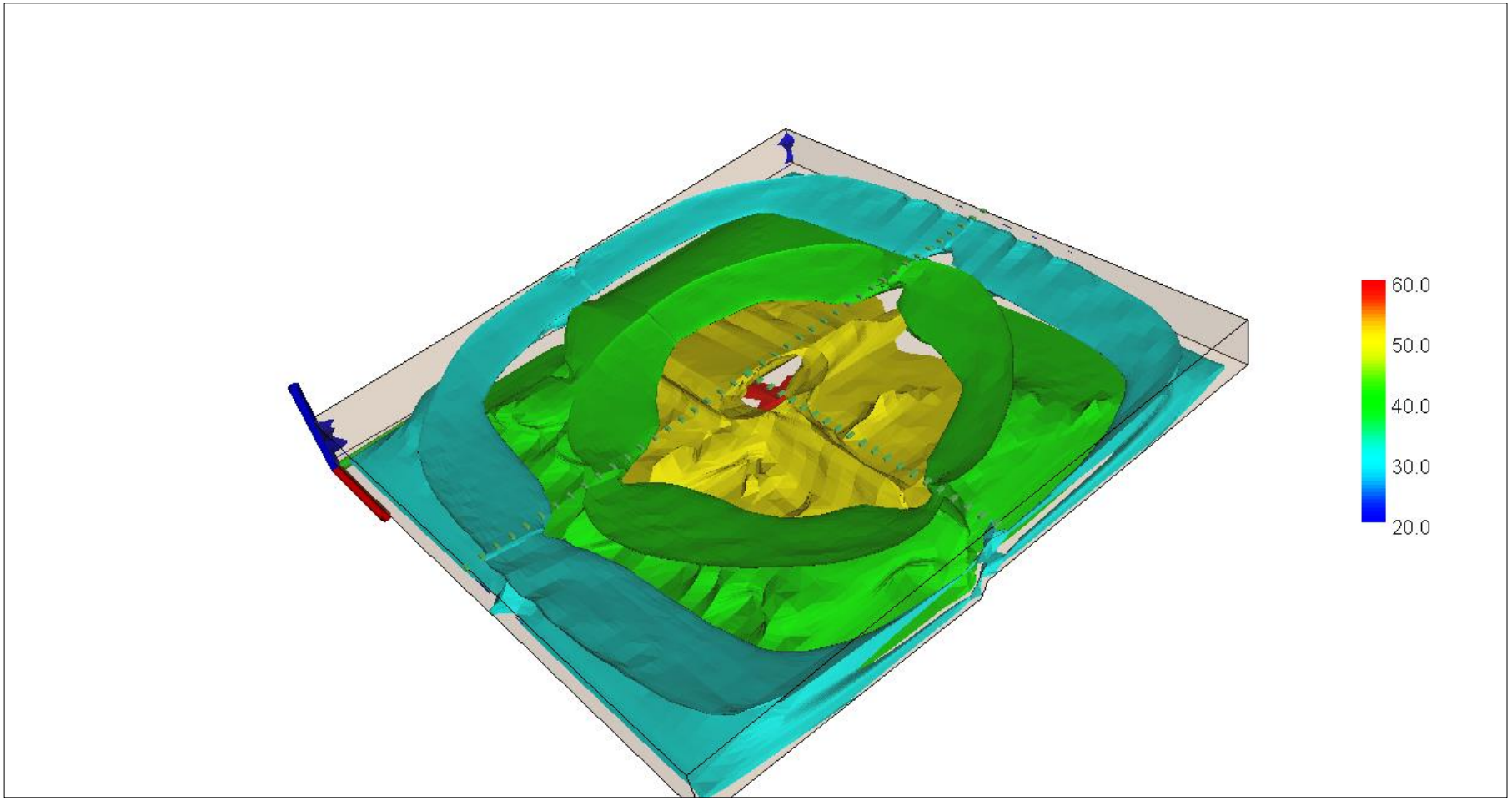

Figure 3.26: Isosurface simulation result of the study area without hydraulic gradient. The legend shows the temperatures. Green cubes are flux boundaries.

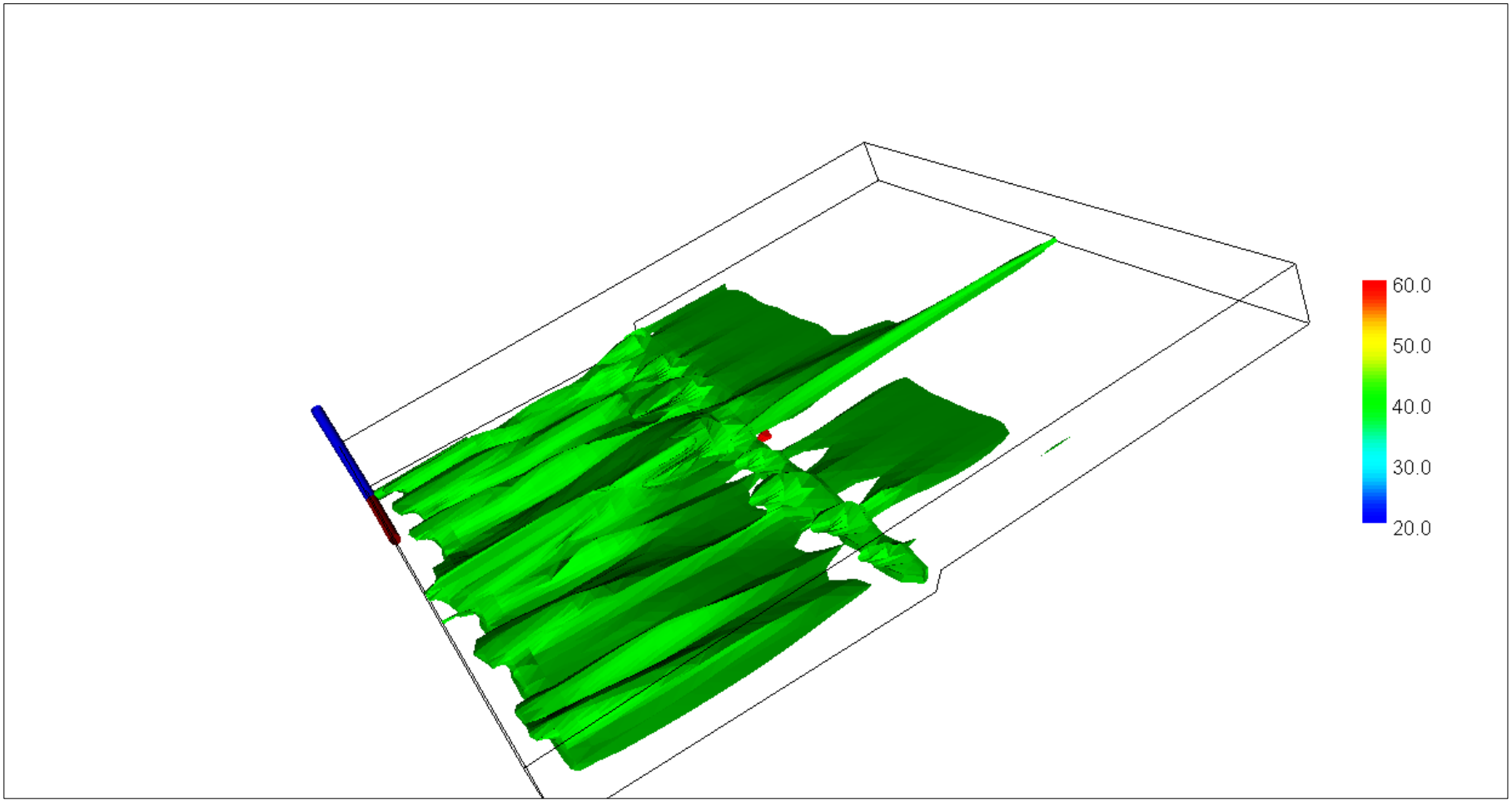

Figure 3.27: Isosurface simulation result of the study area with hydraulic gradient. The legend shows the temperatures.

3.2.5.3 Calibration Simulations

Various simulations done with models having different parameters for evolution scenario 1 are studied. For the sake of readability, scenario 1 results are grouped into two parts, with their calibration results, and model screenshots. The calibration results for part 1 is shown in Appendix 2.

Since the permeability values are not known, models were run with differing isotropic permeability values for formations with trial and error methodology.

The upper formation forming the cold aquifer permeability values were kept as high as much as possible since plio-quartenary formation was reported to be semi consolidated to consolidated from the previous studies. Its values were ranged between 10^{-11} and 5 x 10^{-12} m^2.

The lower formation forming the hot aquifer permeability values were kept between 10^{-12} and 5 x 10^{-13} m^2. For the permeability values, the study of Günay (2012) was taken as a reference, thus values were kept near that value of that study.

For the fault zones, anisotropic and isotropic permeability values were studied, with permeability values ranged from 10^{-12} to 10^{-14} m^2. For all times, +z axis permeability was kept as 10^{-12}, since the two aquifers are intermixed. Permeability values in x and y axes were kept equal, since two faults intersect at right angle with each other.

Table 3.3 : Simulations performed for evolution scenario 1. (Part 1)

Model Number	Upper Aquifer Permeability	Fault Zone Permeability	Lower Aquifer Permability	Bottom Temperature (° C)	RMS Error (%)
1	2 x 10^{-12}	1 x 10^{-14}	2 x 10^{-12}	90	12.09
2	5 x 10^{-12}	1 x 10^{-14}	1 x 10^{-12}	100	12.95
3	5 x 10^{-12}	1 x 10^{-13}	1 x 10^{-12}	100	13.21
4	5 x 10^{-12}	1 x 10^{-12}	1 x 10^{-12}	100	12.55
5	1 x 10^{-11}	1 x 10^{-12}	5 x 10^{-13}	100	13.38
6	1 x 10^{-11}	1 x 10^{-12}	1 x 10^{-12}	100	13.88
7	1 x 10^{-11}	1 x 10^{-14}	1 x 10^{-12}	100	12.92

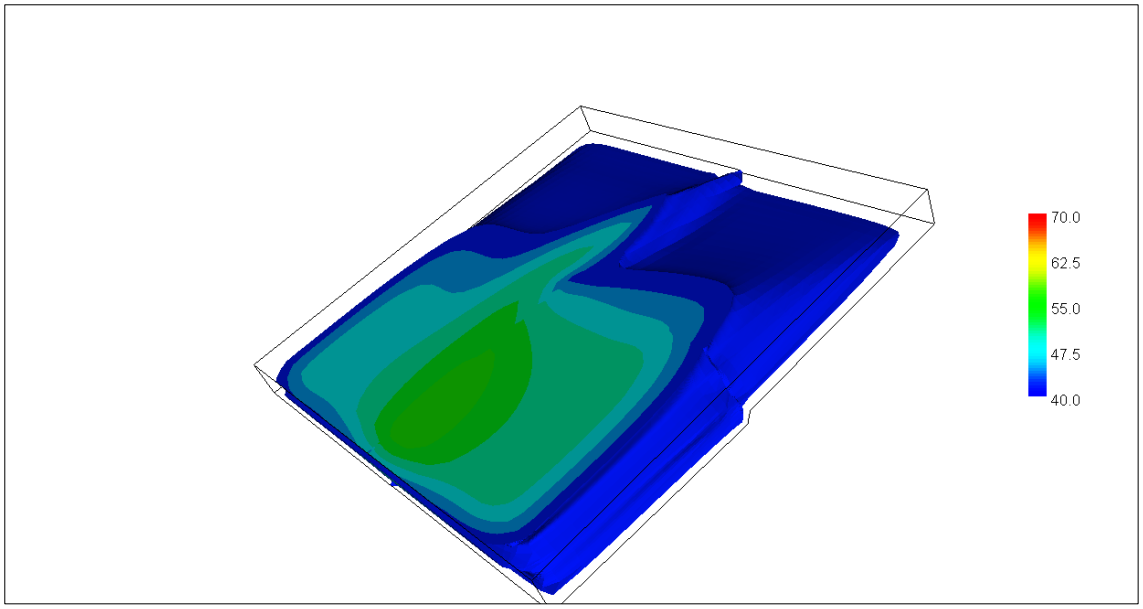

Figure 3.28: Part 1 Model #1 shown with 40 ºC cutoff. Legend shows the temperatures in ºC.

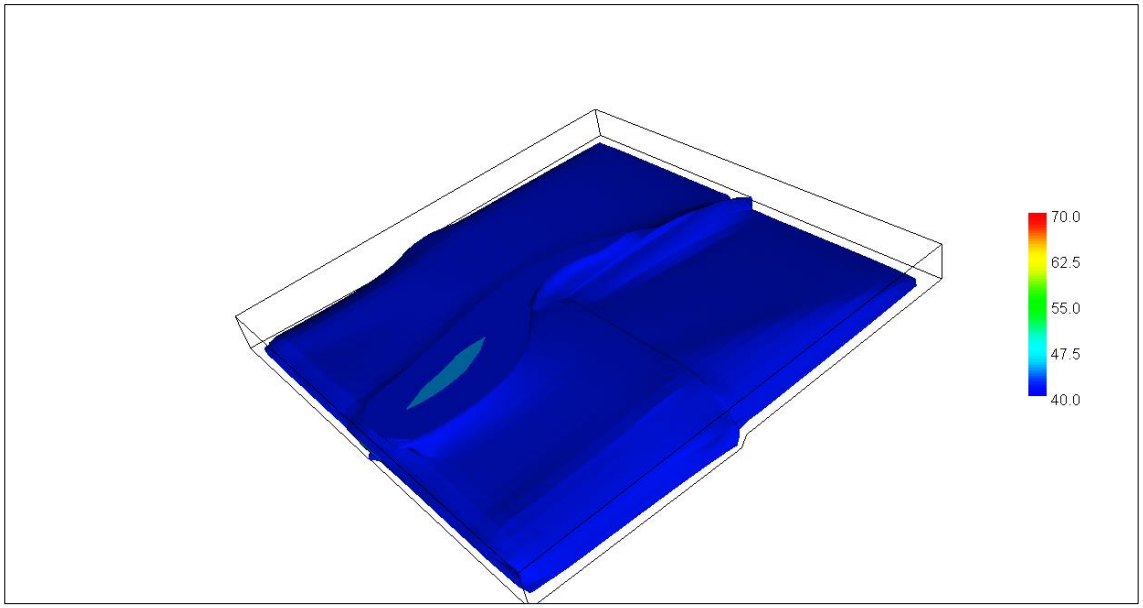

Figure 3.29: Part 1 Model #2 shown with 40 ºC cutoff. Legend shows the temperatures in ºC.

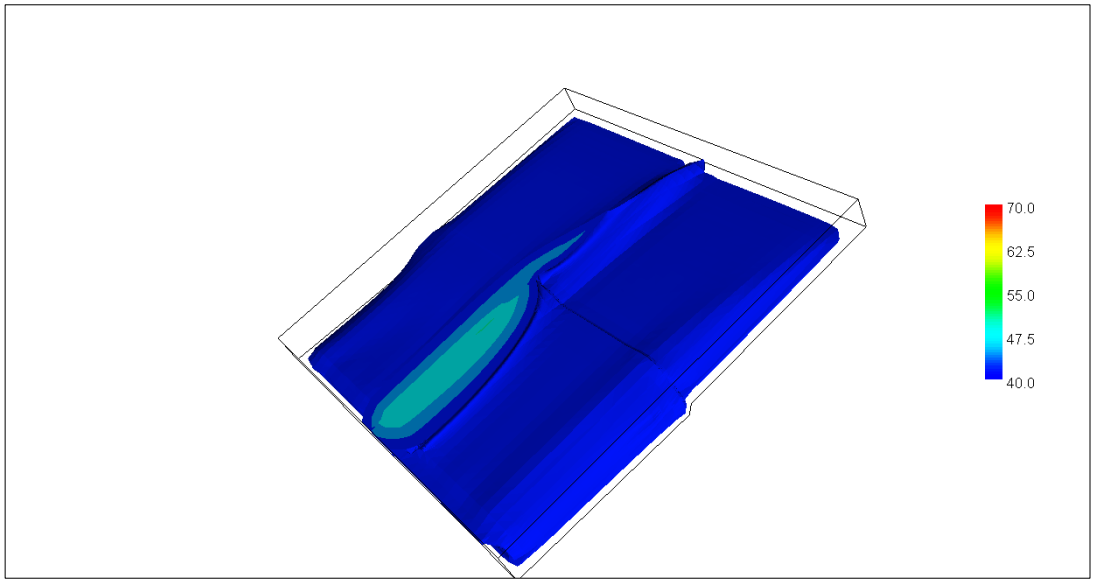

Figure 3.30: Part 1 Model #3 shown with 40 ºC cutoff. Legend shows the temperatures in ºC.

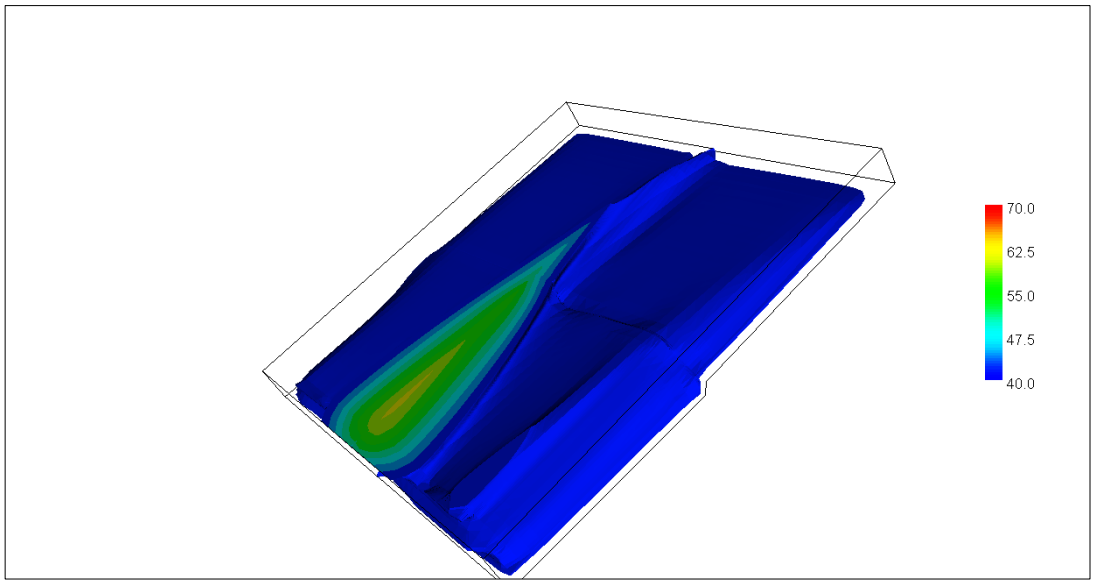

Figure 3.31: Part 1 Model #4 shown with 40 ºC cutoff. Legend shows the temperatures in ºC.

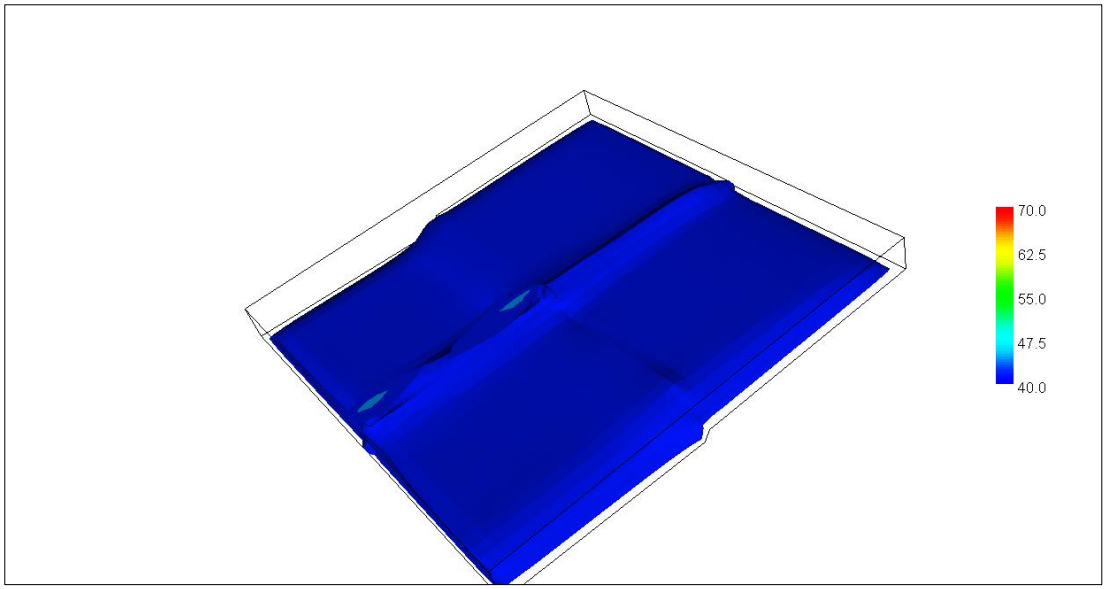

Figure 3.32: Part 1 Model #5 shown with 40 ºC cutoff. Legend shows the temperatures in ºC.

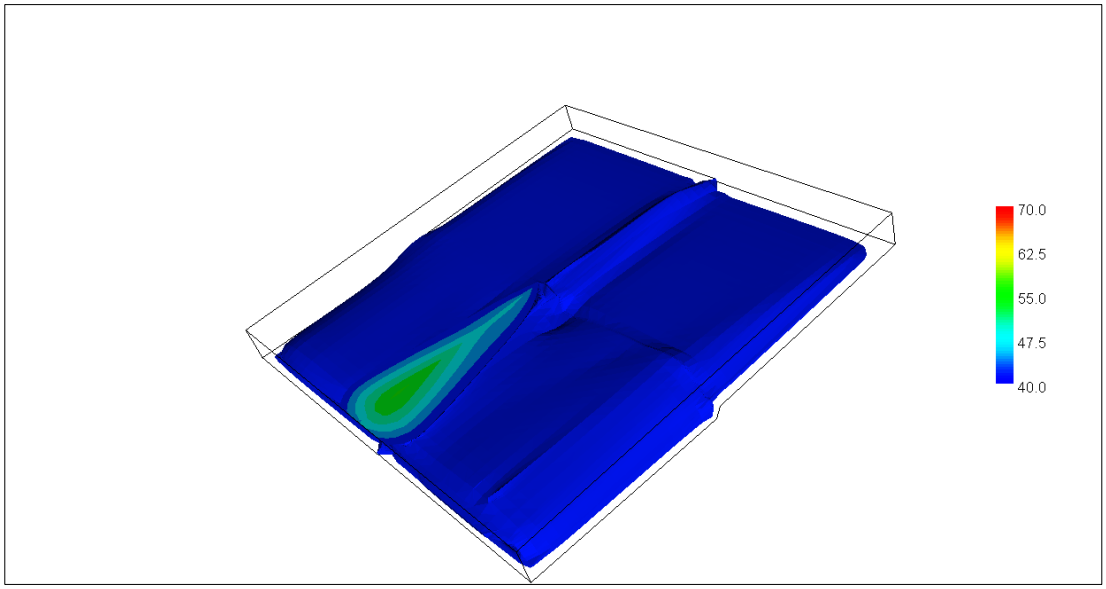

Figure 3.33: Part 1 Model #6 shown with 40 ºC cutoff. Legend shows the temperatures in ºC.

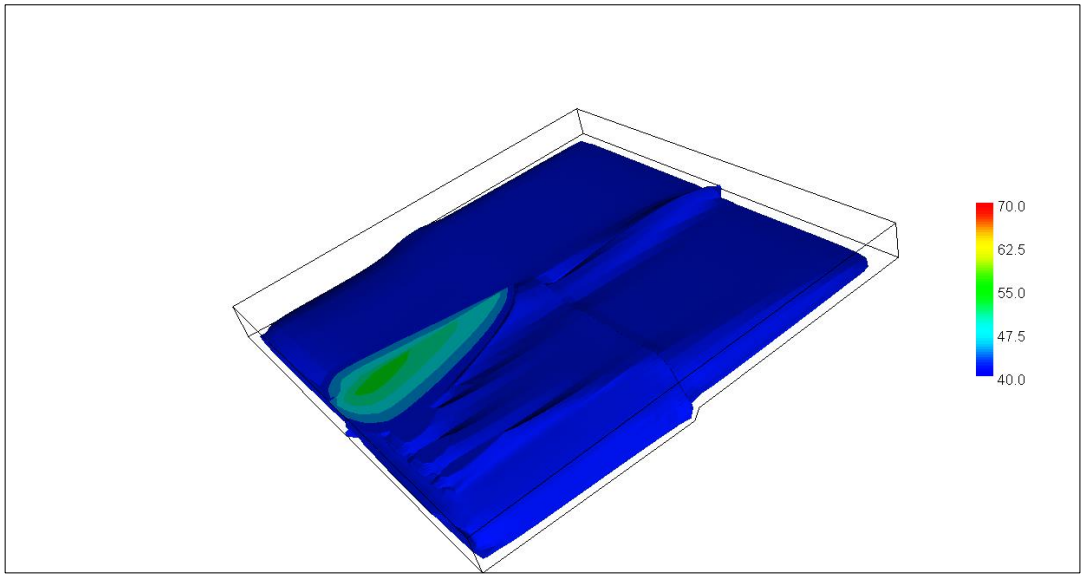

Figure 3.34: Part 1 Model #7 shown with 40 ºC cutoff. Legend shows the temperatures in ºC.

Using part 1 results as a reference, part 2 was modelled with the bottom temperature of 90 º C, and upper aquifer permability with 5 x 10^{-12} m^2, and lower aquifer permability of 1 x 10^{-12} m^2, differing in permeability value of the fault zones.

Table 3.4 : Simulations performed for evolution scenario 1. (Part 2)

Model Number	**Upper Aquifer Permeability**	**Fault Zone Permeability**	**Lower Aquifer Permability**	**Bottom Temperature (º C)**	**RMS Error (%)**
1	5 x 10^{-12}	1 x 10^{-14}	1 x 10^{-12}	90	12.26
2	5 x 10^{-12}	1 x 10^{-13}	1 x 10^{-12}	90	12.07
3	5 x 10^{-12}	1 x 10^{-12}	1 x 10^{-12}	90	11.35
4*	5 x 10^{-12}	1 x 10^{-12}	1x 10^{-12}	90	11.54

* The trapping aquitard was given a permeability of 5 x 10^{-15}, differing from the other models.

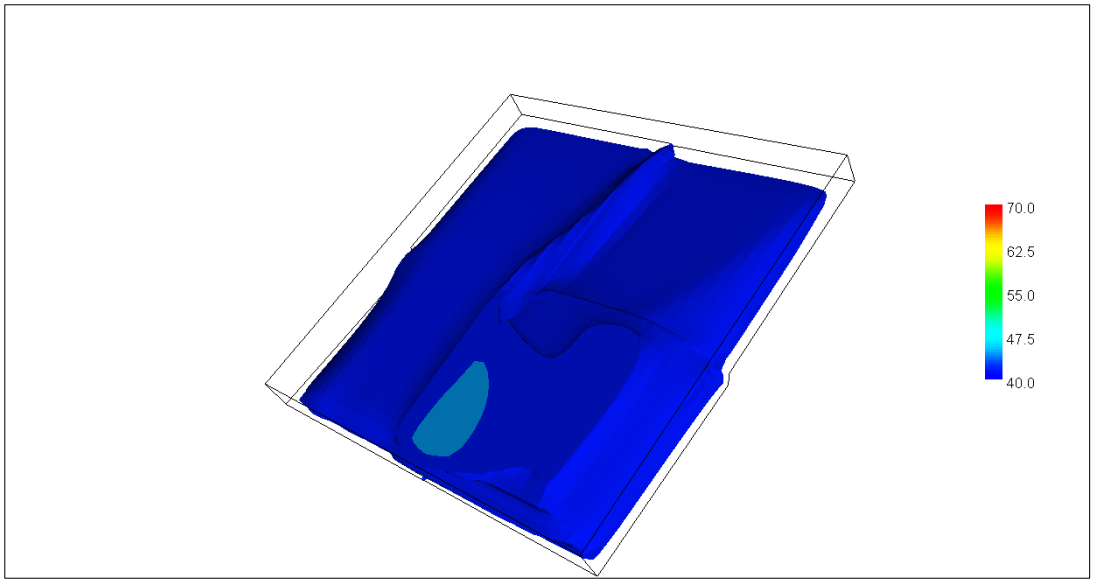

Figure 3.35: Part 2 Model #1 shown with 40 ºC cutoff. Legend shows the temperatures in ºC.

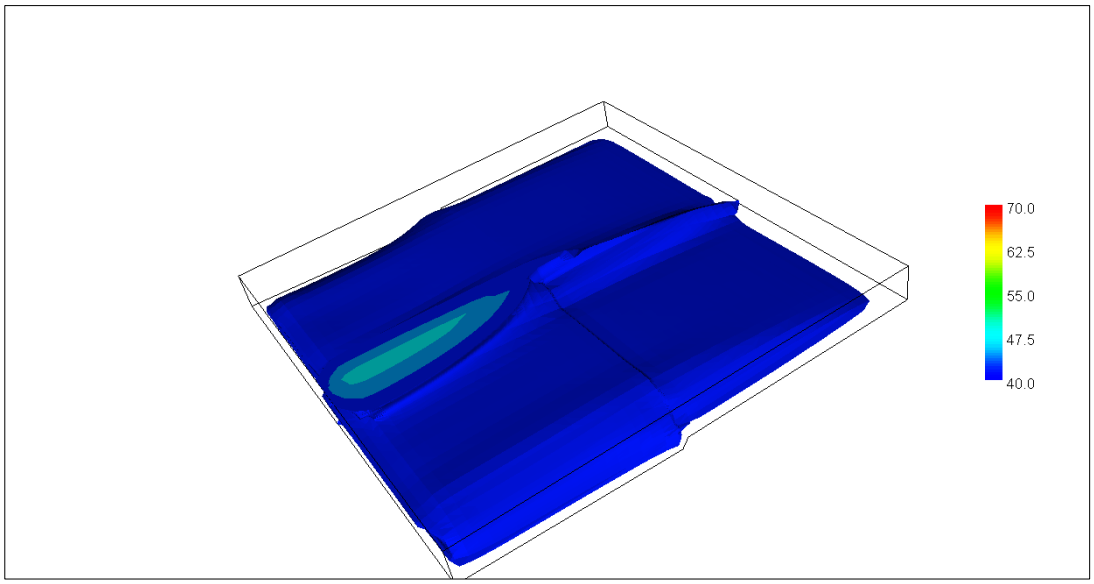

Figure 3.36: Part 1 Model #2 shown with 40 ºC cutoff. Legend shows the temperatures in ºC.

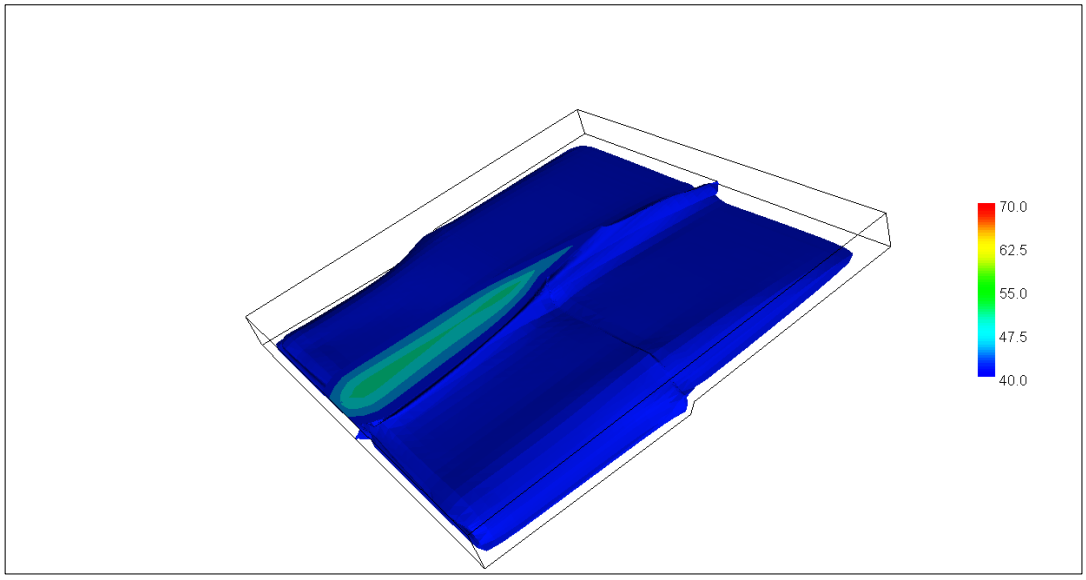

Figure 3.37: Part 1 Model #3 shown with 40 ºC cutoff. Legend shows the temperatures in ºC.

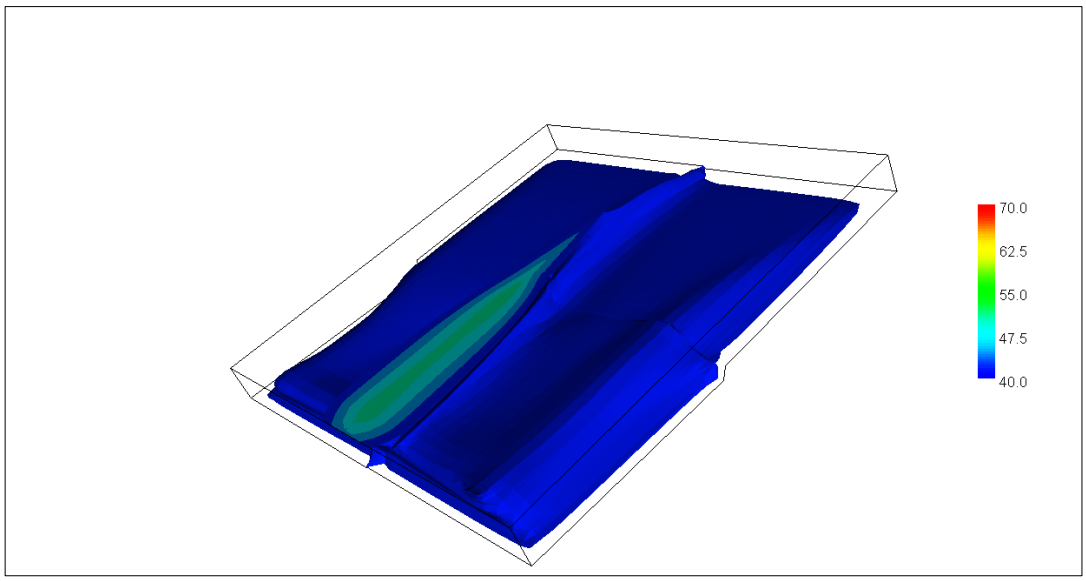

Figure 3.38: Part 1 Model #4 shown with 40 ºC cutoff. Legend shows the temperatures in ºC.

In the evolution scenario 2, various models with different permeability values, bottom temperature and initial lower aquifer temperatures were simulated. The results are shown on tables in Appendix 2. Models in this scenario were produced with variations from the best result obtained from scenario 1.

Table 3.5: Simulations performed for evolution scenario 2.

Model Number	**Upper Aquifer Permeability**	**Fault Zone Permeability**	**Lower Aquifer Permeability**	**Initial Lower Aquifer and Lower Boundary Flux Temperature (° C)**	**Bottom Temperature (° C)**	**RMS Error (%)**
1	5×10^{-12}	1×10^{-13}	1×10^{-12}	60	90	21.31
2	5×10^{-12}	1×10^{-12}	1×10^{-12}	60	80	17.70
3	5×10^{-12}	1×10^{-12}	1×10^{-12}	50	80	13.15
4	5×10^{-12}	1×10^{-14}	1×10^{-12}	40	80	10.31

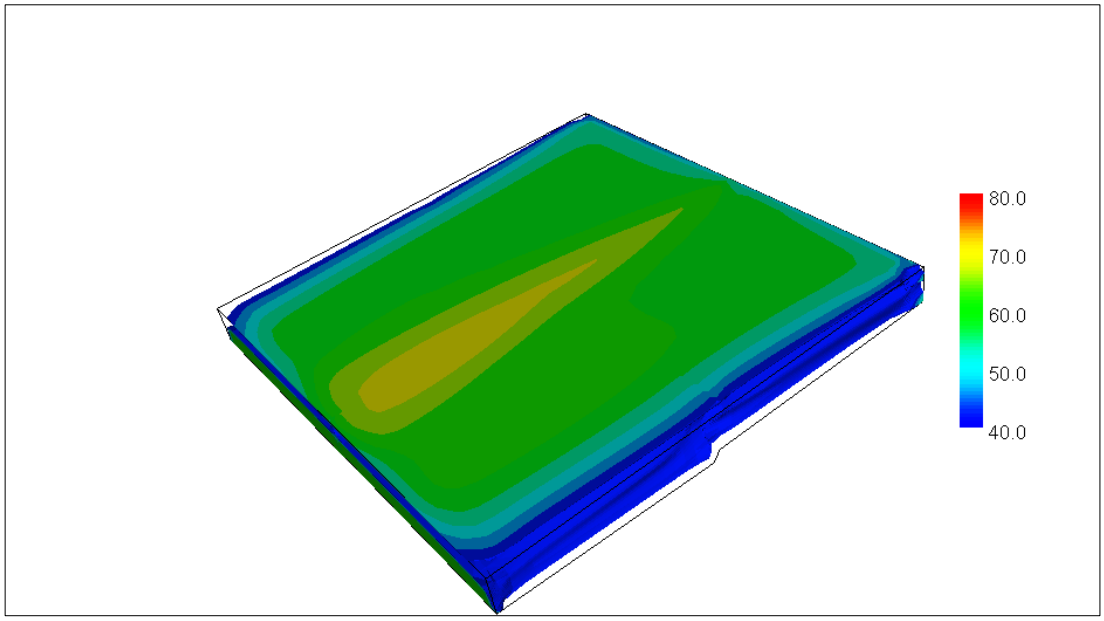

Figure 3.39: Model #1 shown with 40 ºC cutoff. Legend shows the temperatures in ºC.

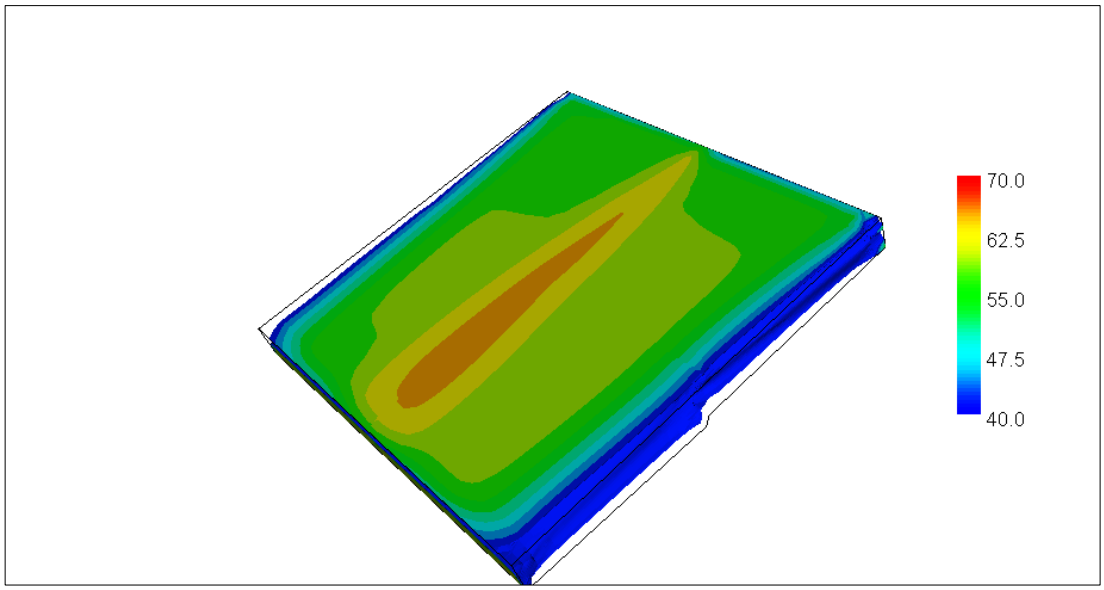

Figure 3.40: Model #2 shown with 40º C cutoff. Legend shows the temperatures in ºC.

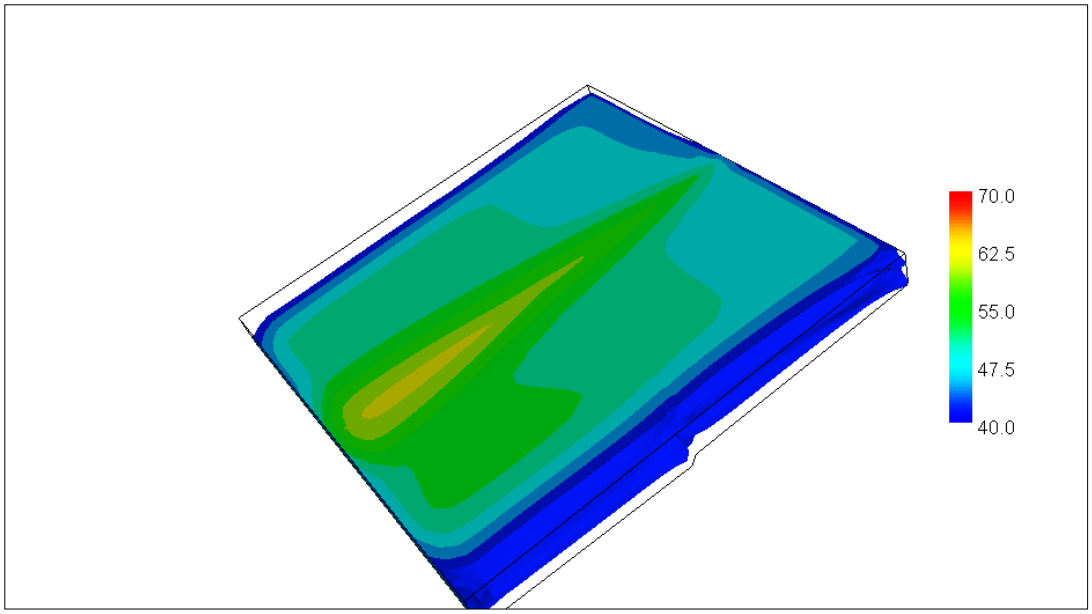

Figure 3.41: Model #3 shown with 40 ºC cutoff. Legend shows the temperatures in ºC.

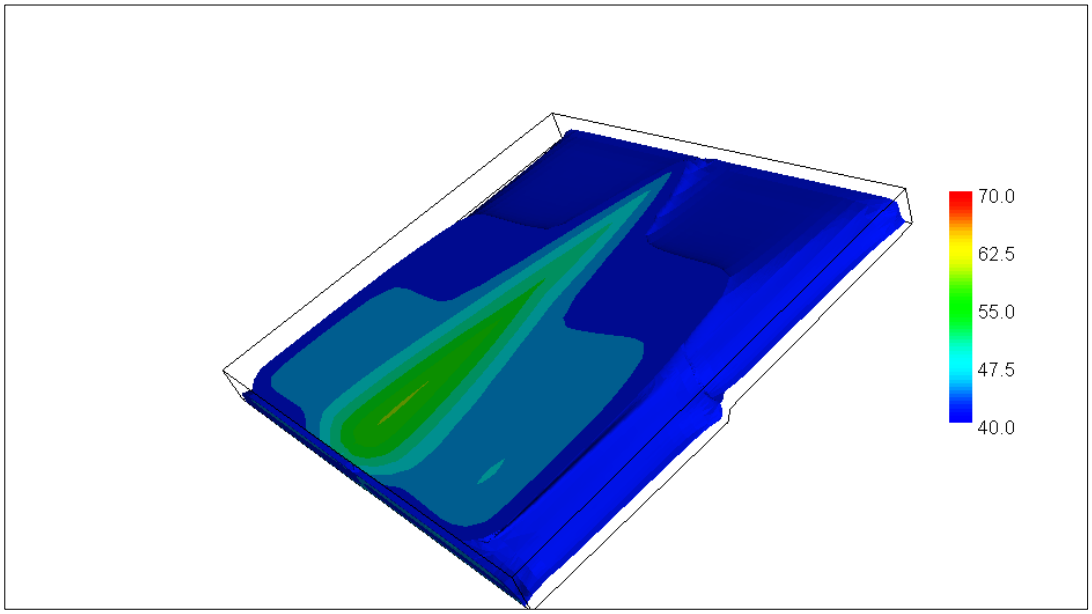

Figure 3.42: Model #4 shown with 40 ºC cutoff. Legend shows the temperatures in ºC.

The best matching result obtained from Root Mean Square Error calculations is from evolutionary scenario 2, model 4, with a value of 10.31% (Figure 3.41). The best matching result for evolutionary scenario 1 is part 2, model 3, with a value of 11.35%.

However there are some uncertainties with the observed well data. The cold water well DSI-7 has a depth of 132 meters, which is actually inside the impermeable layer for partition 2. However, as those wells are opened for irrigation and the actual well screen is not known, for the best matching scenarios above, the well depth has been raised to 90 meters, which is near the bottom of the upper aquifer. The modified calculated values are as follows:

Table 3.6: Modified Temperatures after DSI-7 Well Modification

DSI – 7 Actual	Scenario 2 Model 4	Scenario 1 Part 2 Model 3
21 º C	47.7 º C	35.5 º C

From these results, the RMSE for scenario 1, Part 2 Model 3 has been changed to 11.24%, and scenario 2, model 4 has been changed to 10.12%.

Another observation is the well ED-3's temperature values obtained from borehole data. Although this well is as close to the faults like other wells, the well temperature data from that borehole is noticeably lower than other deep hot water wells in the region. Besides, in the study of Avşar (2011), the well temperature has been reported to be 62º C, which does not match the borehole data. (See Table 2.1 & Appendix 1) In calibration studies, this well had the most significant errors in error calculations.

Lastly, although in RMSE calculations, scenario 2 model 4 gave better results, it should be pointed out that in terms of the cold wells' calibration data, scenario 1 errors are smaller.

Table 3.7: Cold well mean square errors for best fit models.

Well Name	Observed	Scenario 1 Part 2 Model 3	MSE	Scenario 2 Model 4	MSE
DERMAN	53	44.60	70.93	51.90	1.23
ENTUR	51	42.30	75.15	50.50	0.28
YAGCI	42	40.80	1.35	49.30	52.99
DSI6	39	37.10	3.71	47.90	78.48
DOGAN	32	35.90	15.58	45.20	174.92
DSI9	32	39.50	56.20	48.40	269.95
HASTANE	31	31.30	0.12	42.70	136.65
DSI5	30	34.30	18.23	46.40	268.90
DSI7	21	35.50	210.83	47.70	713.42
DSI8	18	25.10	50.55	40.20	493.52
RMSE			7.09		14.80

3.2.3.4 Summary for Calibration Studies

The calibration simulations performed by the 3-dimensional analysis with two different evolution scenario assumptions yielded various results for the integrated 3-dimensional modelling of two aquifers. The assumptions and characteristics of the models can be summarized below:

1 – Structural and formational borders needed a partition of the study area into 4 parts.

2- The formation data from the field obtained from the boreholes drilled by MTA (2001) and İB (2007) was matched per partition separately, and a 3 dimensional model was constructed, assuming the formations are horizontal in each partition.

3- Two buried and intersecting fault data from Avşar (2011) was incorporated into the model.

4- The 3-dimensional models, consisting of 65596 nodes and 60750 elements were constructed with 45 nodes in x and y dimensions and 31 nodes in the z dimension, making 74.5 m x 74.5 m x 10 m elements. The elements in the fault

volume are made up of 5 nodes with 4 m x 4 m x 10 m elements, to discretize the fault zone more precisely.

5- Two different evolutionary scenarios; namely, heating after faulting and faulting after heating were assumed prior to simulations. The boundary and initial conditions were formed using those two evolutionary scenarios.

6- Since the permeability values are not known from previous studies, models were run with differing isotropic permeability values for formations.

7- In the first studies, the effect of 6.5 meter hydraulic head difference was studied, thus upper aquifer permeability values were lowered to 10^{-11}, and lower aquifer permeability values were lowered to 10^{-12} maximum, since in the model computed with hydraulic gradient with upper aquifer permeability of 10^{-10} m^2 and lower aquifer permeability of 10^{-11} m^2, little heat accumulation was observed. (Figure 3.25 and Figure 3.26)

8- The upper formation forming the cold aquifer permeability values were kept as high as much as possible since plio-quartenary formation was reported to be semi consolidated to consolidated from the previous studies. Its values were ranged between 10^{-11} and 5 x 10^{-12} m^2.

9- The lower formation forming the hot aquifer permeability values were kept between 10^{-12} and 5 x 10^{-13} m^2. Since the permeability values were not known from field studies, study of Günay (2012) was taken as a reference, thus values were kept near that value of that study.

10- For the fault zones, anisotropic and isotropic permeability values were studied, with permeability values ranged from 10^{-12} to 10^{-14} m^2. For all times, +z axis permeability was kept as 10^{-12}, since the two aquifers are intermixed. Permeability values in x and y axes were kept equal, since two faults intersect at right angle with each other.

11- Water discharge was incorporated to the system at the +z boundaries, but from the faults only, with 1 m^3/s flux.

12- Calibration studies were performed done using the well temperature data from previous studies, using Root Mean Square Error statistical method.

The results obtained from the calibration studies are as follows:

1- The best matching result obtained from Root Mean Square Error calculations is from evolutionary scenario 2, model 3, with a value of 10.12%. (Figure 3.41)

2- The best matching result for evolutionary scenario 1 is part 2, model 3, with a value of 11.24%. (Figure 3.36)

3- The upper aquifer permeability value should be higher than 10^{-11} m^2, for the upper aquifer to "hold" the temperature coming from the lower aquifer in aforementioned conditions. Values around 5 x 10^{-12} m^2 are good candidates.

4- The lower aquifer permeability values around 10^{-12} m^2 are good candidates to "hold" the temperature in the lower aquifer.

5- Bottom temperatures around 80~90º C are good candidates for the –z boundary to create optimum amount of temperature for the system.

6- For the fault zones, isotropic permeability value of 10^{-12} m^2 yielded the best results for the system. With lower values, more temperature is accumulated in the lower aquifer, and by forming a "dam-like" structure against the flow, the upper aquifer is heated more as well. (See Figure 3.34)

7- From the results obtained from the 3-dimensional studies of the system, the 2-dimensional model needs to be revised, since the upper aquifer permeability value had to be lowered from 10^{-10} m^2, which was the value used in 2-dimensional studies.

8- 75 m x 75 m x 10 m finite elements were adequate to perform the calibration studies. Approximately, an area 4 times bigger than this study area can be studied with these element dimensions within the software limits, provided that deep well data are available.

9- There is no best model for the study area with many unknown values, but different alternative models are made available by the calibration studies. The results obtained from these calibration models can be used in the future as a reference to the precise modelling of the study area.

3.2.5.5 Revision

With the information obtained from the 3-dimensional calibration studies, the 2-dimensional model needed to be revised. The permeability value for the 2-dimensional model was lowered down to $2x10^{-12}$ m^2. The higher permeability zone defined in 2-dimensional simulation was lowered to $6x\,10^{-12}$ m^2. The simulation was re-run using Flow with Varying Permeability conditions stated in chapter 3.2.2.3, with steady-state simulation with 6 areal borders and 38 constant head points. (Figure 3.42)

The root mean square error was recalculated, with the results shown in Table 3.11.

Table 3.8: Revised 2-Dimensional Model Error calculations

MSE of Ural's Study Area	**MSE of Avşar's Study Area**
1.35	0.19

The result of this revised simulation didn't differ much from the simulation results obtained in chapter 3.2. The hydraulic head difference is 6.5 meters, the same as calculated before.

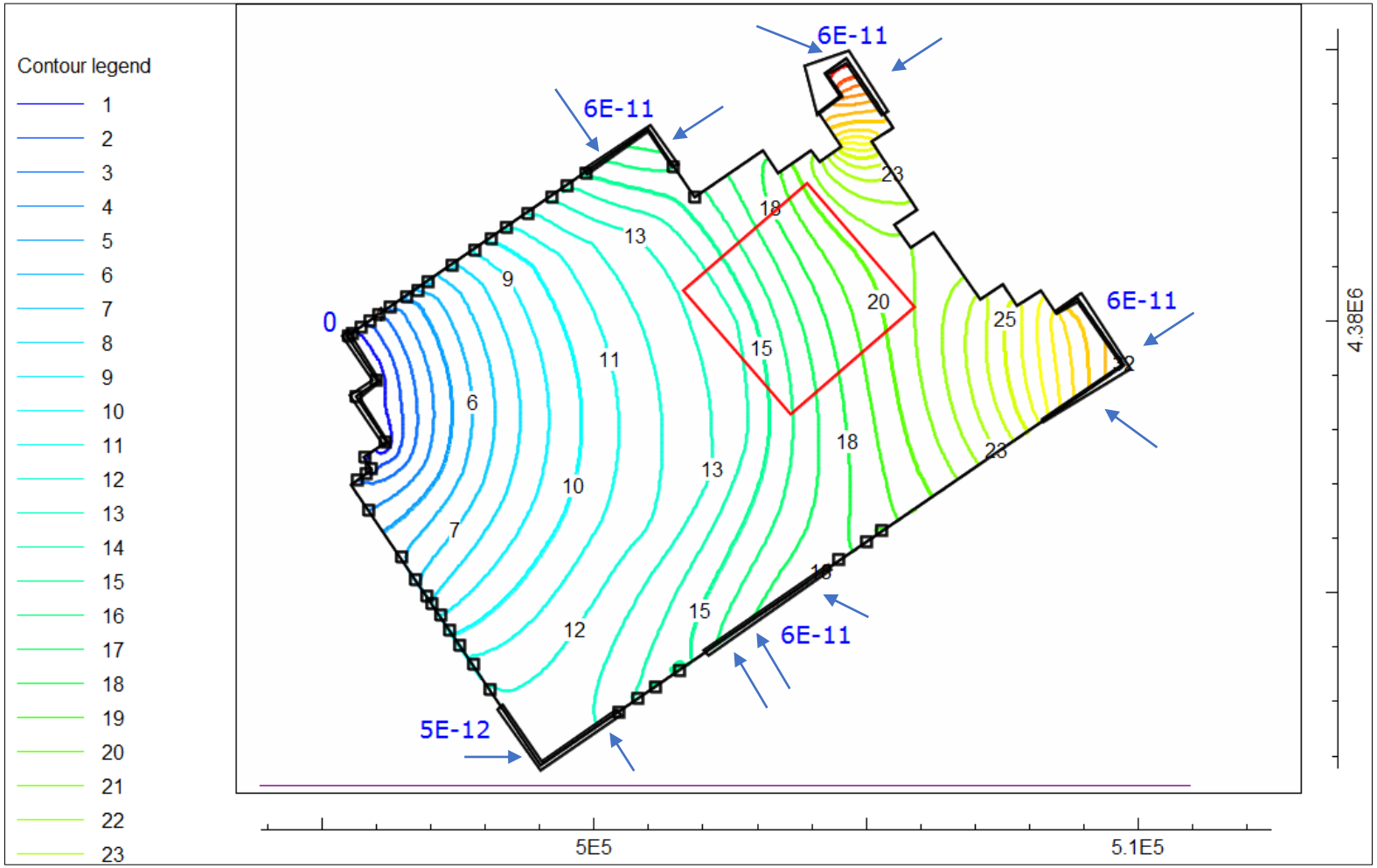

Figure 3.43: Revised steady-state 2-dimensional model. Blue arrows show the flux in m^3/s.

CHAPTER 4

NUMERICAL APPLICATIONS

4.1 Introduction

In this chapter, the calibration data obtained from Chapter 3 is used to calculate the response of the geothermal system to pumping. Various hypothetical production scenarios are studied with differing pump rates over various time periods. Pressure and temperature losses are recorded, and the recovery of the system is observed with the help of modeling. Lastly, a hypothetical reinjection scenario with production schedule is modelled.

4.2 Edremit Geothermal Heating System Specifics

The Edremit Geothermal Heating System is studied in detail by Can Coşkun (2007) in his master's thesis. A representative diagram of the heating system including production wells can be seen in Figure 4.1. Also, in that study he had found out that the Edremit Geothermal Heating System requires 100 kg/s of hot water in winter for heating and 10 kg/s of hot water is needed for hot water in summer months for 1648 equivalent residences for the year 2006. In the production schematic, three wells are shown as not pumping, because the Edremit Central Heating System realization was planned in three stages, for 1500, 5000 and lastly 7500 equivalent residence heating. It was reported that for the first stage, wells ED-1, ED-3 and EDJ-3 were assigned to the system and wells EDJ-4, EDJ-5 and EDJ-7 were not producing at that time. Currently, the private firm is operating 9 wells, for which information is not known fully. Thus, the realized and planned production data of 2007 is used in this study, with maximum requirements for second stage of production which is for 5000 equivalent residences, approximately equaling 360 kg/s of hot water requirement for winter months and 36 kg/s for summer months.

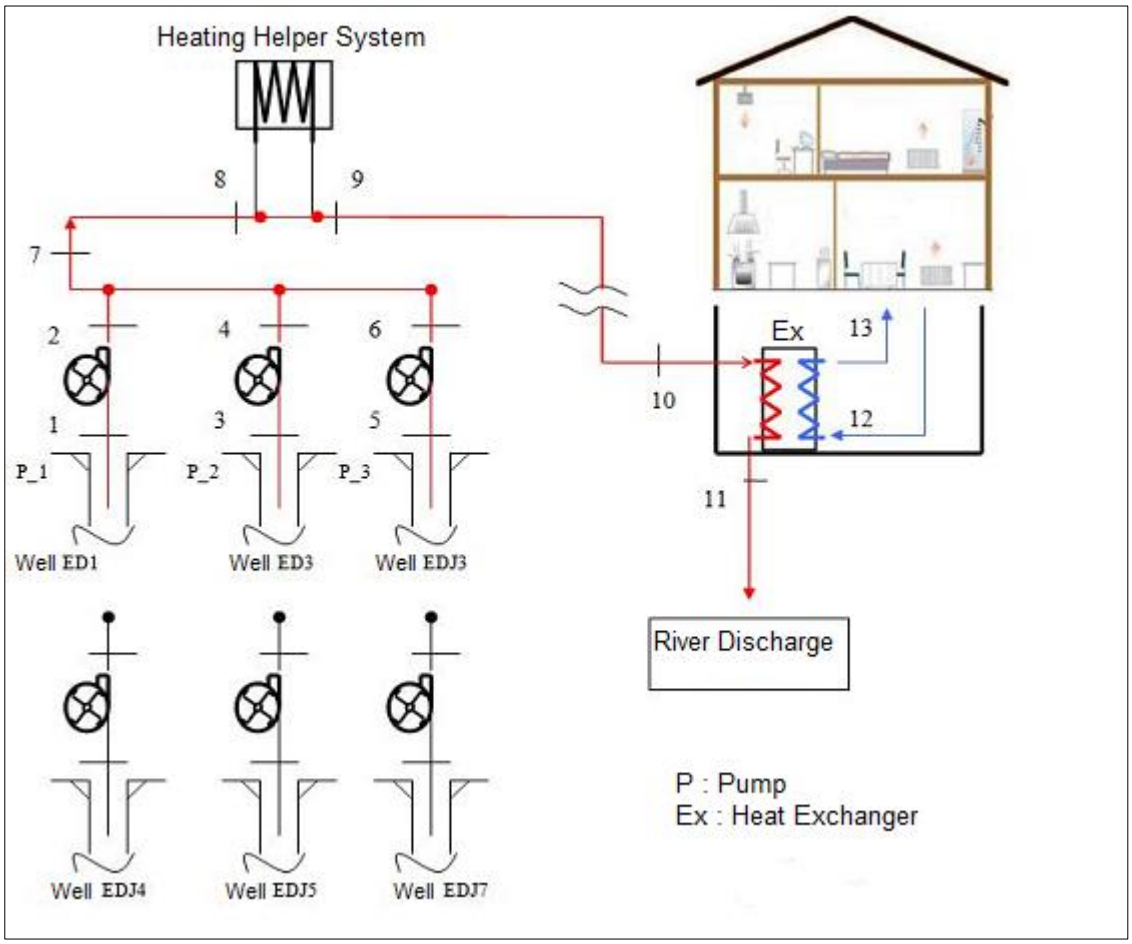

Figure 4.1: Generalized flow schematic of Edremit Geothermal Heating System. (Modified after Coşkun (2007))

The system works with 3 wells pumping hot water at 60º C to the exchangers installed at the bottom of the residences, which exchange heat with the closed circulation system. Then the water which leaves the exchangers at temperatures around 40º C is discharged to the Edremit Stream. The well pumps were reported to be operating with between 18 kg/s and 86 kg/s of pumping rates (Coşkun, 2007).

4.3 Production Modelling

In this study, the requirements for a geothermal heating system which were defined in 4.2 were modelled with 3 well systems and 6 well systems with various time frames, and the reservoir responses were calculated with the help of calibration studies performed in Chapter 3.

The production schedule for the system is 6 months of winter months pumping with 100 kg/s of hot water requirement for 1500 equivalent residences, and 10 kg/s of hot water for 6 months of summer. For the second production realization plan, the equivalent residence number is 5000, and the required hot water for winter months is taken as 360 kg/s and for summer months, 36 kg/s of pumping was required.

The current system is operating since 2006, equaling 10 years of production with different production wells, with different pumping rates. In this study however, hypothetical pumping scenarios are studied with 10 and 30 year time frames with various pumping rates based on documented pumping rate requirements. It is also assumed that all the wells can operate fully with equal production rates in the scenarios.

For the production scenarios, the best matching model of evolutionary scenario 1 of chapter 3 is used in numerical scenarios. The wells are observed at the well head which was taken as 0 meters, and at the well bottoms. Recovery response of the reservoir for different pumping rates are simulated by shutting down all the wells in the scenario after production schedules and are documented after the pumping scenario results in their relevant sub chapters. Recoveries for temperatures are studied for bottom of the wells only.

4.3.1 Three Well Pumping Scenarios

In three well pumping scenarios, wells ED-1, ED-3 and EDJ-3 were operated in the pumping schedule, which was planned for 1500 equivalent residence requirement. For summer months, the pumping rates are one-tenth of the rate of winter months.

4.3.1.1 100 kg/s Pumping for 10 Years

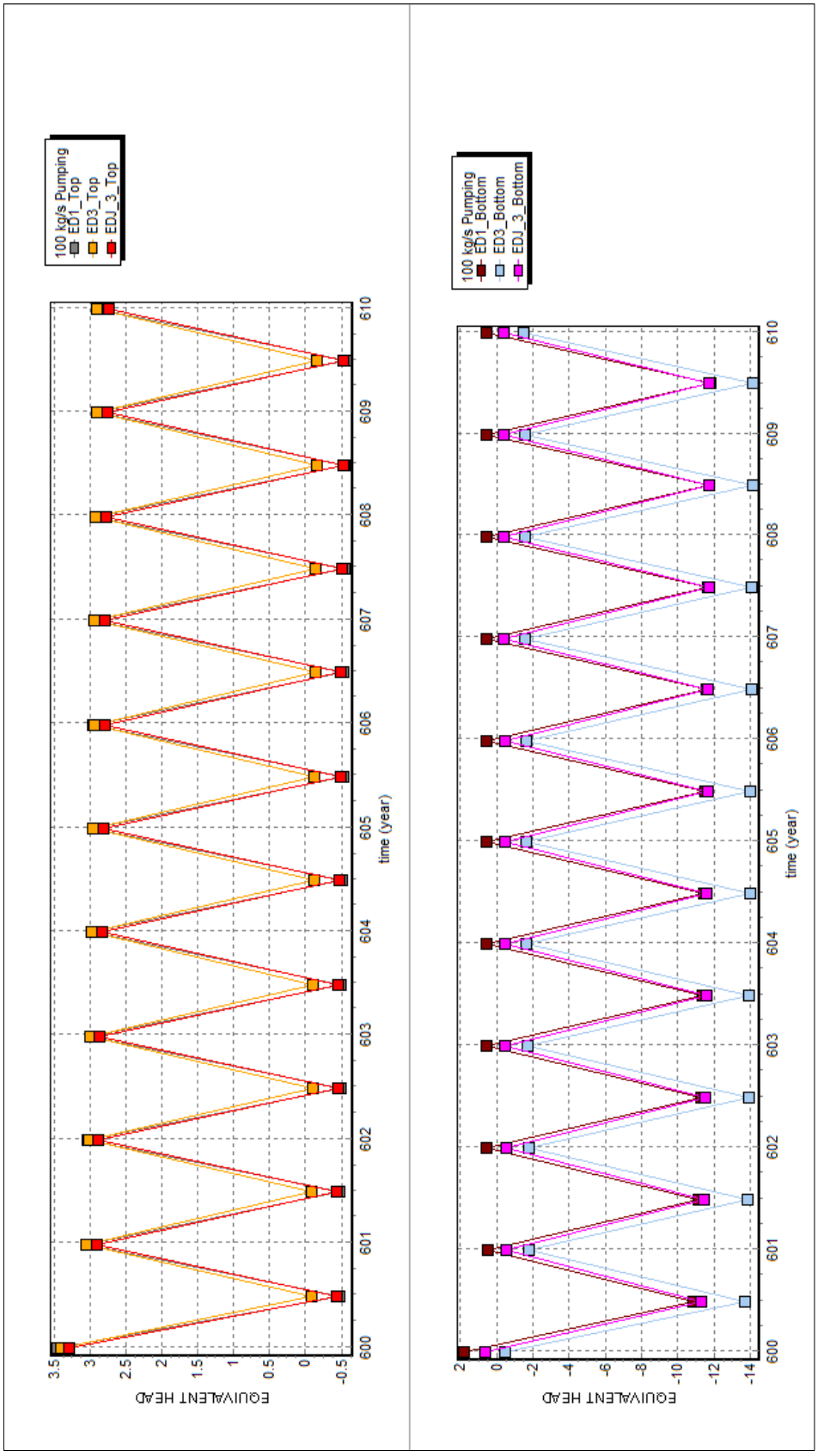

Figure 4.2: Pressure at well heads and bottoms for 100 kg/s 10 year pumping scenario.

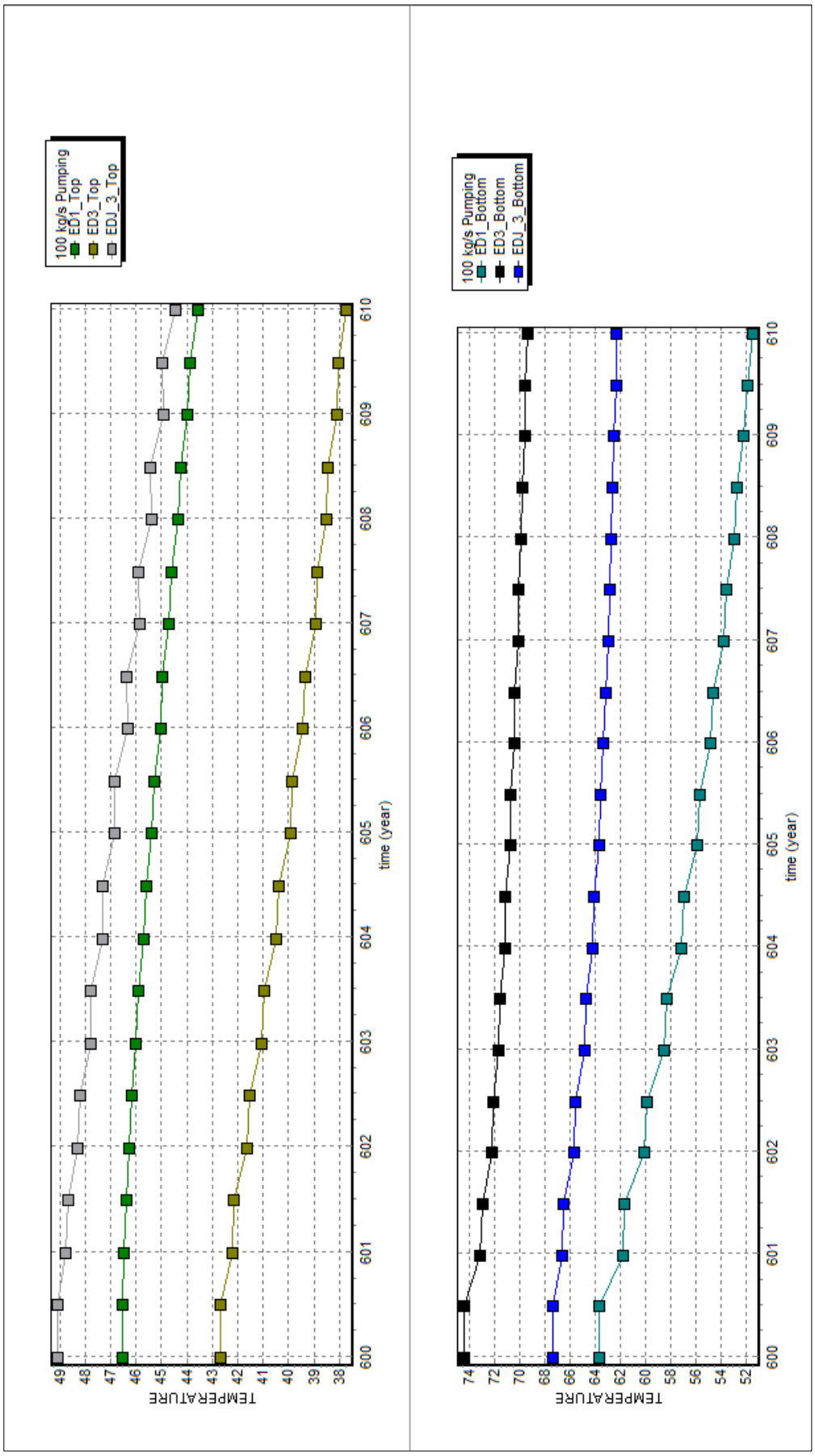

Figure 4.3: Temperatures at well head and bottom for 100 kg/s 10 year pumping scenario.

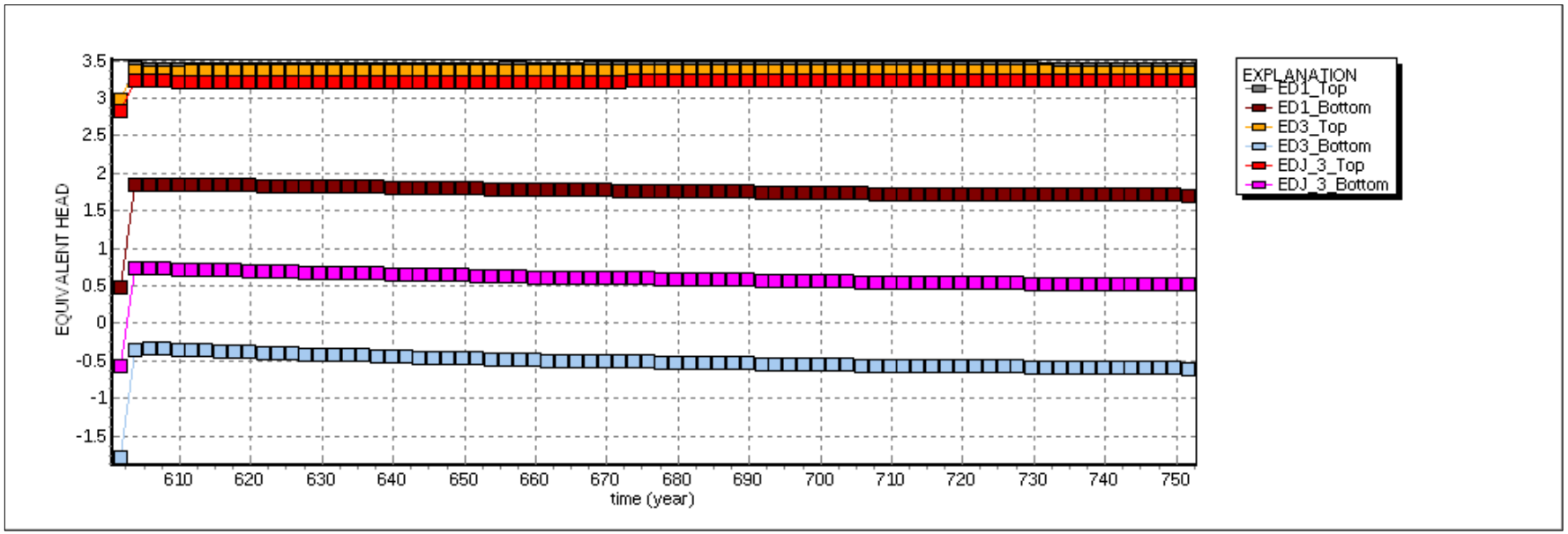

Figure 4.4: Pressure Recoveries at well head and bottom for 100 kg/s 10 year pumping scenario.

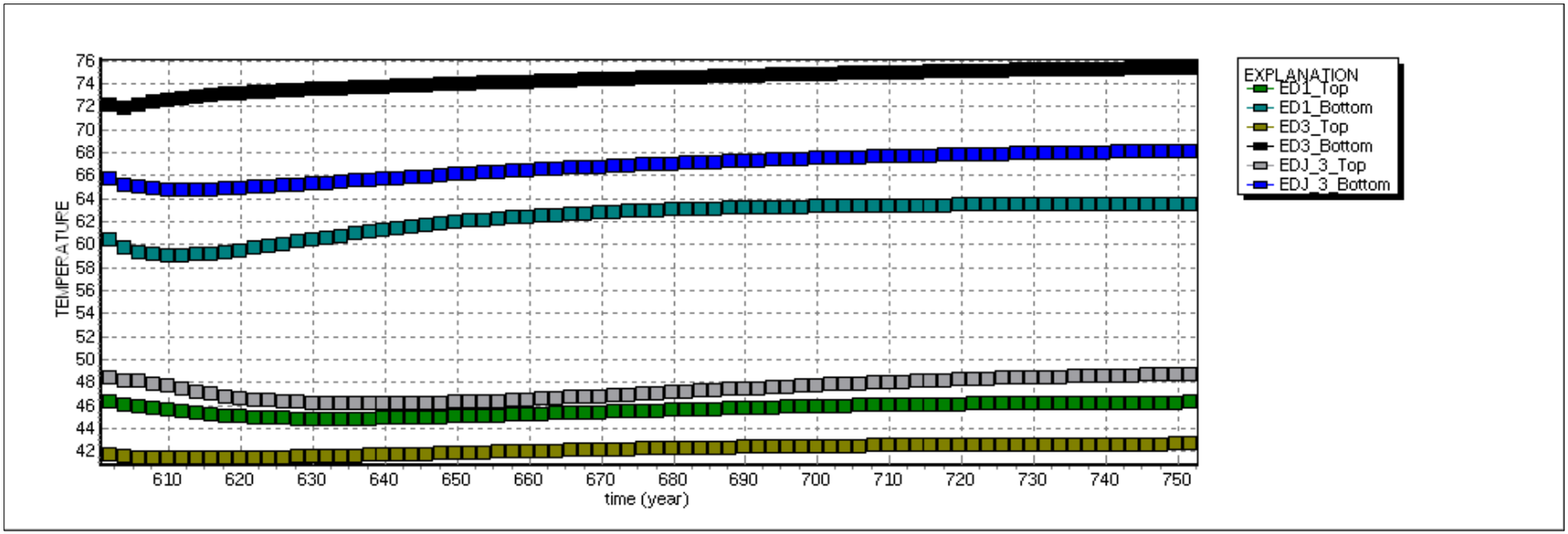

Figure 4.5: Temperature Recoveries at well bottom for 100 kg/s 10 year pumping scenario.

4.3.1.2 100 kg/s Pumping for 30 Years

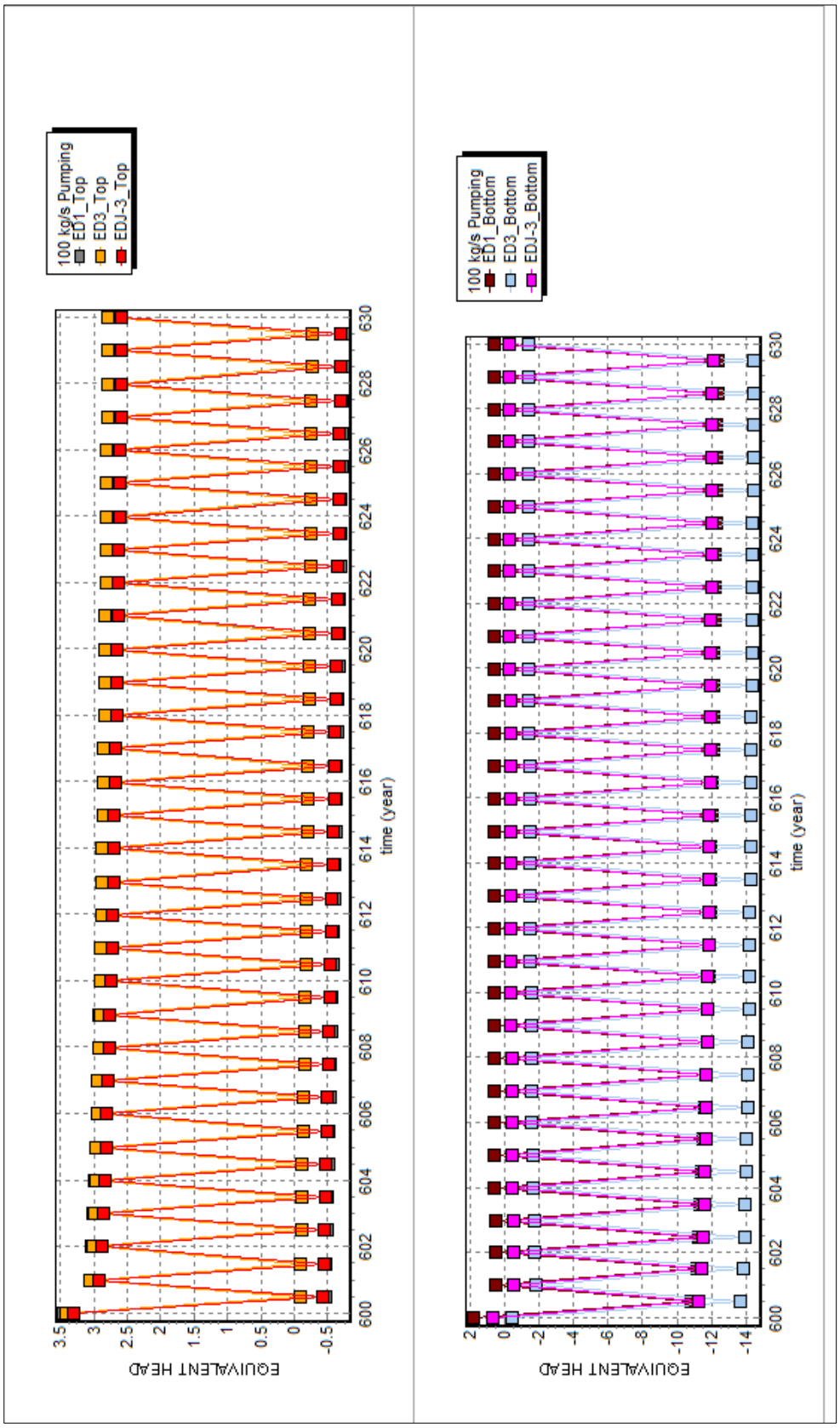

Figure 4.6: Pressures at well head and bottom for 100 kg/s 30 year pumping scenario.

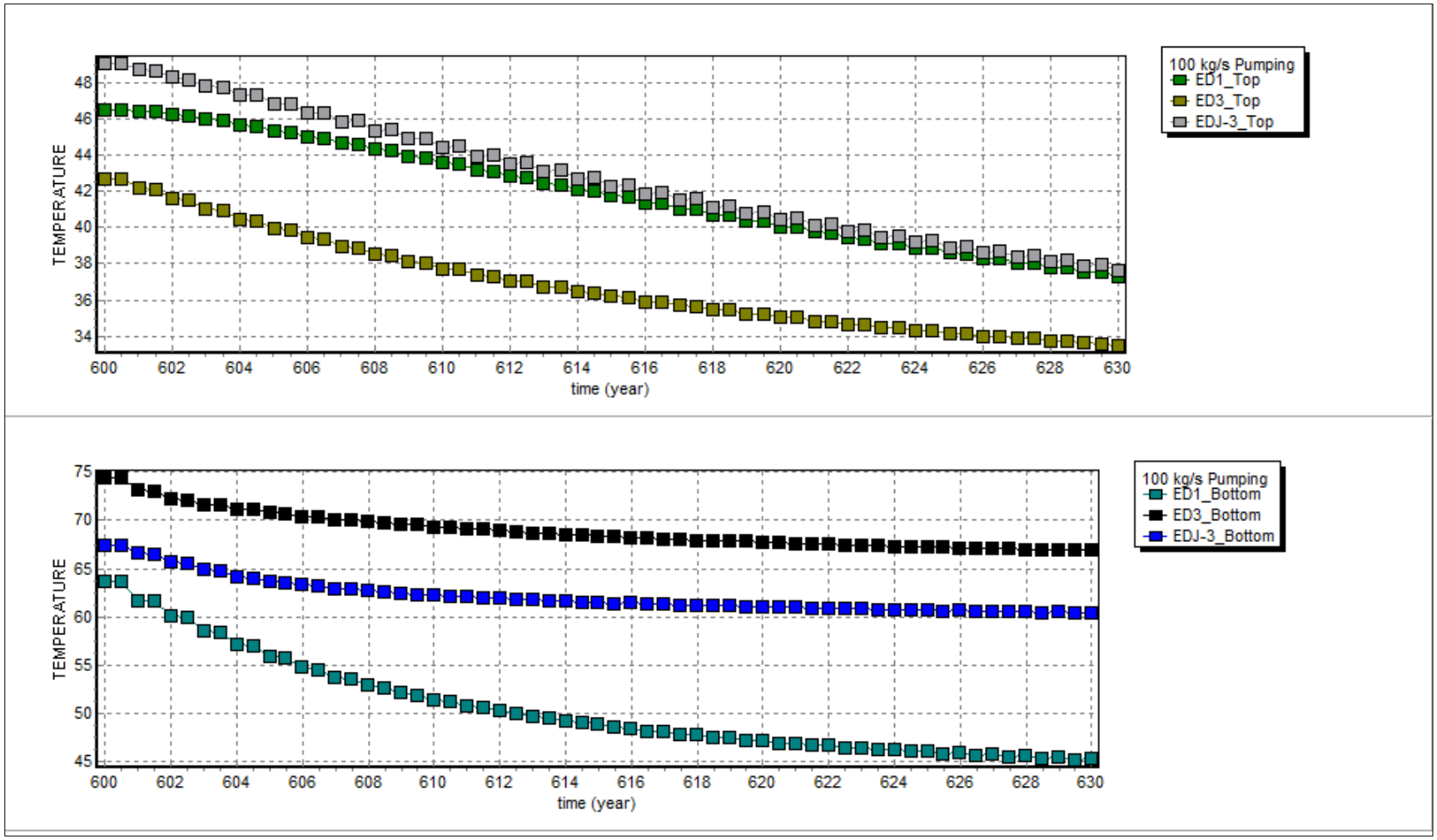

Figure 4.7: Temperatures at well head and bottom for 100 kg/s 30 year pumping scenario.

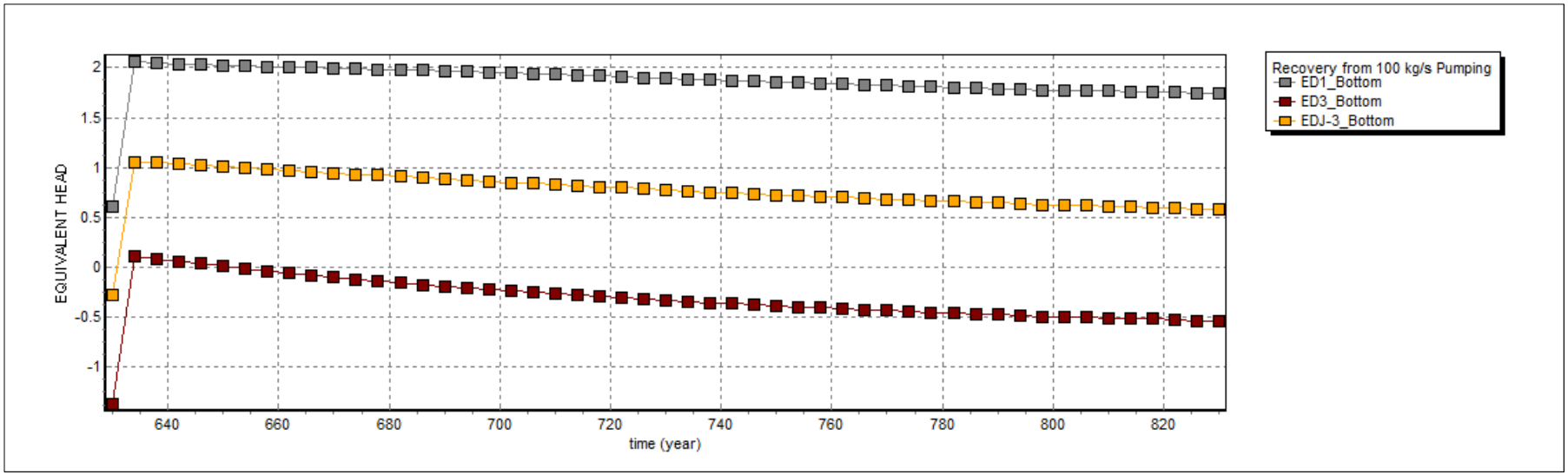

Figure 4.8: Pressure Recovery at well bottom for 100 kg/s 30 year pumping scenario.

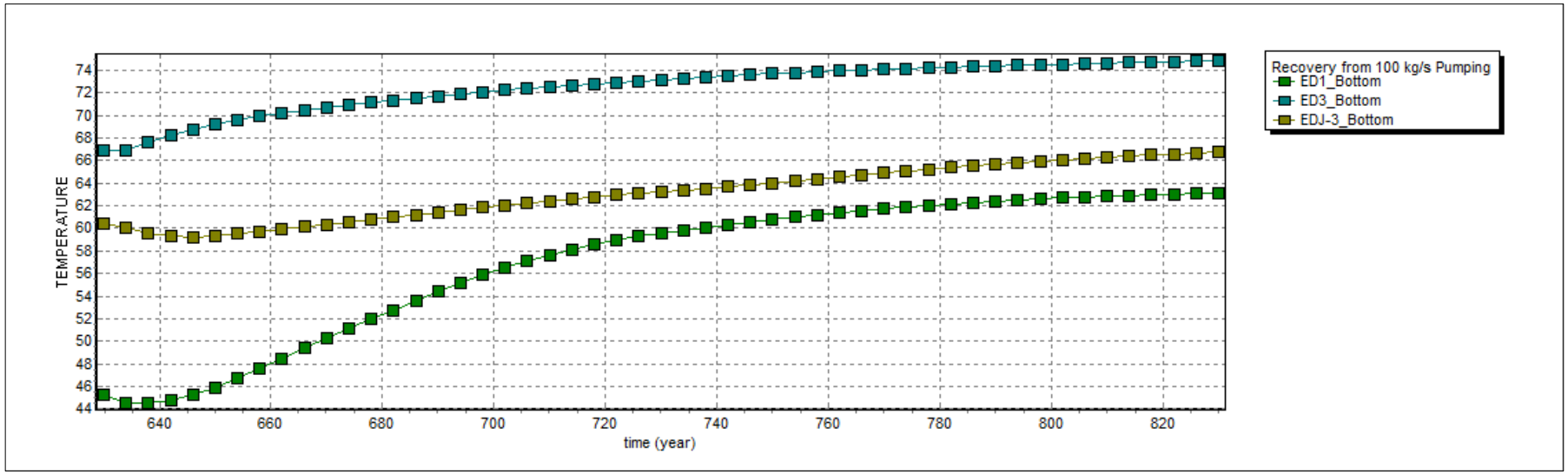

Figure 4.9: Temperature Recovery at well bottom for 100 kg/s 30 year pumping scenario.

4.3.1.3 200 kg/s Pumping for 10 Years

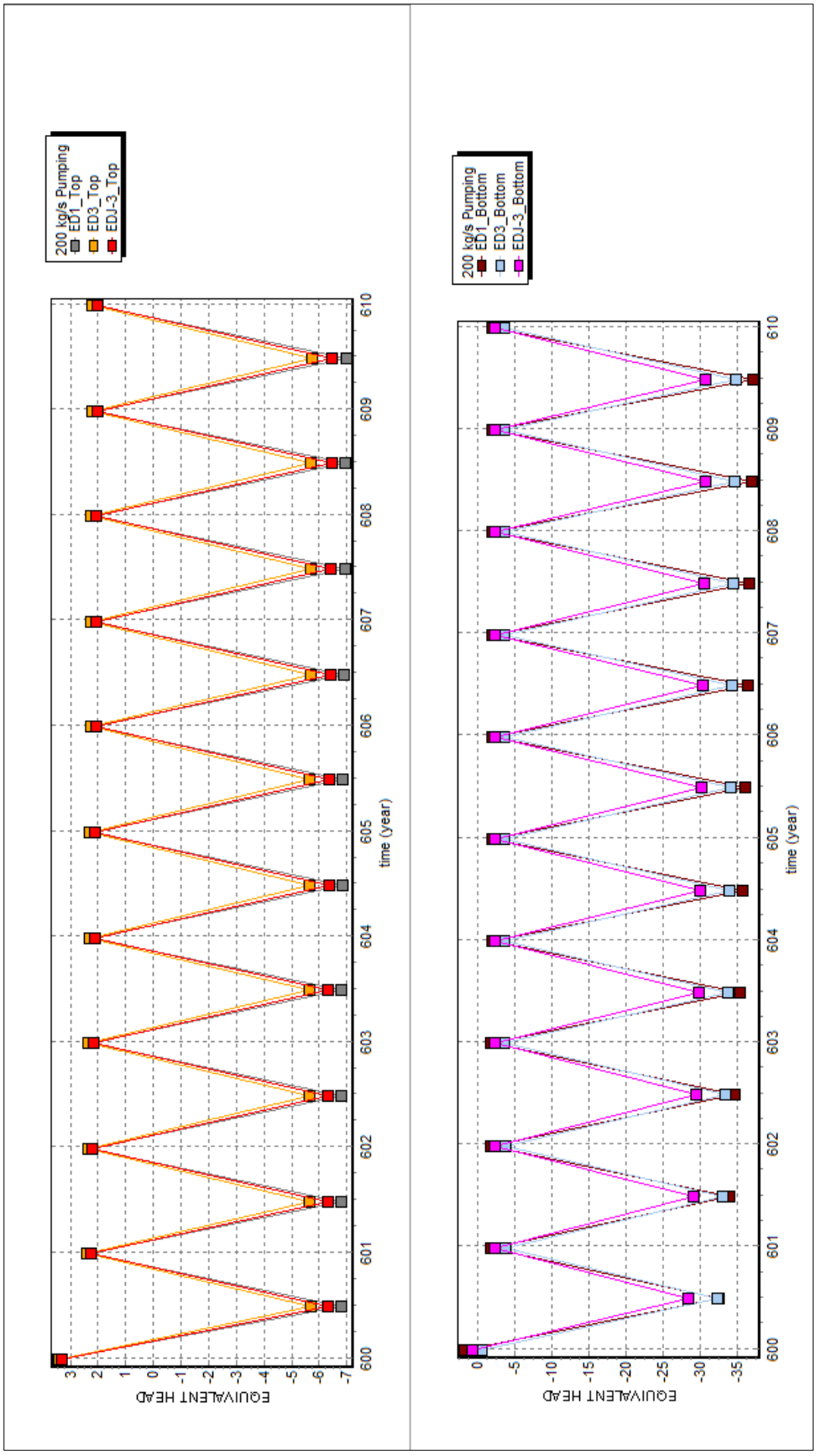

Figure 4.10: Pressures at well head and bottom for 200 kg/s 10 year pumping scenario.

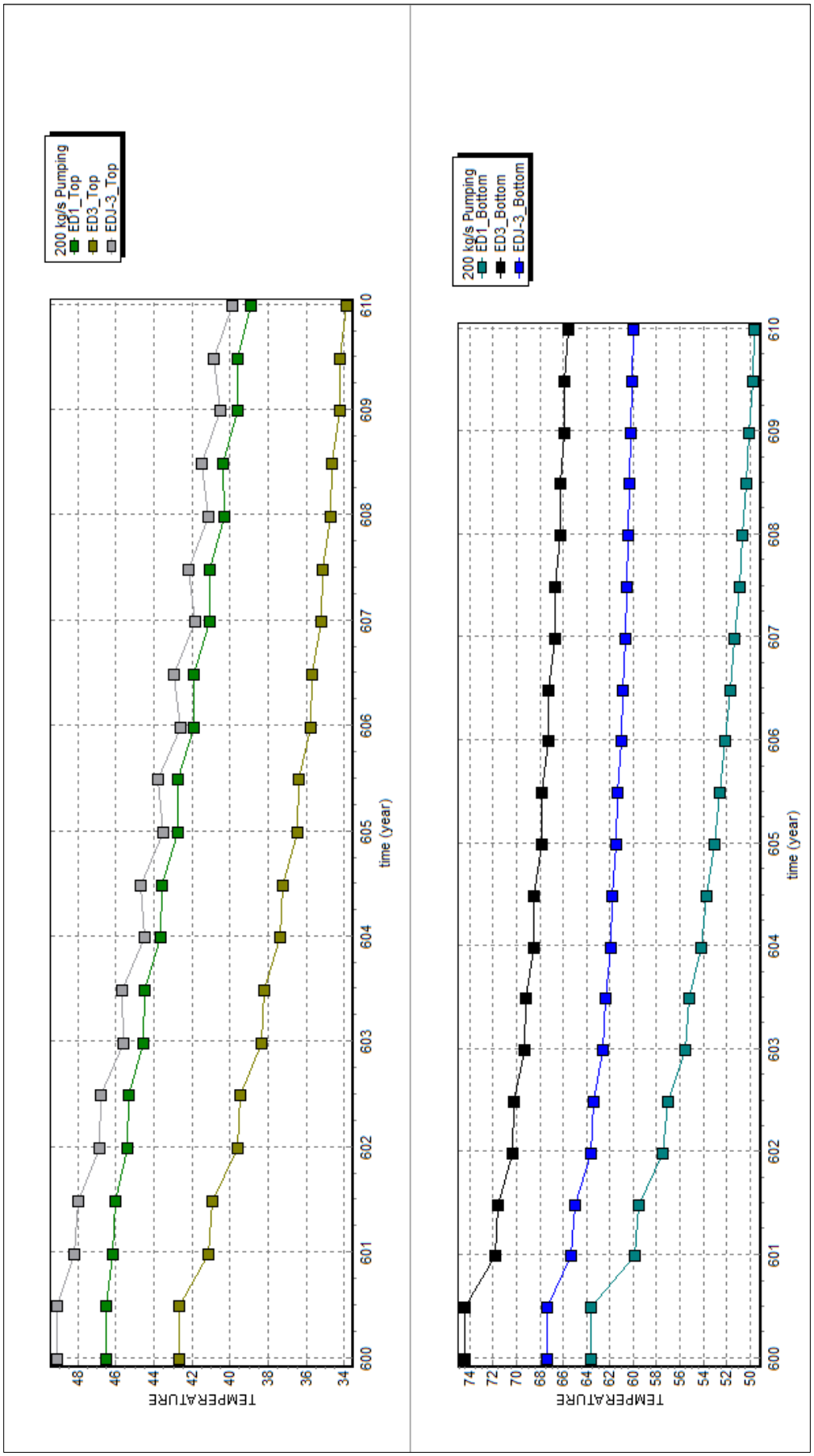

Figure 4.11: Temperatures at well head and bottom for 200 kg/s 10 year pumping scenario.

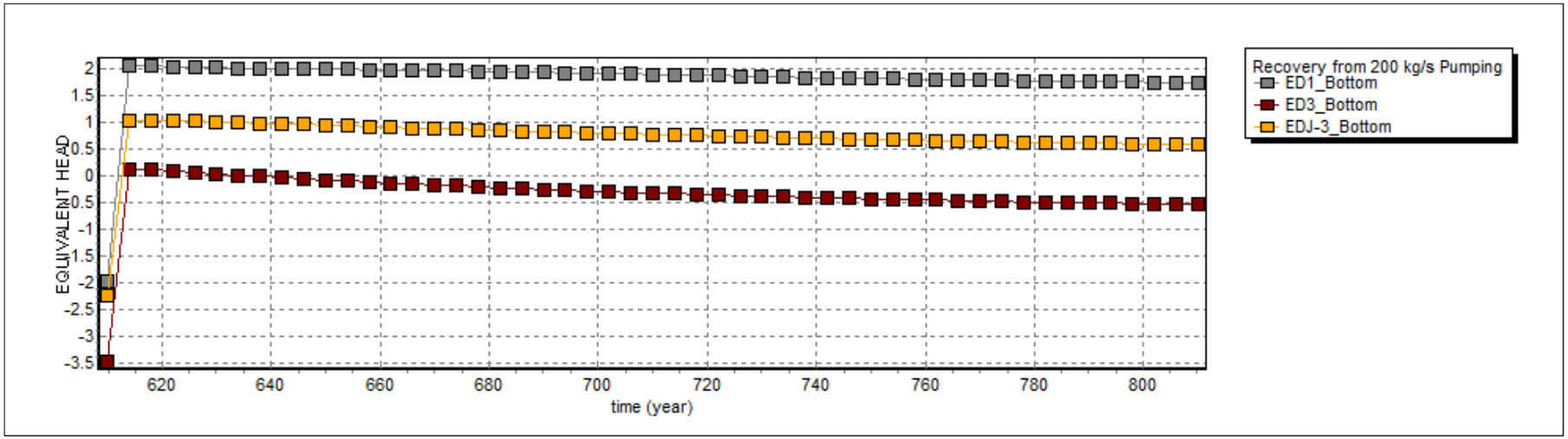

Figure 4.12: Pressure Recovery at well bottom for 200 kg/s 10 year pumping scenario.

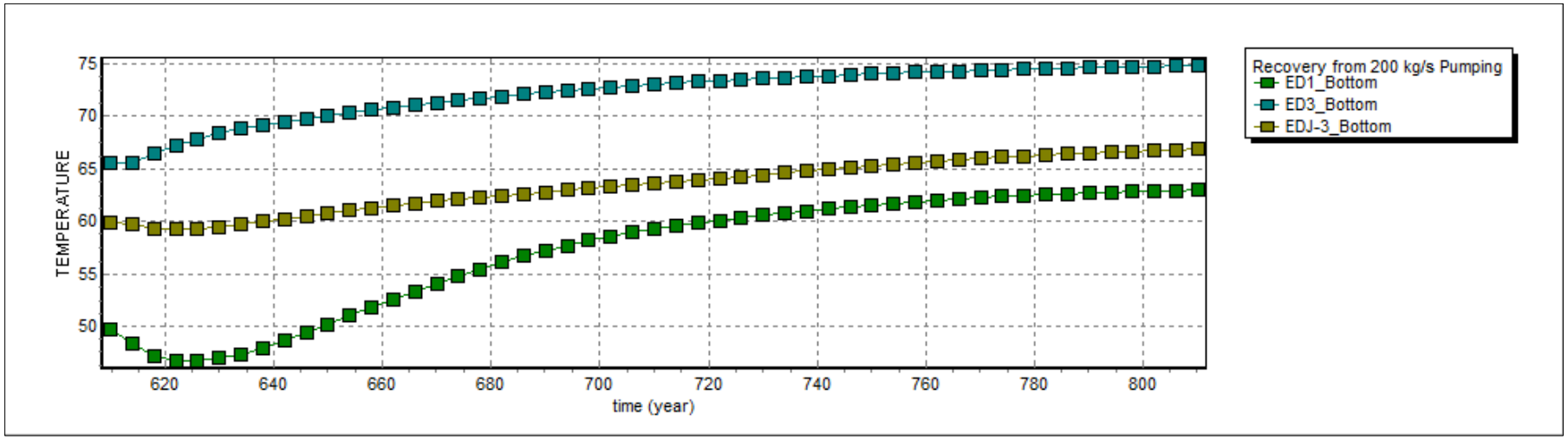

Figure 4.13: Temperature Recovery at well bottom for 200 kg/s 10 year pumping scenario.

4.3.1.4 200 kg/s Pumping for 30 Years

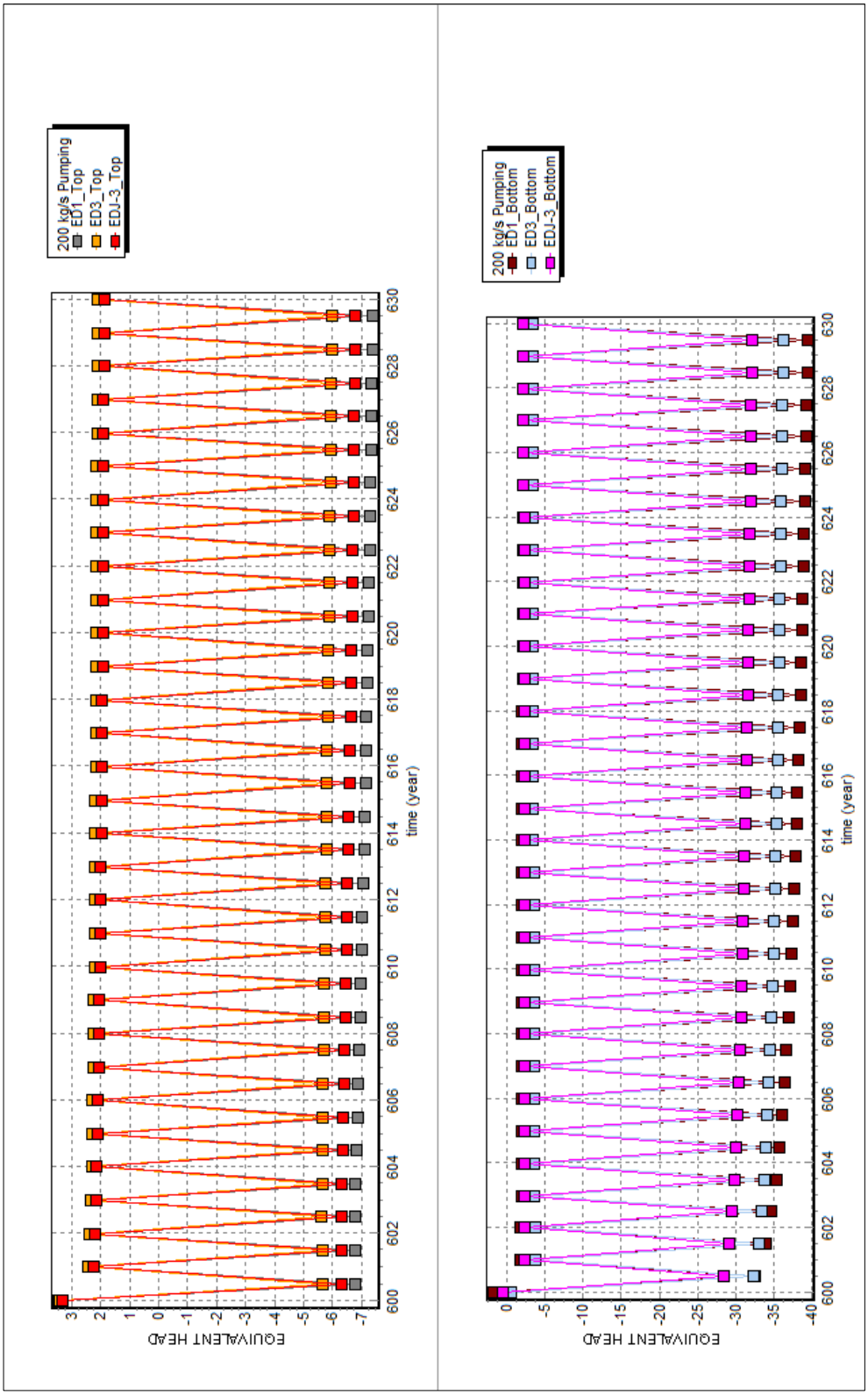

Figure 4.14: Pressures at well head and bottom for 200 kg/s 30 year pumping scenario.

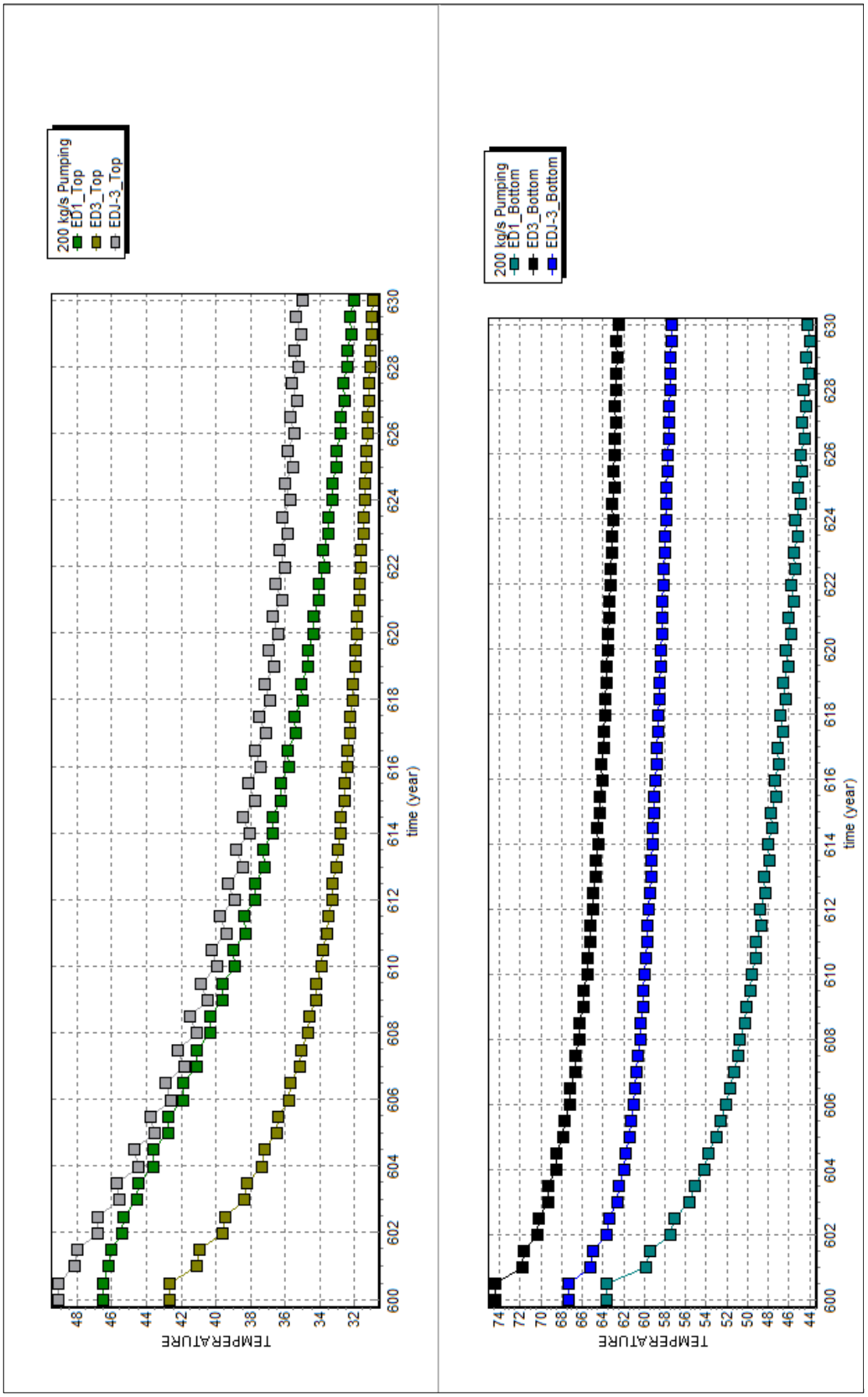

Figure 4.15: Temperatures at well head and bottom for 200 kg/s 30 year pumping scenario.

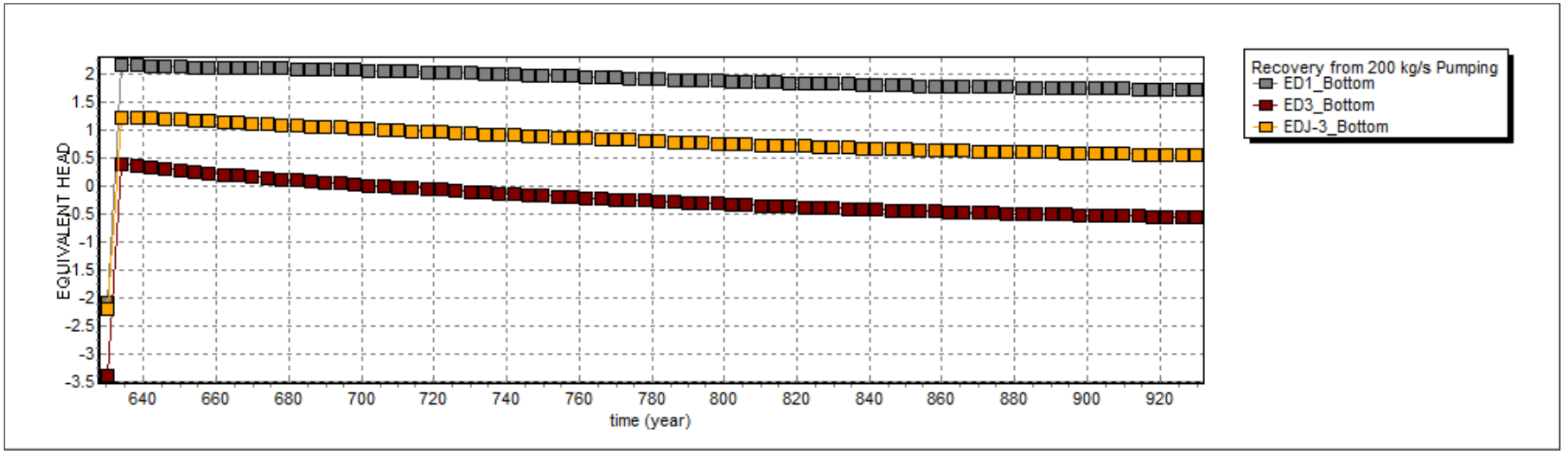

Figure 4.16: Pressure Recovery at well bottom for 200 kg/s 30 year pumping scenario.

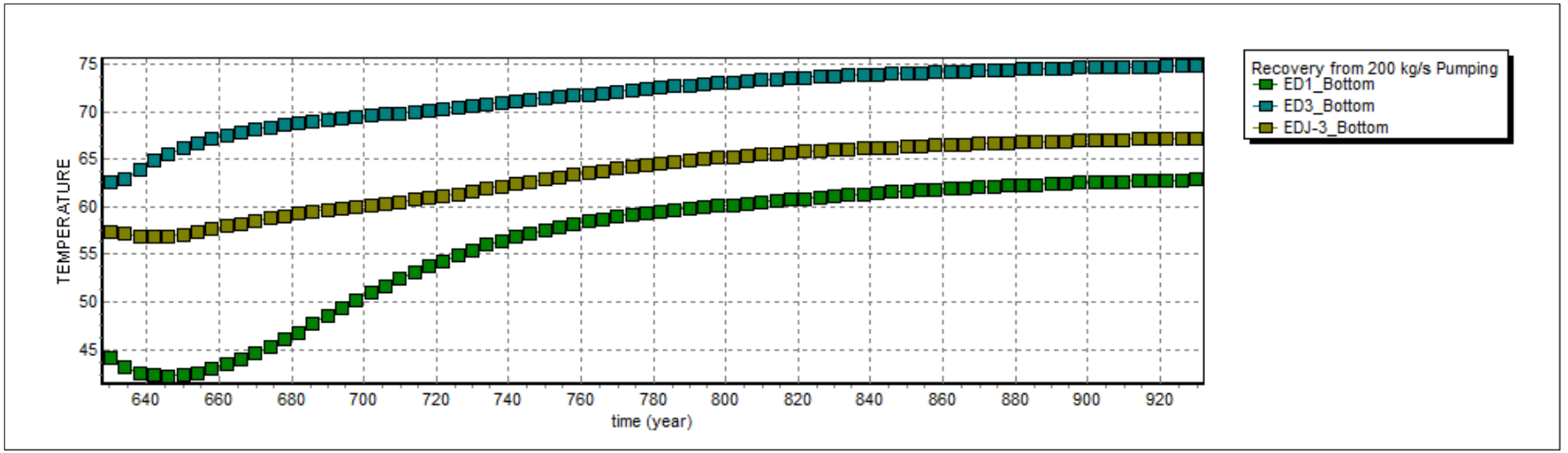

Figure 4.17: Temperature Recovery at well bottom for 200 kg/s 30 year pumping scenario.

Table 4.1: Results after 100kg/s Pumping Scenario for 10 Years

Observation Location	Original T (ºC)	After T (ºC)	Difference (ºC)	Before P (Pa)	After P (Pa)	Difference (m)
ED1_Top	46.52	43.58	-2.94	33894.75	28443.21	-0.56
ED1_Bottom	63.66	51.43	-12.24	1782309.20	1770363.70	-1.22
ED3_Top	42.66	37.73	-4.93	33420.67	28437.07	-0.51
ED3_Bottom	74.42	69.35	-5.07	3034631.40	3024244.70	-1.06
EDJ_3_Top	49.08	44.43	-4.65	32315.08	26906.88	-0.55
EDJ_3_Bottom	67.38	62.26	-5.13	2417991.50	2408006.20	-1.02

Table 4.2: Results after 100 kg/s Pumping Scenario for 30 Years

Observation Location	Original T (ºC)	After T (ºC)	Difference (ºC)	Before P (Pa)	After P (Pa)	Difference (m)
ED1_Top	46.52	37.31	-9.21	33894.75	26887.78	-0.71
ED1_Bottom	63.66	45.27	-18.39	1782309.20	1770659.80	-1.19
ED3_Top	42.66	33.47	-9.19	33420.67	27293.67	-0.62
ED3_Bottom	74.42	66.90	-7.52	3034631.40	3025787.70	-0.90
EDJ_3_Top	49.08	37.64	-11.44	32315.08	25303.06	-0.71
EDJ_3_Bottom	67.38	60.45	-6.93	2417991.50	2409065.60	-0.91

Table 4.3: Results after 200 kg/s Pumping Scenario for 10 Years

Observation Location	Original T (ºC)	After T (ºC)	Difference (ºC)	Before P (Pa)	After P (Pa)	Difference (m)
ED1_Top	46.52	38.92	-7.59	33894.75	20713.81	-1.34
ED1_Bottom	63.66	49.64	-14.02	1782309.20	1745501.50	-3.75
ED3_Top	42.66	33.88	-8.77	33420.67	21742.12	-1.19
ED3_Bottom	74.42	65.54	-8.88	3034631.40	3005139.80	-3.01
EDJ_3_Top	49.08	39.89	-9.19	32315.08	19820.63	-1.27
EDJ_3_Bottom	67.38	59.95	-7.44	2417991.50	2389822.60	-2.87

Table 4.4: Results after 200 kg/s Pumping Scenario for 30 Years

Observation Location	Original T (ºC)	After T (ºC)	Difference (ºC)	Before P (Pa)	After P (Pa)	Difference (m)
ED1_Top	46.52	32.03	-14.49	33894.75	18977.75	-1.52
ED1_Bottom	63.66	44.18	-19.48	1782309.20	1744282.30	-3.88
ED3_Top	42.66	30.93	-11.72	33420.67	20673.87	-1.30
ED3_Bottom	74.42	62.53	-11.90	3034631.40	3006043.10	-2.91
EDJ_3_Top	49.08	35.00	-14.08	32315.08	18425.30	-1.42
EDJ_3_Bottom	67.38	57.32	-10.06	2417991.50	2390220.00	-2.83

4.3.2 Six Well Pumping Scenarios

In six well pumping scenarios, wells ED-1, ED-3, EDJ-3, EDJ-4, EDJ-5 and EDJ-7 were operated in the pumping schedule, which was planned for 5000 equivalent residence requirement. For summer months, the pumping rates are one-tenth of the rate of winter months.

4.3.2.1 360 kg/s Pumping For 10 Years

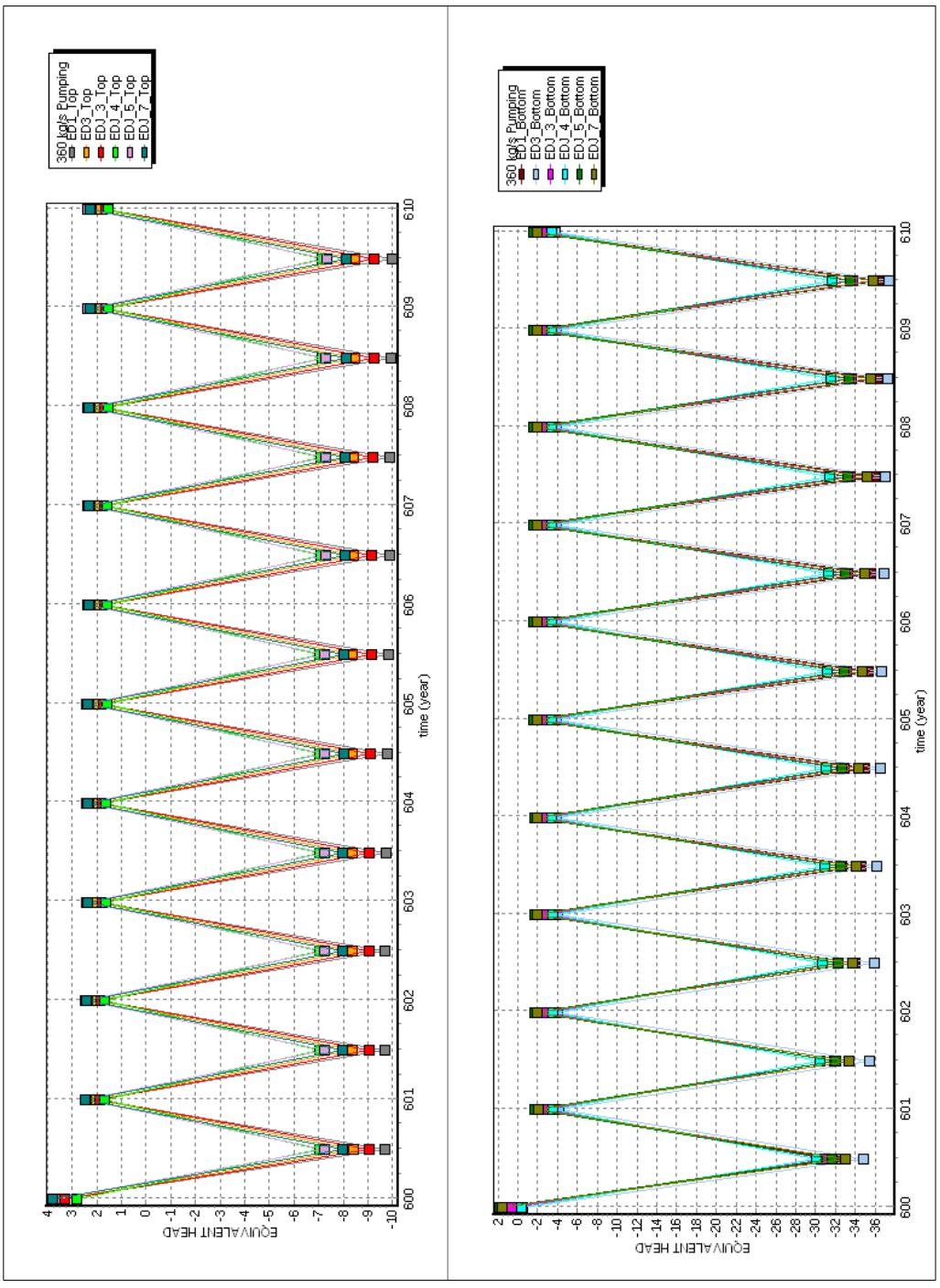

Figure 4.18: Pressures at well head and bottom for 360 kg/s 10 year pumping scenario.

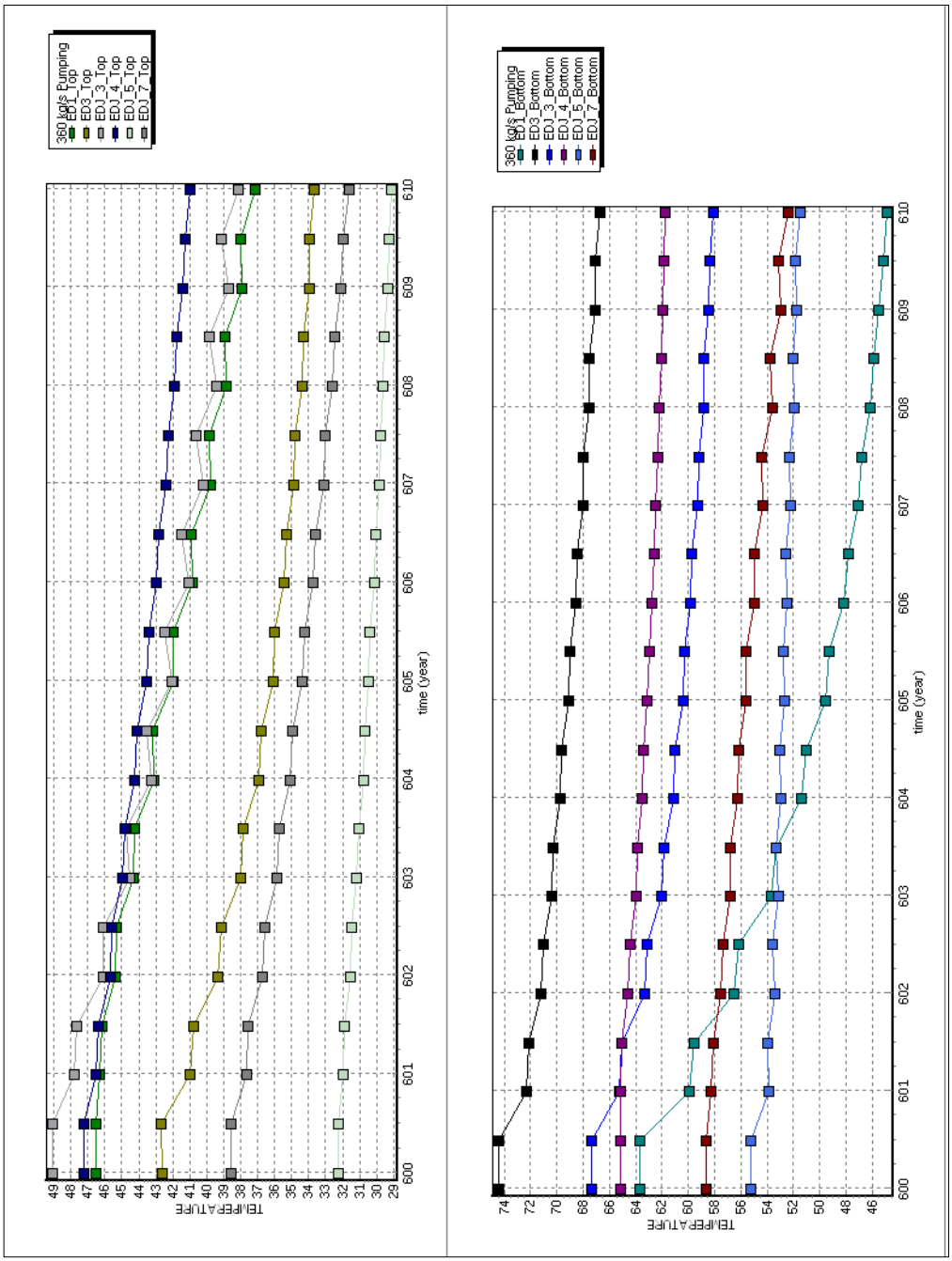

Figure 4.19: Temperatures at well head and bottom for 360 kg/s 10 year pumping scenario.

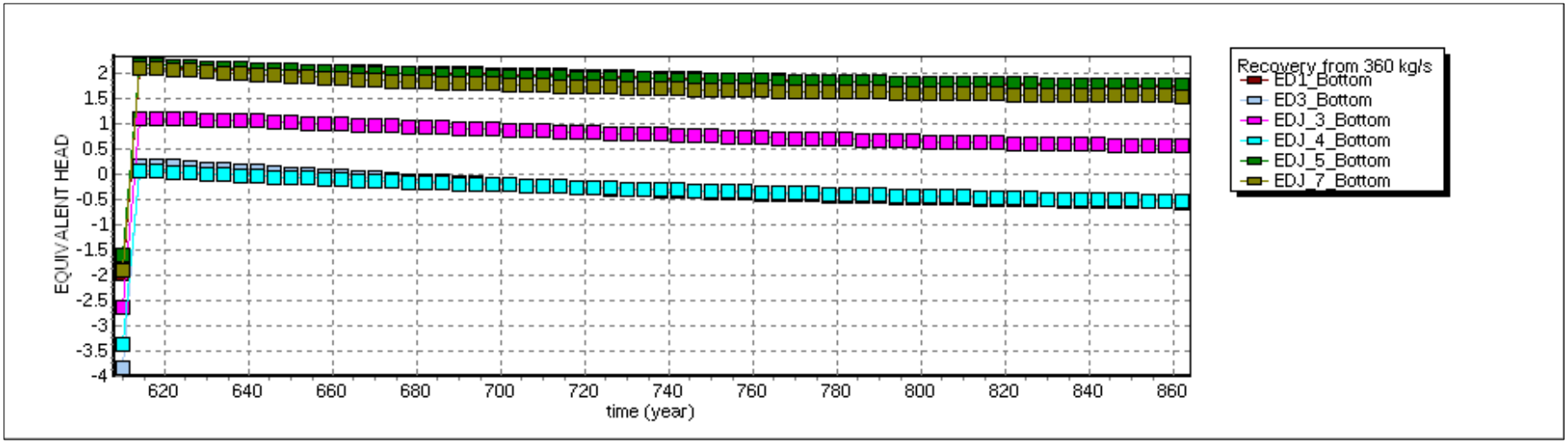

Figure 4.20: Pressure recovery at well bottom for 360 kg/s 10 year pumping scenario.

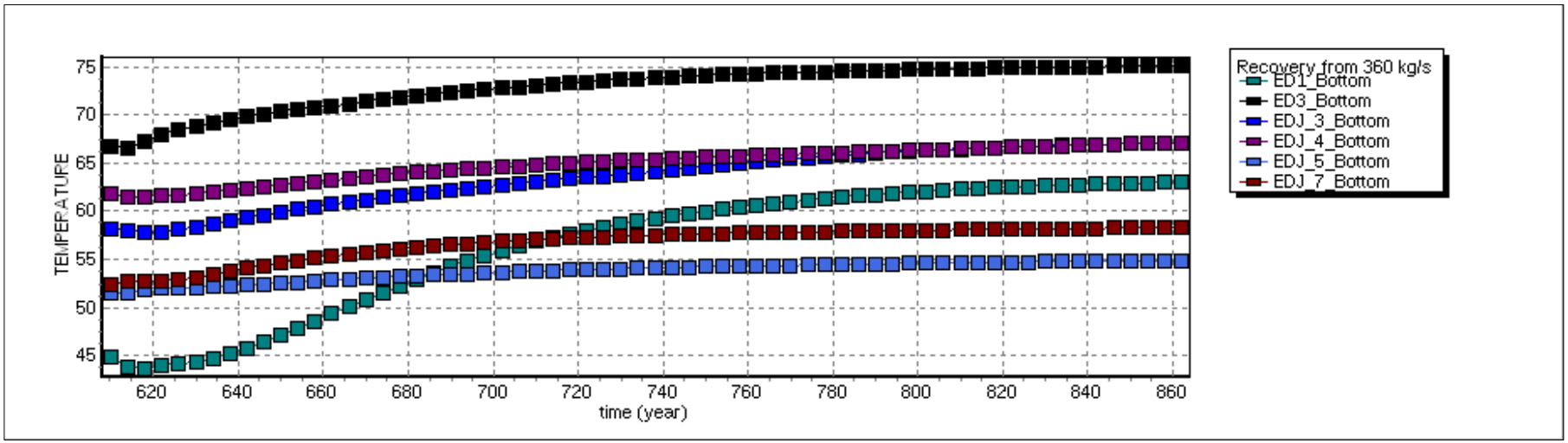

Figure 4.21: Temperature recovery at well bottom for 360 kg/s 10 year pumping scenario.

4.3.2.2 360 kg/s Pumping For 30 Years

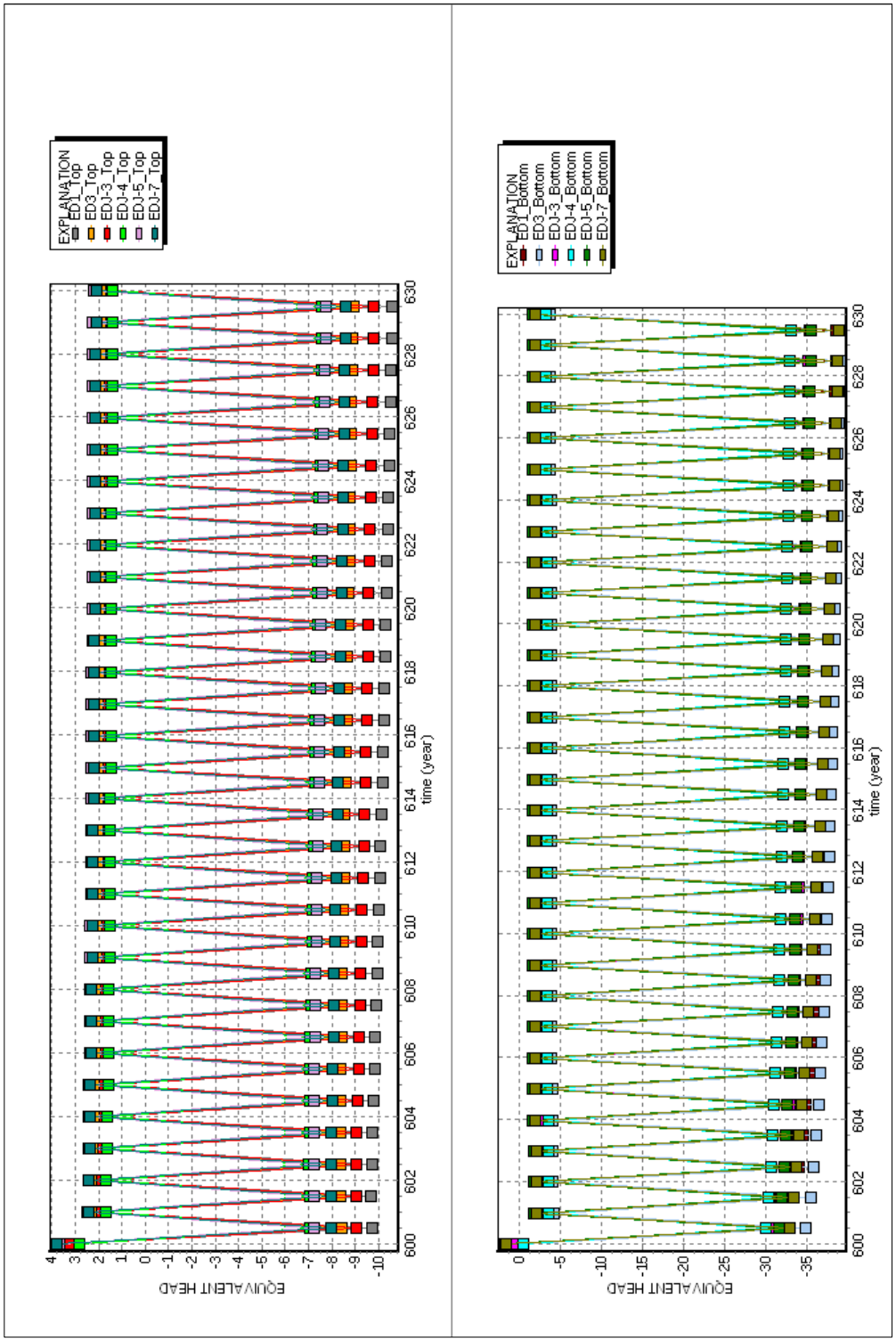

Figure 4.22: Pressures at well head and bottom for 360 kg/s 30 year pumping scenario.

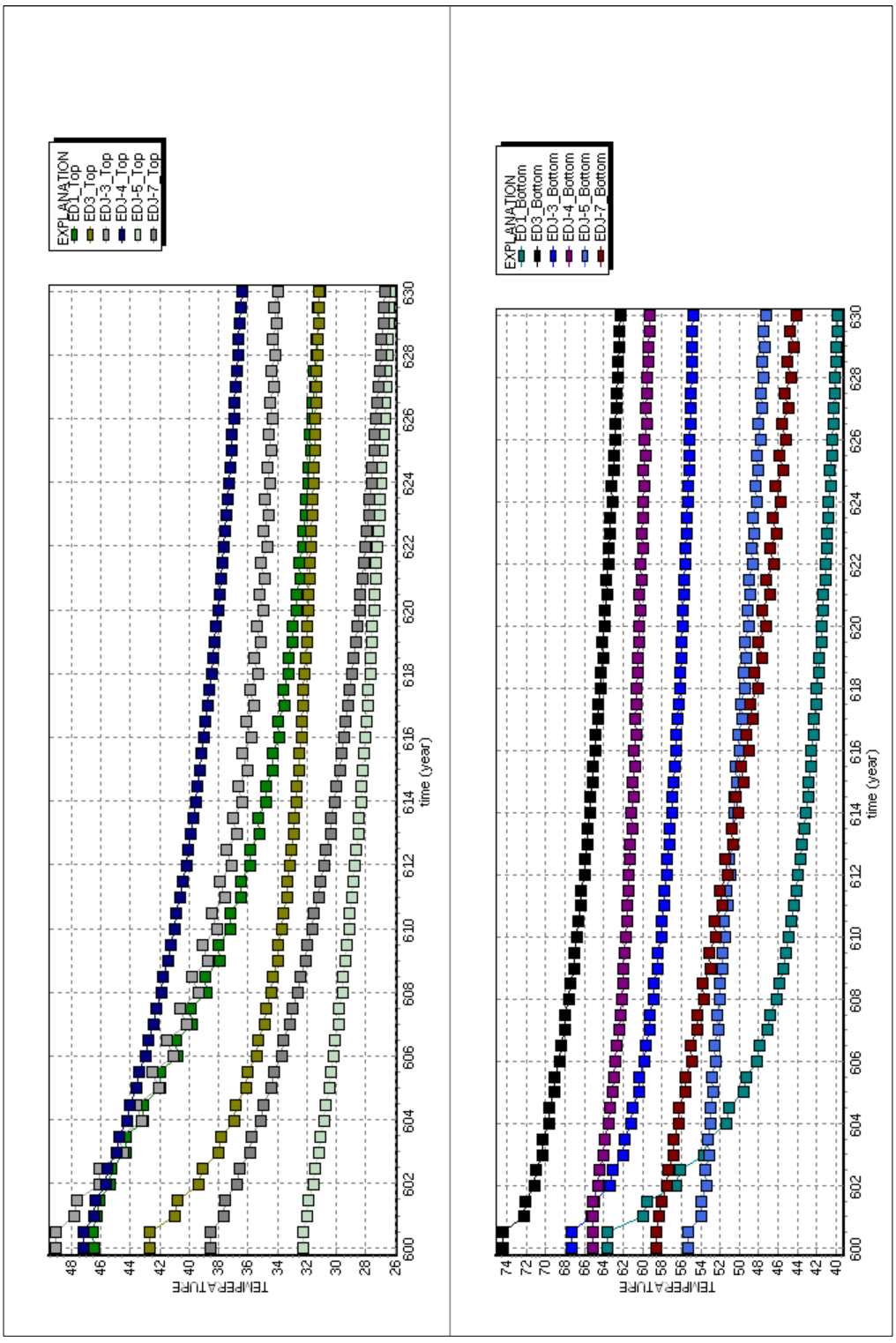

Figure 4.23: Temperatures at well head and bottom for 360 kg/s 30 year pumping scenario.

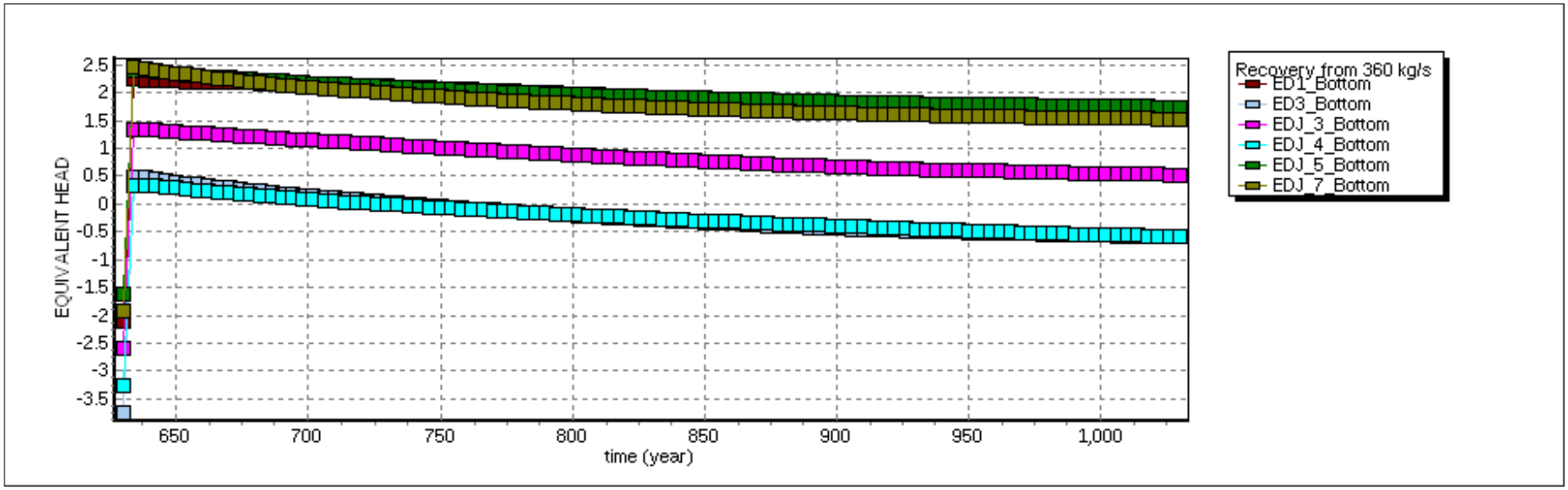

Figure 4.24: Pressure recovery at well bottom for 360 kg/s 30 year pumping scenario.

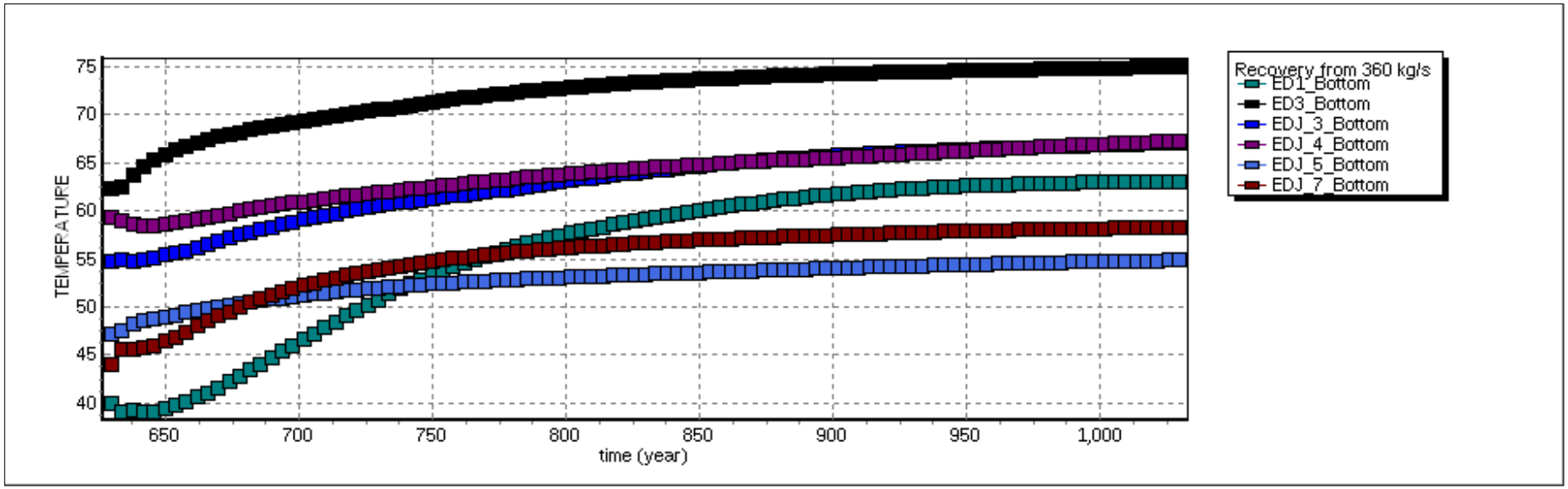

Figure 4.25: Temperature recovery at well bottom for 360 kg/s 30 year pumping scenario.

4.3.2.3 720 kg/s Pumping For 10 Years

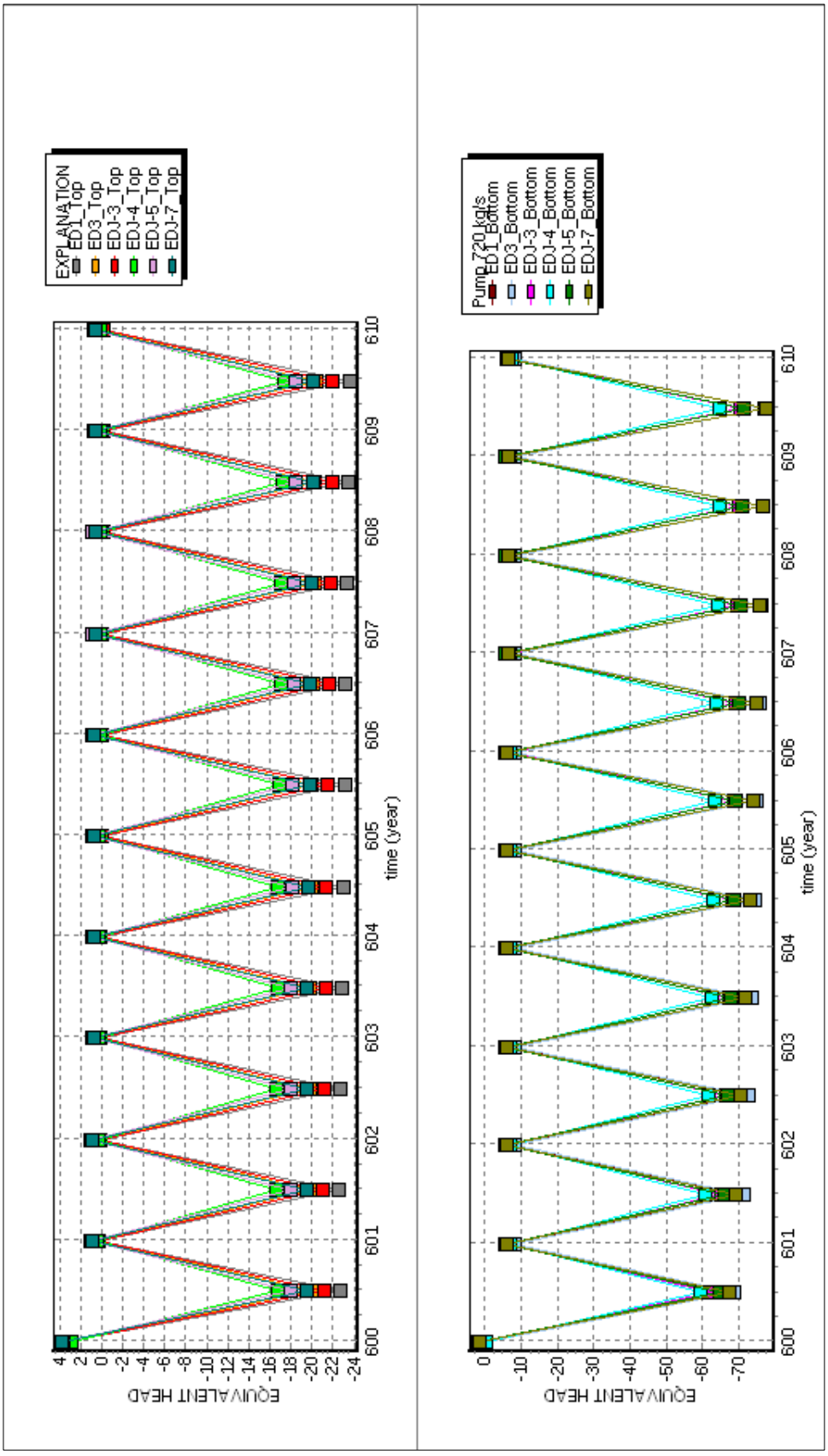

Figure 4.26: Pressures at well head and bottom for 720 kg/s 10 year pumping scenario.

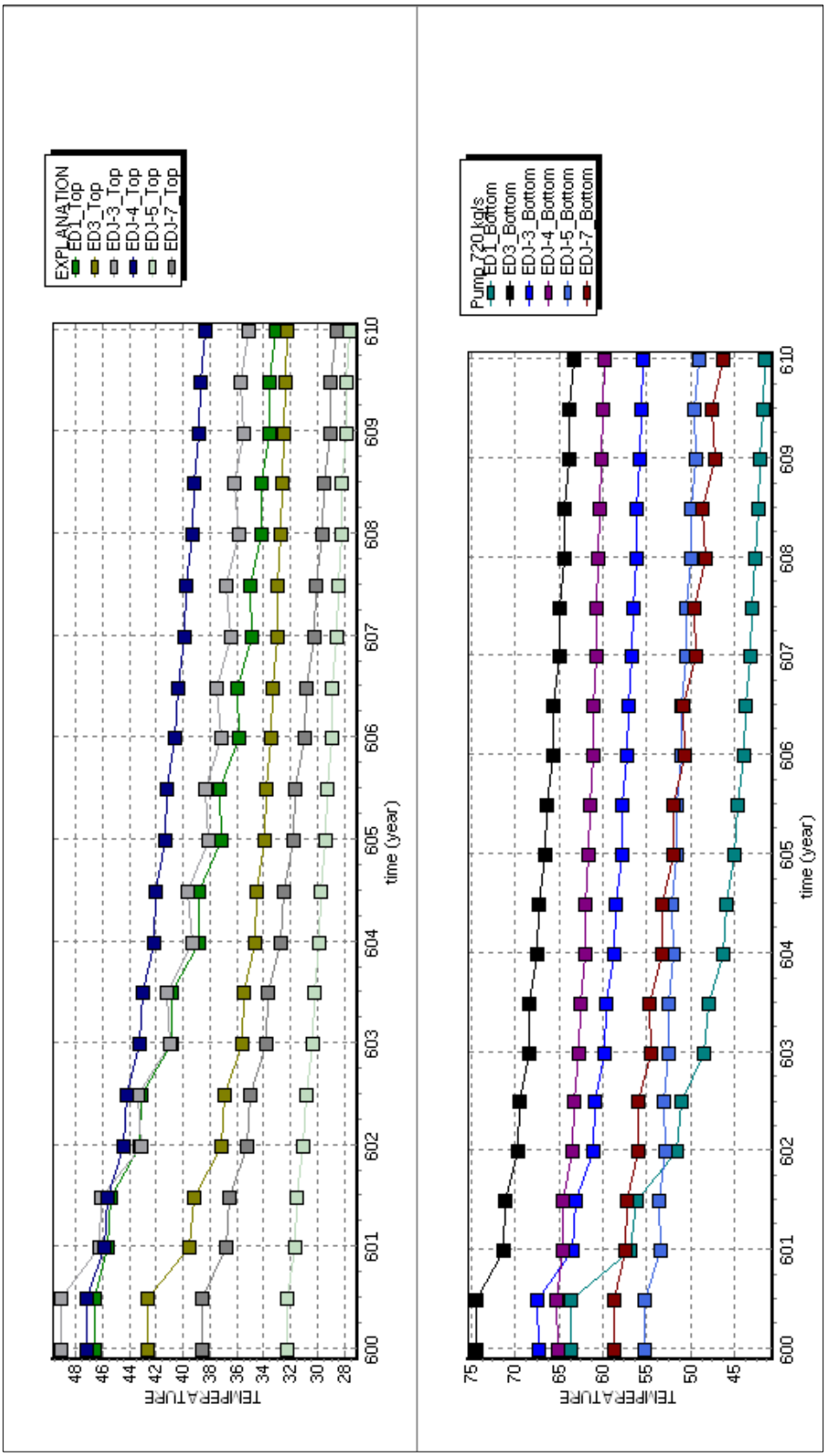

Figure 4.27: Temperatures at well head and bottom for 720 kg/s 10 year pumping scenario.

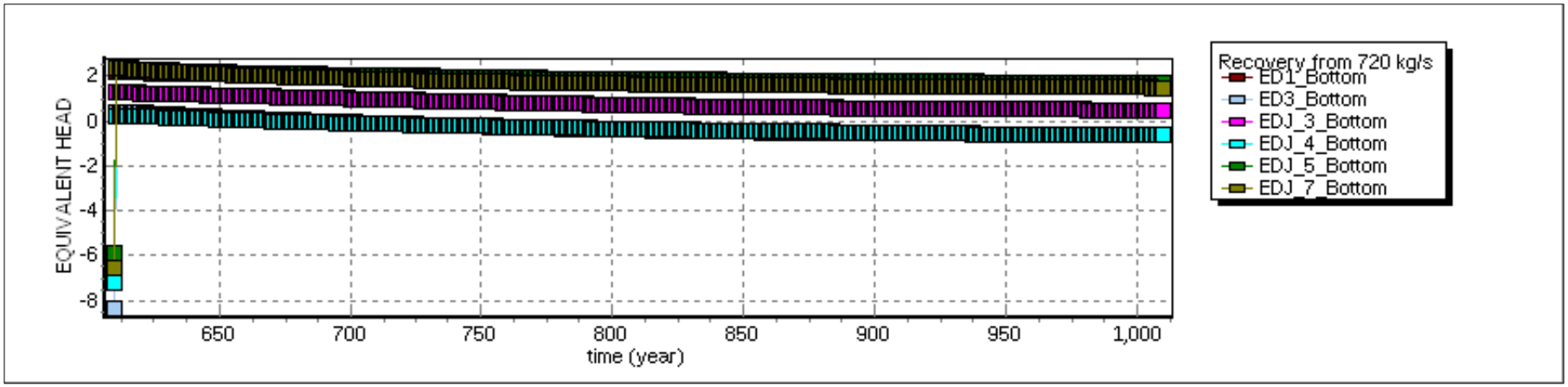

Figure 4.28: Pressure recovery at well bottom for 720 kg/s 10 year pumping scenario.

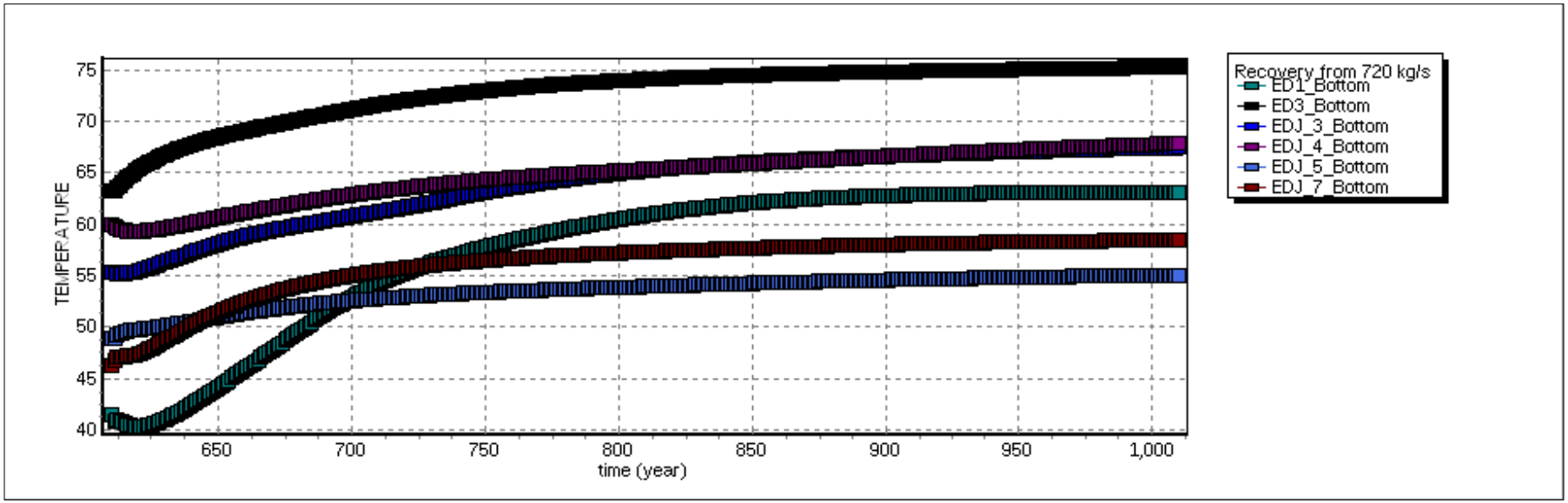

Figure 4.29: Temperature recovery at well bottom for 720 kg/s 10 year pumping scenario.

4.3.2.4 720 kg/s Pumping For 30 Years

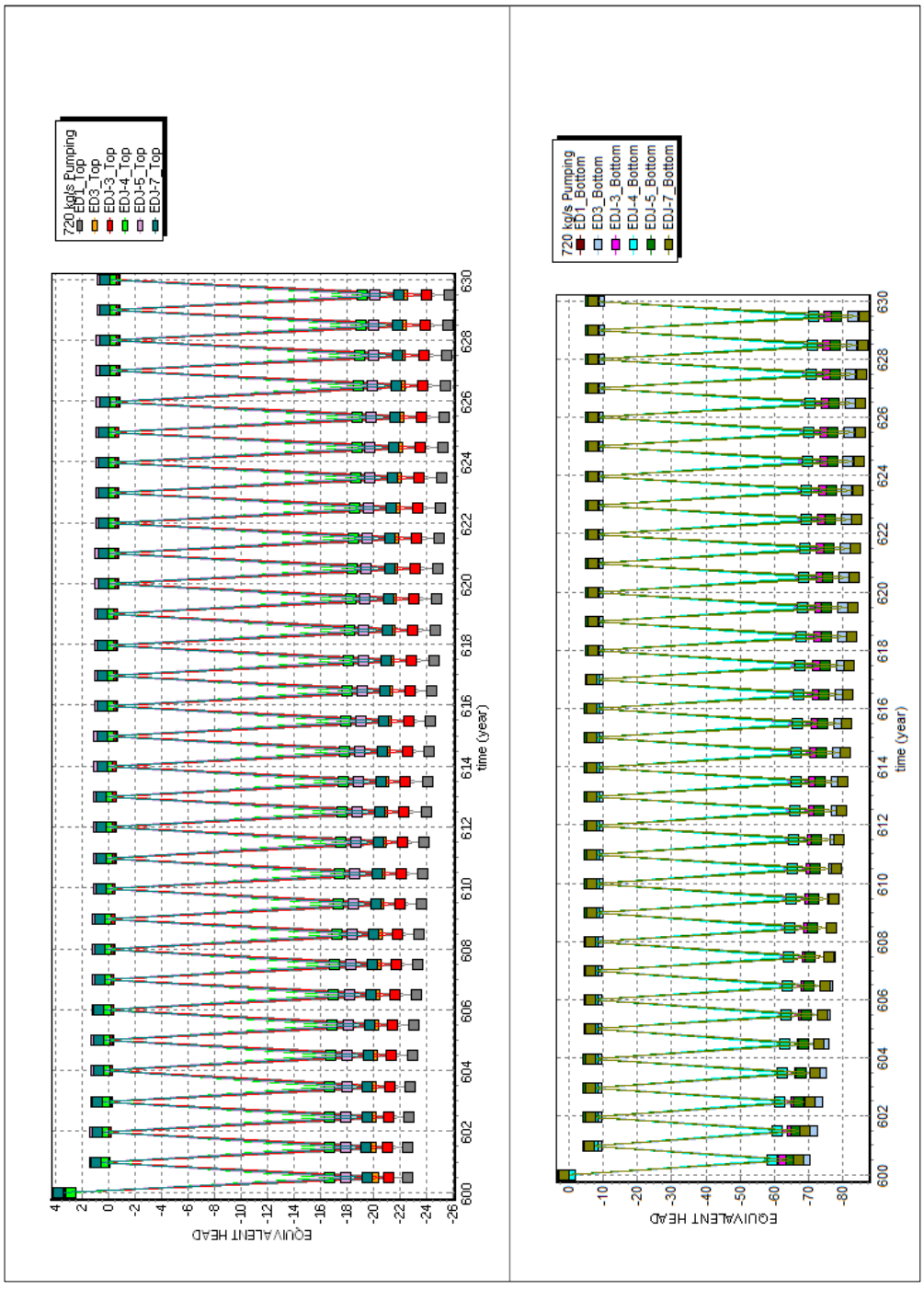

Figure 4.30: Pressures at well head and bottom for 720 kg/s 30 year pumping scenario.

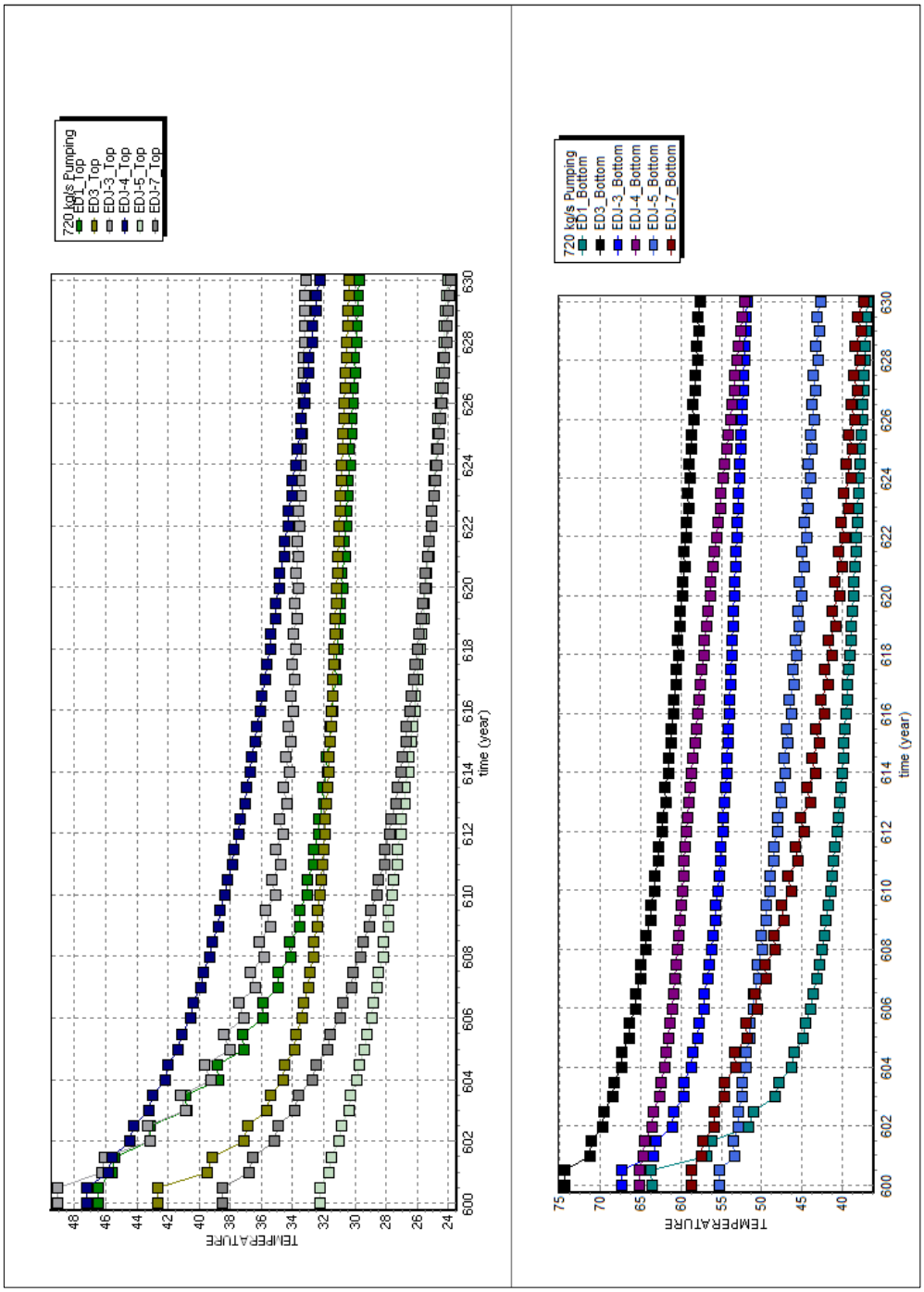

Figure 4.31: Temperatures at well head and bottom for 720 kg/s 30 year pumping scenario.

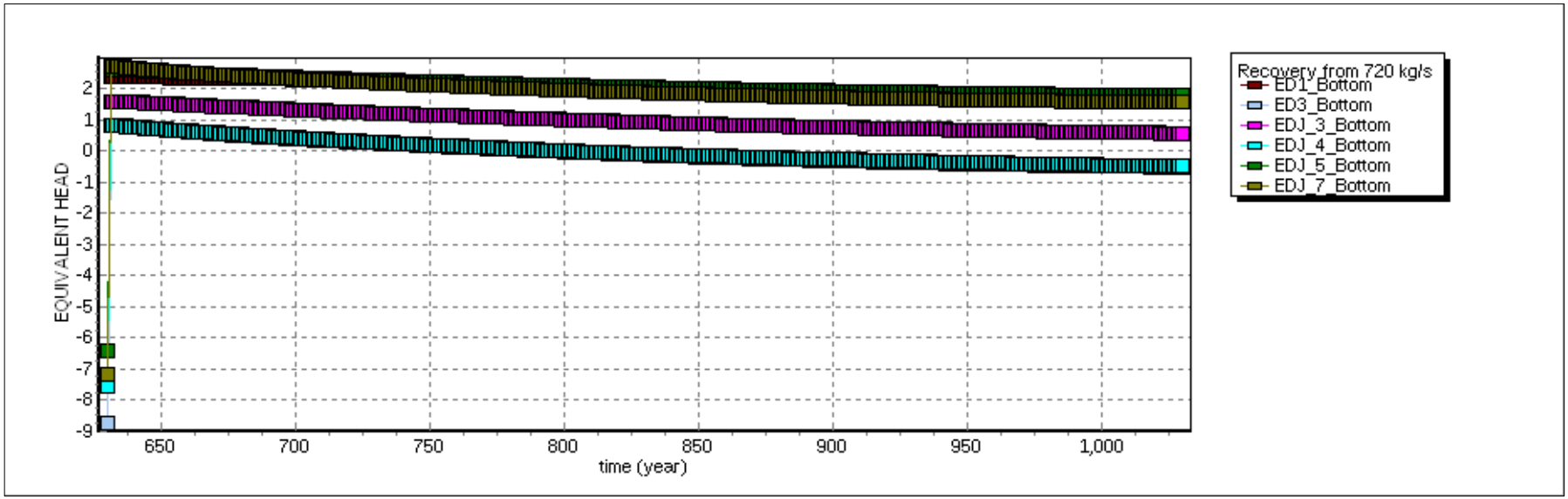

Figure 4.32: Pressure recovery at well bottom for 720 kg/s 30 year pumping scenario.

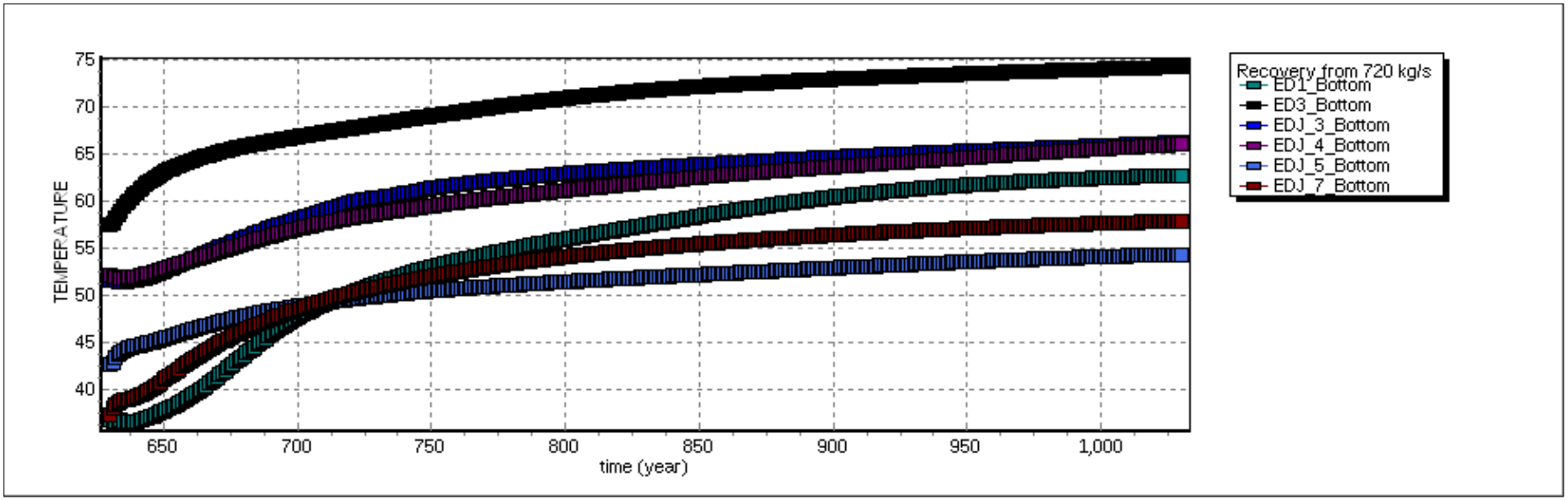

Figure 4.33: Temperature recovery at well bottom for 720 kg/s 30 year pumping scenario.

Table 4.5: Results after 360 kg/s Pumping Scenario for 10 Years

Observation Location	Original T (ºC)	After T (ºC)	Difference (ºC)	Before P (Pa)	After P (Pa)	Difference (m)
ED1_Top	46.52	37.16	-9.36	33894.75	16664.17	-1.76
ED1_Bottom	63.66	44.88	-18.78	1782309.20	1745341.20	-3.77
ED3_Top	42.66	33.65	-9.00	33420.67	18052.94	-1.57
ED3_Bottom	74.42	66.72	-7.71	3034631.40	3001585.90	-3.37
EDJ_3_Top	49.08	38.12	-10.96	32315.08	15996.24	-1.66
EDJ_3_Bottom	67.38	58.10	-9.28	2417991.50	2386056.40	-3.26
EDJ_4_Top	47.22	40.98	-6.24	27721.58	15024.70	-1.29
EDJ_4_Bottom	65.19	61.76	-3.43	2937254.00	2908237.60	-2.96
EDJ_5_Top	32.27	29.13	-3.15	36329.66	23033.31	-1.36
EDJ_5_Bottom	55.29	51.47	-3.82	2370798.80	2337102.10	-3.43
EDJ_7_Top	38.54	31.61	-6.93	37166.25	22252.97	-1.52
EDJ_7_Bottom	58.65	52.36	-6.28	2368598.20	2334312.80	-3.49

Table 4.6: Results after 360 kg/s Pumping Rate for 30 Years

Observation Location	Original T (ºC)	After T (ºC)	Difference (ºC)	Before P (Pa)	After P (Pa)	Difference (m)
ED1_Top	46.52	31.10	-15.41	33894.75	14842.72	-1.94
ED1_Bottom	63.66	39.92	-23.75	1782309.20	1744138.40	-3.89
ED3_Top	42.66	31.14	-11.51	33420.67	16890.40	-1.69
ED3_Bottom	74.42	62.27	-12.15	3034631.40	3002517.80	-3.27
EDJ_3_Top	49.08	34.01	-15.07	32315.08	14506.63	-1.82
EDJ_3_Bottom	67.38	54.79	-12.59	2417991.50	2386363.80	-3.22
EDJ_4_Top	47.22	36.42	-10.80	27721.58	13754.36	-1.42
EDJ_4_Bottom	65.19	59.33	-5.86	2937254.00	2909319.80	-2.85
EDJ_5_Top	32.27	26.32	-5.96	36329.66	21825.17	-1.48
EDJ_5_Bottom	55.29	47.18	-8.11	2370798.80	2337075.40	-3.44
EDJ_7_Top	38.54	26.67	-11.87	37166.25	20640.40	-1.68
EDJ_7_Bottom	58.65	44.11	-14.54	2368598.20	2334175.00	-3.51

Table 4.7: Results after 720 kg/s Pumping Scenario for 10 Years

Observation Location	Original T (ºC)	After T (ºC)	Difference (ºC)	Before P (Pa)	After P (Pa)	Difference (m)
ED1_Top	46.52	33.03	-13.48	33894.75	-1496.80	-3.61
ED1_Bottom	63.66	41.50	-22.16	1782309.20	1699097.60	-8.48
ED3_Top	42.66	32.25	-10.40	33420.67	2129.04	-3.19
ED3_Bottom	74.42	63.24	-11.19	3034631.40	2957290.70	-7.88
EDJ_3_Top	49.08	35.09	-13.99	32315.08	-956.43	-3.39
EDJ_3_Bottom	67.38	55.38	-12.00	2417991.50	2344378.40	-7.50
EDJ_4_Top	47.22	38.31	-8.90	27721.58	1093.05	-2.71
EDJ_4_Bottom	65.19	59.88	-5.31	2937254.00	2870402.50	-6.81
EDJ_5_Top	32.27	27.60	-4.68	36329.66	7736.57	-2.91
EDJ_5_Bottom	55.29	48.92	-6.36	2370798.80	2295047.20	-7.72
EDJ_7_Top	38.54	28.58	-9.96	37166.25	5798.15	-3.20
EDJ_7_Bottom	58.65	46.33	-12.32	2368598.20	2289042.50	-8.11

Table 4.8: Results after 720 kg/s Pumping Scenario for 30 Years

Observation Location	Original T (ºC)	After T (ºC)	Difference (ºC)	Before P (Pa)	After P (Pa)	Difference (m)
ED1_Top	46.52	29.71	-16.81	33894.75	-4984.14	-3.96
ED1_Bottom	63.66	36.86	-26.80	1782309.20	1693075.10	-9.10
ED3_Top	42.66	30.40	-12.25	33420.67	-716.20	-3.48
ED3_Bottom	74.42	57.58	-16.84	3034631.40	2953461.10	-8.27
EDJ_3_Top	49.08	33.13	-15.95	32315.08	-4197.80	-3.72
EDJ_3_Bottom	67.38	51.73	-15.65	2417991.50	2340143.80	-7.94
EDJ_4_Top	47.22	32.28	-14.94	27721.58	-2188.77	-3.05
EDJ_4_Bottom	65.19	52.14	-13.04	2937254.00	2867058.90	-7.16
EDJ_5_Top	32.27	24.05	-8.22	36329.66	4804.79	-3.21
EDJ_5_Bottom	55.29	42.66	-12.63	2370798.80	2289922.10	-8.24
EDJ_7_Top	38.54	23.88	-14.66	37166.25	2496.82	-3.53
EDJ_7_Bottom	58.65	37.37	-21.28	2368598.20	2282571.80	-8.77

4.3.3 Production Summary

From the production scenario results, it is evident that there is a delicate natural balance for temperatures of the reservoir. Even in low production rates, the temperatures had not reached a thermal steady-state, and showed a decline in temperatures. The time for temperature recoveries vary between 200 and 400 years, based on pumping rates between 100 and 720 kg/s respectively. The most adversely affected well from production is found to be well ED-1, which loses 26.8º C temperature at 720 kg/s pumping rate; however that particular well exhibited the highest recovery rate also. This is most probably that the well is located at the intersection of two faults in the study area (Figures 4.25 & 4.27).

The pressure levels drop at most 9.1 meters at well bottoms for 720 kg/s pumping rate. However, the pressure levels show a rapid recovery even in 6 month low production schedule. As can be seen in Figure 4.24, the pressure is lowered to 72 meters during winter months, but rises again by 62 meters in summer months rapidly. (Figure 4.26) In all scenarios, the pressure recovery had been reached in at most 4 years. This is most probably because of the high hydraulic gradient present in the study area.

In the production scenario of 360 kg/s for 10 years, the well bottoms showed an average temperature decline around 8.22 ºC. That production rate was selected to be close to the real operating production rates for 5000 equivalent residences, requirements which were compiled from the study of Coşkun (2007). The current operating temperatures were reported to be 51.46 ºC as of 2016 with 9 wells (excluding EDJ-4, which is assigned to a thermal spa facility), operating for 7500 residences; which was 60º C with 3 wells for 1648 equivalent residences as of 2007 (See Chapter 2.3). These close values of temperature declines between real and simulated values somehow support the validity of the hypothetical production schedule assumptions that was made in Chapter 4.2 of this study.

Temperatures before and after production simulation results can be observed visually from figures 4.34 and 4.35.

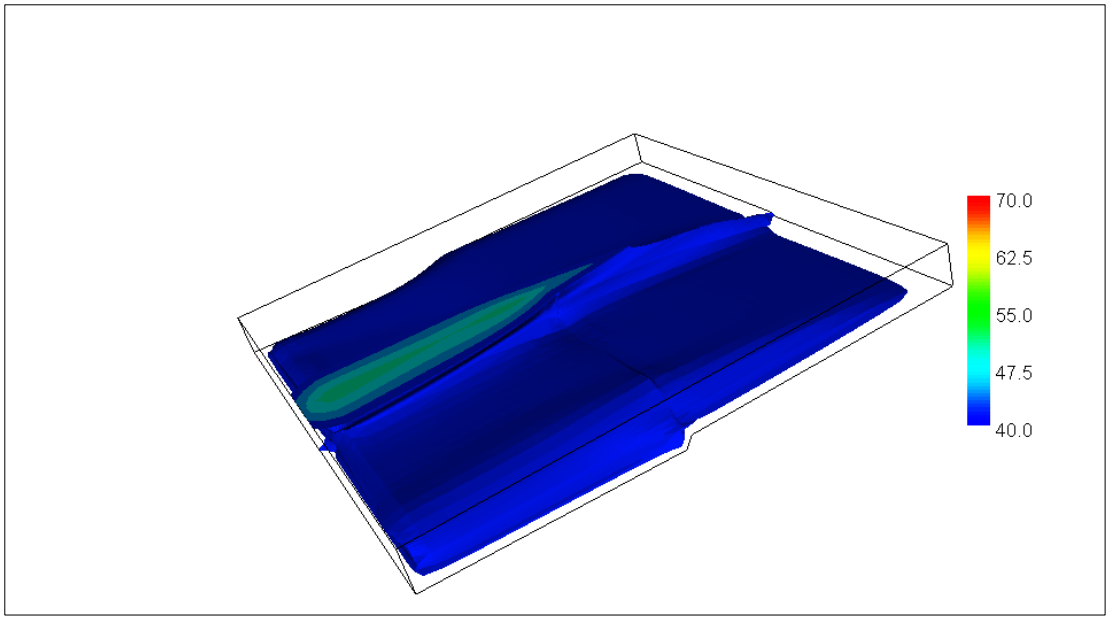

Figure 4.34: Study area simulation before production scenarios. Legend shows the temperatures in ºC.

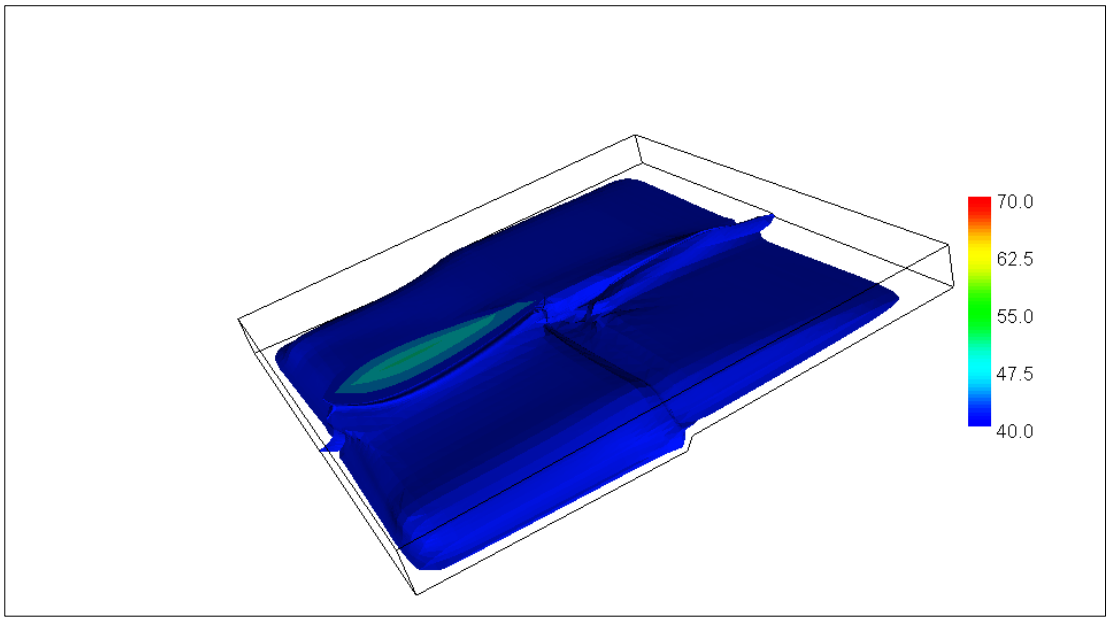

Figure 4.35: Study area simulation after 360 kg/s Pumping Scenario for 10 Years. Legend shows the temperatures in ºC.

4.4 Reinjection

Reinjection in the study area had not been performed by the operating firm up to now, and the waters are still discharged to the river after heating the exchangers in the residences. In this study, a hypothetical reinjection schedule is performed to model the reservoir response to reinjection while production is also performed for 10 years.

It is assumed that the production rate of 360 kg/s had been performed for 10 years without reinjection, representing the planned conditions of 10 years of production done actually in the study area. Reinjection is performed after 10 years, simultaneously with production rates, and the simulation was run for 10 years. For comparison, another simulation with that production rate but without reinjection had also been performed.

For reinjection, three wells are chosen which are approximately 350 meters to the east from the wells EDJ-5, ED-2 and EDJ-7. That location was chosen because of the effect of hydraulic gradient, and the location of production wells of EDJ-5 and EDJ-7, which are between the fault and the positive hydraulic gradient boundary.

The reinjection rate is taken to be 252 kg/s, which is 70% of the production rate, and the temperatures are taken as 35º C, which is the discharge temperature to the river. The reinjection to all wells are distributed equally, and done at depths between 100 and 240 meters, which is the lower hot aquifer and in winter months only.

Temperature and pressure changes in reinjection and no reinjection scenarios that were performed can be seen between figures 4.36 and 4.39.

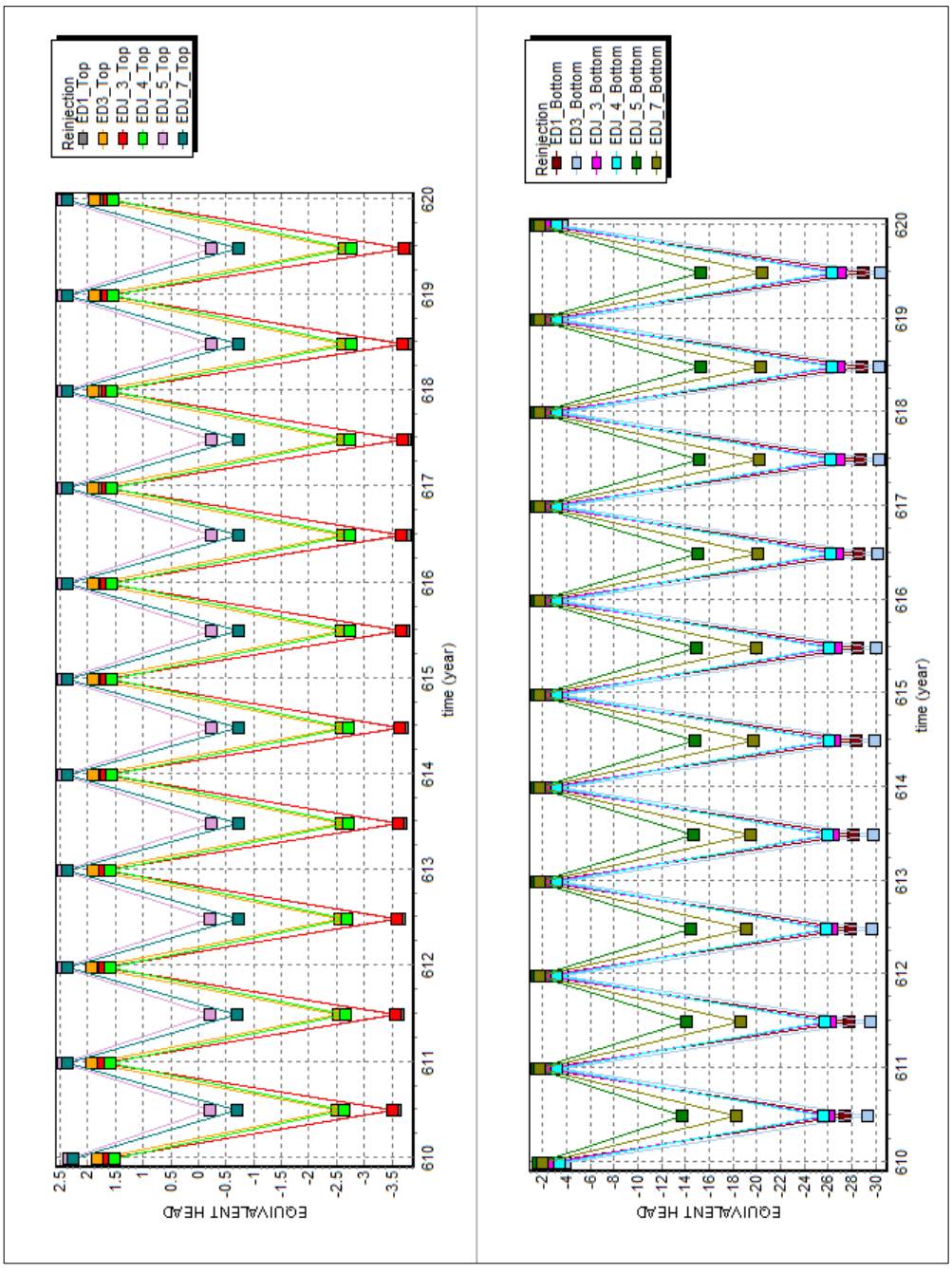

Figure 4.36: Pressures at well head and bottom for reinjection scenario.

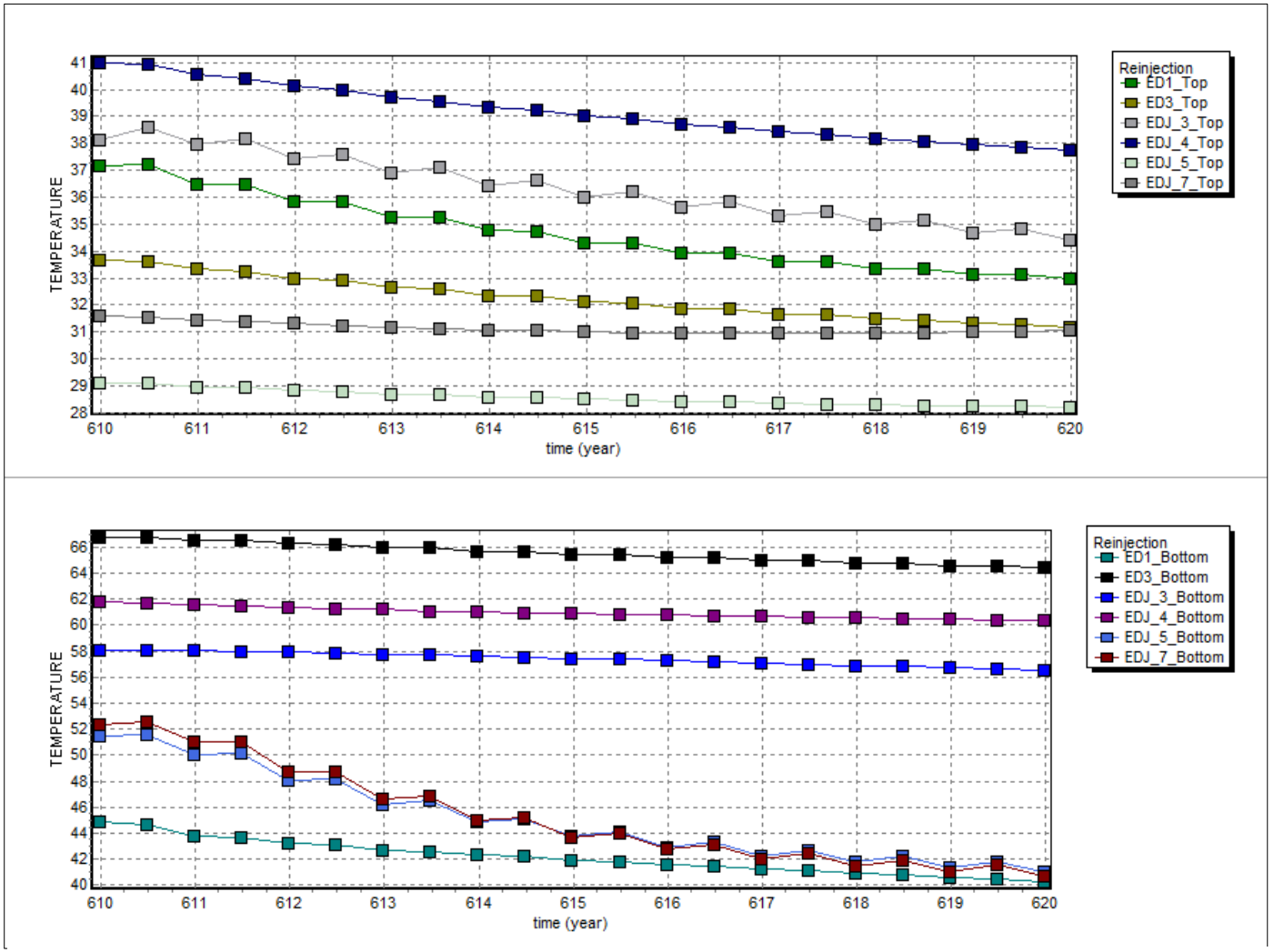

Figure 4.37: Temperatures at well head and bottom for reinjection scenario.

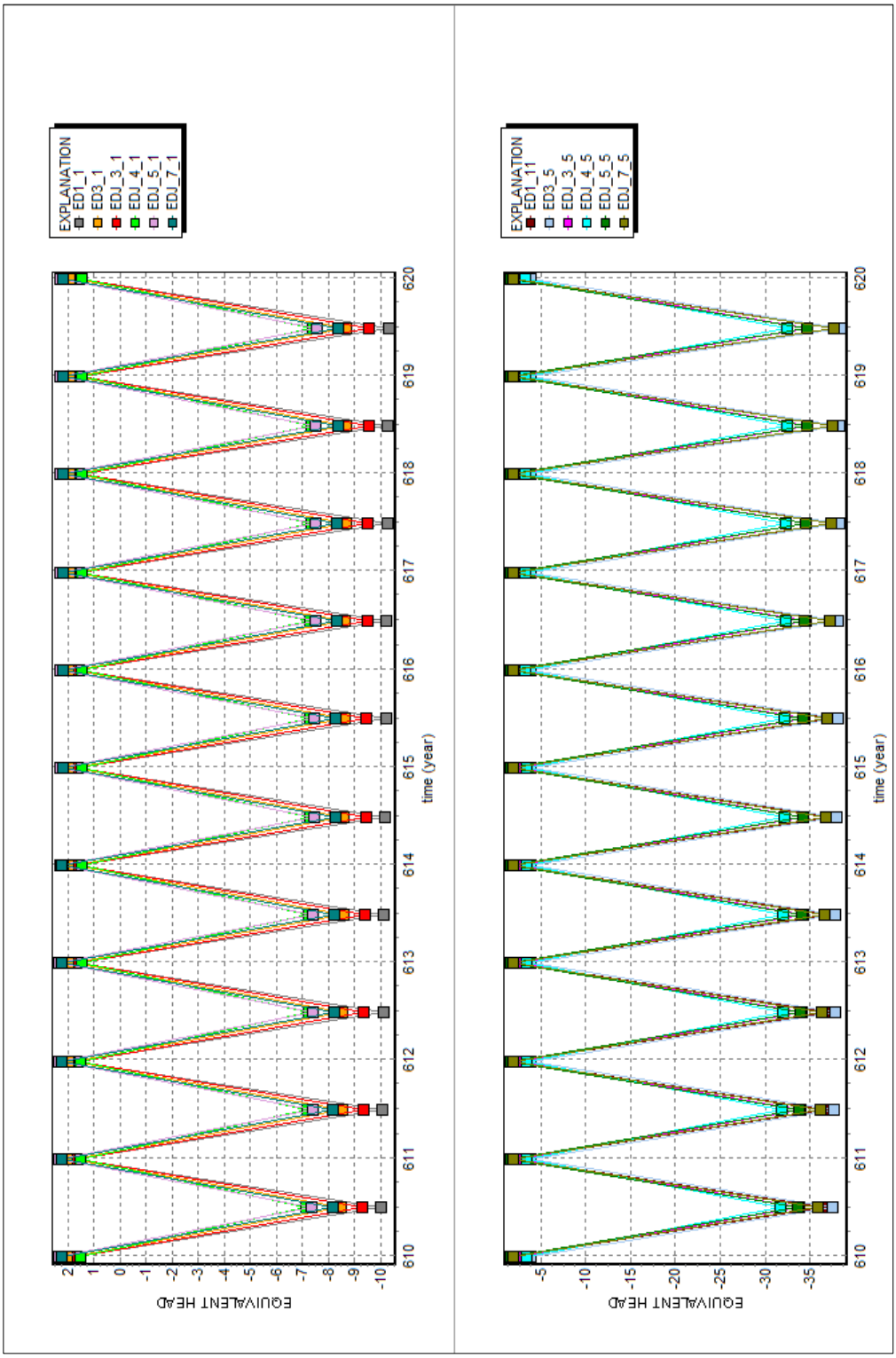

Figure 4.38: Pressures at well head and bottom for no reinjection scenario.

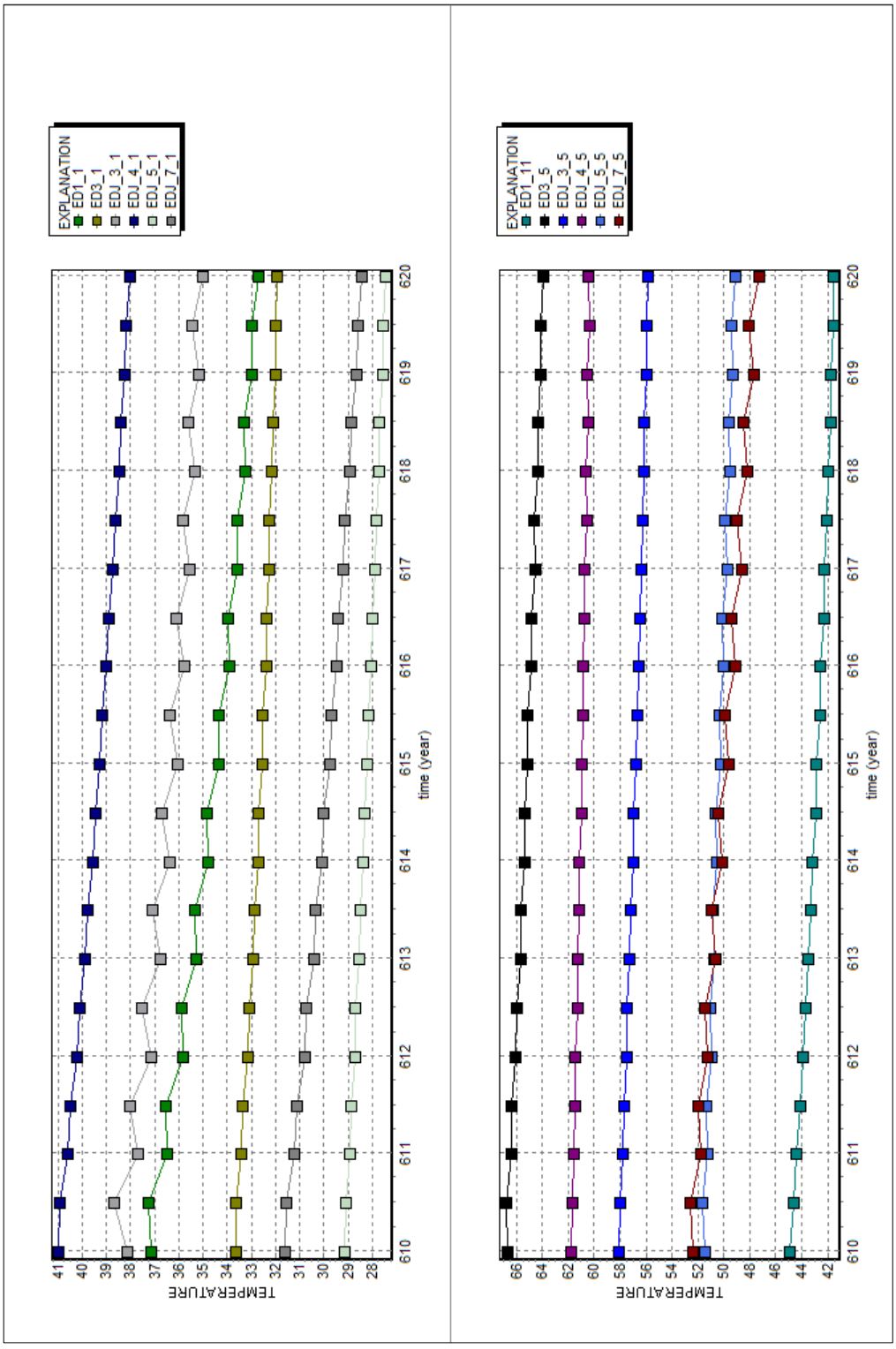

Figure 4.39: Temperatures at well head and bottom for no reinjection scenario.

4.4.1 Reinjection Results

Production with reinjection simulation can be compared with production with no reinjection throughout figures 4.36 and 4.39. There is a water level gain of 7 meters at the bottom of the wells, and 6.5 to 7 meters of water level gains at the top of the wells from reinjection for winter months. For summer months, the gains in pressure levels are around 0.5 meters at the well tops, and 1 meter at the well bottoms.

When compared with no reinjection scenario, the temperatures at the well bottoms are reduced by 2.46 º C. The pressure losses are 0.15 meters average at the well bottoms at the end of reinjection scenario. The gain in water levels is 0.14 m in average, and temperature losses are 1.07 º C in average. The highest temperature losses are observed at the well bottoms of EDJ-5 and EDJ-7 with 8.08 and 6.58 ºC respectively.

Production simulations for the study area showed that reinjection is not needed for pressure level gains because of the hydraulic gradient present in the area which can fill the pressure drops rapidly.

Reinjection simulations showed that reservoir response to reinjection is negligible. However, reinjection can still serve the local community considering the adverse effects of discharge to the river from geothermal heat production on agriculture and environment while having little effect on geothermal production.

Table 4.9: Temperature Observations for Reinjection / No Reinjection Scenarios

Observation Location	Reinjection (ºC)	No Reinjection (ºC)	Difference (ºC)
ED1_Top	32.95	32.72	0.23
ED1_Bottom	40.25	41.55	-1.30
ED3_Top	31.16	31.91	-0.75
ED3_Bottom	64.40	63.90	0.51
EDJ_3_Top	34.42	35.00	-0.58
EDJ_3_Bottom	56.55	55.85	0.70
EDJ_4_Top	37.73	38.04	-0.30
EDJ_4_Bottom	60.42	60.43	-0.02
EDJ_5_Top	28.20	27.44	0.76
EDJ_5_Bottom	41.01	49.09	-8.08
EDJ_7_Top	31.06	28.43	2.63
EDJ_7_Bottom	40.74	47.32	-6.58
AVG			-1.07

Table 4.10: Pressure Observations for Reinjection / No Reinjection Scenarios

Observation Location	Reinjection (Pa)	No Reinjection (Pa)	Difference (m)
ED1_Top	16725.42	15470.49	0.13
ED1_Bottom	1745883.70	1744608.70	0.13
ED3_Top	18542.24	17339.88	0.12
ED3_Bottom	3003897.60	3002242.90	0.17
EDJ_3_Top	16031.71	15024.96	0.10
EDJ_3_Bottom	2387928.00	2386298.70	0.17
EDJ_4_Top	15190.70	14240.64	0.10
EDJ_4_Bottom	2910406.50	2908921.70	0.15
EDJ_5_Top	23956.28	22326.86	0.17
EDJ_5_Bottom	2338500.70	2337193.00	0.13
EDJ_7_Top	23267.59	21276.95	0.20
EDJ_7_Bottom	2335623.80	2334383.00	0.13
AVG			0.14

CHAPTER 5

RESULTS AND DISCUSSIONS

This study was made in order to simulate the Edremit Geothermal Field, which has an upper cold aquifer and a lower hot aquifer, separated by an impermeable layer, and is now currently operated with a geothermal central heating system installed.

Because of the lack of structural, stratigraphical and hydrogeological data in permeability values and water levels, the system could not have been fully simulated, however using previous studies and observation data from the field, a similar or equivalent 3 dimensional simulation was performed using finite element methodology.

The boundary conditions and permeability values were computed using the data that was calculated 40 years prior. Boundary conditions with permeability values were computed with 2-Dimensional steady state finite element methodology for the entire Edremit Basin. The older data was georeferenced with geographical information system and calibration was accomplished with current technology.

For 3-Dimensional simulations, a 3 km by 3 km part of the study area was selected because of available deep well data limitation. Boundary conditions and permeability values from 2-Dimensional simulations were integrated to form the 3-Dimensional model. Different permeability values for formations and fault zones were studied with two different geothermal evolutionary scenarios.

Calibration studies for 3-Dimensional simulations were performed with around 11% accuracy according to Root Mean Square Error calculations. For two geothermal

evolutionary scenarios, calculations showed similar results.

During calibration studies, the permeability values obtained from 2-Dimensional simulation was found to be inadequate, thus a revision of the 2-Dimensional model was performed using the findings from 3-Dimensional simulations.

Numerical simulations were performed using compiled data from studies 10 years prior to this study, at the beginning of the geothermal system operations by the private firm that uses the geothermal system for district heating purposes. It was found out that the temperature levels had not reached a steady state, but declined continuously with the pumping rates. On the other hand, pressure levels exhibited a very rapid recovery, even in a small time frame of 6 months.

For the sustainable production of the geothermal system, a hypothetical reinjection scenario was studied with 70% amount of the extracted water at 35º C, with 3 wells located between two production wells and positive hydraulic gradient boundary, in which the production wells are located between faults and positive hydraulic gradient boundary. The reinjection scenario revealed that the gain in water levels is 0.14 m average, and temperature losses are 1.07 º C in average.

CHAPTER 6

CONCLUSIONS AND RECOMMENDATIONS

The following conclusions have been reached from this research:

1- An Integrated 3-Dimensional Finite Element Model of the Edremit Geothermal system had been performed using previous studies and current software technology.

2- A fully representative 3-Dimensional model of the Edremit Geothermal Field cannot be performed without adequate amount of permeability and water level data; however a similar or equivalent model can be derived from previous studies that can help in future models.

3- 3-Dimensional models do help in understanding the model. With current technology, using time dimension, 4-Dimensional geothermal models are possible.

4- Two geothermal evolutionary scenarios are possible for the Edremit Geothermal Field; however, more deep well data is required to be precise.

5- Hypothetical production scenarios were performed using data compilation from previous studies, which revealed that the temperature level drops do not reach a steady state, and recovery from 10 to 30 year pumping with rates between 100 kg/s and 720 kg/s would take 200 to 400 years for the model to restore the original temperature values. However; the pressure levels in the model do recover in a very short time period of 6 months.

6- Reinjection simulations performed on the model revealed that there is not much temperature or pressure levels that can be obtained by reinjection, but for saving the environment it can be performed.

The following items are recommended from this thesis:

1- New wells near DSI-7, DSI-8, HASTANE and DSI-9 wells need to be drilled down to the Kazdağ metamorphics or Eybek granodiorite to determine the geological formations and temperatures at the bottom aquifer to obtain a more precise formation and geothermal system knowledge of the area around pumping wells.

2- Permeability and current water level values should be determined from field studies to obtain a precise model of the region around the pumping wells.

3-The simulations showed that current pumping rates do decrease the temperature at the production wells and the temperature levels had not reached a steady state. Thus, at the current rates, sustainable production for temperature levels does not seem possible in the long term. A reevaluation of the production rates is advised.

4- It is still unknown whether the geothermal system is a local phenomenon. Thus, deep wells should be drilled towards the edges of the 3-Dimensional study area and more importantly to the southwestern and southeastern directions not only to identify the geological conditions that had shaped the Edremit Geothermal System, but also for prospecting other possible hot water well locations.

5-Sensitivity analysis was not performed after calibrations. It would be better if sensitivity analyses are done for future studies.

REFERENCES

A.M.C. Şengör, The North Anatolian Transform Fault: its age, offset and tectonic significance, J. Geo. Soc., London 136 (1979) 269-282.

A.M.C. Şengör, Ege'nin neotektonik evrimini yöneten etkenler, in: O. Erol, V. Oygür (Eds), Batı Anadolu'nun Genç Tektonigi ve Volkanizması Paneli. Congress of the Geological Society of Turkey, 1982, pp. 59-72.

Avşar, 2011, Geochemical evaluation and conceptual modeling of Edremit geothermal field, Ph. D. Thesis, Middle East Technical University, Ankara, p. 158.

Bingöl, E., Akyürek, B., Korkmazer, B., 1973. Biga yarımadas ın ın jeolojisi ve Karakaya formasyonunun baz ı özellikleri. *Proceedings, Cumhuriyetin 50. Yılı yerbilimleri kongresi,* Ankara p. 70-76.

Bozkurt, E. and Rojay, B., 2005. Episodic two-stage Neogene extension and short term intervening compression in Western Turkey: field evidence from the Kiraz Basin and Bozdağ Horst. Geodinamica Acta. 18, 299-316.

C. Kissel, C. Laj, The Tertiary geodynamical evolution of the Aegean arc: a paleomagnetic reconstruction, Tectonophysics, Volume 146, Issues 1–4, 30 January 1988, pg 183-201

Convection Cells in a gravity field, http://commons.wikimedia.org/wiki/File: ConvectionCells.svg, last accessed at May 2016

Coşkun (2007), Energetic And Exergetic Analyses Of The Balikesir Geothermal District Heating Systems, M.S. thesis, Balıkesir University, Balıkesir

Dewey 1998;Extensional Collapse of Orogens, Tectonics Journal, Vol7, Dec 1998,pg 1123,1139

DSİ, 1977. Edremit ve Armutova (Gömeç) ovaları hidrojeokimyasal etüt raporu, *Gn. Directorate of State Hydraulic Works, Rep.No. 86940*, unpublished

Duru, M., Pehlivan, Ş., Şentürk, Y., Yavaş, F., Kar, H., 2004. New results on the lithostratigraphy of the Kazdağ Massif in northwest Turkey. *Turkish Journal of Earth Sciences,* 13, 177-186

Edremit Jeotermal, http://www.edremitjeotermal.com.tr/hakkimizda.asp ,as of March, 2016.

Emre and Sözbilir, Tectonic Evolution of the Kiraz Basin, Küçük Menderes Graben: Evidence for Compression/Uplift-related Basin Formation Overprinted by Extensional Tectonics in West Anatolia,Turkish Journal of Earth Sciences (Turkish J. Earth Sci.), Vol. 16, 2007, pp. 441–470

Faulds et al. 2009, Structural controls on Geothermal systems in Western Turkey: A Preliminary Report, GRC Transactions, Vol. 33, 2009.

Günay, 2012. Numerical Modeling of Edremit Geothermal Field, M.S. thesis, Middle East Technical University, Ankara

İB, 2005. Edremit (Balıkesir) Belediyesi EDJ-3, EDJ-4, EDJ-5 ve EDJ-7 numaralı jeotermal kuyuları bitirme raporu, *Gn. Directorate ofBank of Provinces, Rep.No. İLB-JTE / 65*, unpublished.

İB, 2009. Edremit (Balıkesir) Belediyesi JTE-10/014 ve JTE-10/015 numaralı jeotermal kuyuları bitirme raporu, *Gn. Directorate of Bank of Provinces, Rep.No. İLB-JTE / 117*, unpublished.

İB, 2010. Edremit (Balıkesir) Belediyesi İLB-10/004 (EDJ-7) ve İLB-10/014 (EDJ-8) numaralı jeotermal kuyuları ölçüm ve inceleme raporu. *Gn. Directorate of Bank of Provinces, Rep.No. İLB-JTE / 128*, unpublished.

J. E. Meulenkamp, et al, 1988;On the Hellenic subduction zone and the geodynamic evolution of Crete since the Late Middle Miocene, Tectonophysics 146(1):203-215,January 1988

J.F. Dewey, A.M.C. Şengör, 1979; Aegean and Surrounding Regions: Complex multiplate and continuum tectonics in a convergent zone, Geol.Soc.Am.Bull.90, 84-92

Jacob, Bear. Dynamics of Fluids in Porous Media. Dover Publications, New York. 1988.

Jackson, J. & McKenzie, D. The relationship between plate motions and seismic moment tensors, and the rates of active deformation in the Mediterranean and Middle East. Geophysical Journal, 93, 45-73.

Kaya, O., Ünay, E., Göktaş, F. and Saraç, G.,2007. Early Miocene stratigraphy of central west Anatolia, Turkey: implications for the tectonic evolution of the eastern Aegean area. Geological Journal, 42, 85-109.

Kaya et al., 2014. Geological and Geophysical Observations on the Tectonic Features of Western Part of the Afyon-Akşehir Graben: A Contribution to the Arguments on the Two-stage Extension Model, Bulletin of the Earth Sciences Application and Research Centre of Hacettepe University.

Koçyiğit et al, 1999,Evidence from the Gediz graben for episodic two-stage extension in western Turkey. Journal of the Geological Society, London, 156, 605-16.

Koçyiğit et al., 2000; Episodic graben formation and extensional neotectonic regime in west central Anatolia and the Isparta Angle: a case study in the Akşehir-Afyon graben, Turkey. In: Bozkurt, E., Winchester, J.A. and Piper,J.D.A. (eds), Tectonics

and Magmatism in Turkey and the Surrounding Area. Geological Society, London, Special Publications, 173, 405-421.

Koçyiğit and Özacar, 2003; Extensional neotectonic regime through the NE edge of the outer Isparta Angle, SW Turkey: New field and seismic data. Turkish Journal of Earth Sciences, 12, 67-90.

Koçyiğit, 2005; The Denizli graben-horst system and the eastern limit of western Anatolian continental extension: basin fill, structure, deformational mode, throw amount and episodic evolutionary history, SW Turkey. Geodinamica Acta, 18(3-4), 167-168.

MTA, 2001. Balıkesir-Edremit-Derman jeotermal alanı ED-1, ED-2, ED-3 sondajları kuyu bitirme raporu, *Gn. Directorate of Mineral Research and Exploration, Rep.No. 10512,* unpublished.

MTA, 2005. Türkiye Jeotermal Kaynakları Envanteri. *Gn. Directorate of Mineral Research and Exploration, Envanter Serisi-201*, Ankara, pg. 849.

MTA, 2007. 1:100 000 ölçekli Türkiye jeoloji haritaları No: 97 Balıkesir İ18 paftası, *Gn. Directorate of Mineral Research and Exploration,* Ankara.

Mertoğlu, Şimşek, Başarır, 2015. Geothermal Country Update Report of Turkey (2010-2015) Proceedings World Geothermal Congress 2015, Melbourne, Australia, 19-25 April 2015.

Mutlu, 2007. Constraints on the Origin of the Balıkesir Thermal Waters (Turkey) from Stable Isotope (δ18O, δD, δ13 C, δ34 S) and Major-Trace Element Compositions, Turkish Journal of Earth Sciences(Turkish J. Earth Sci.), Vol. 16, 2007, pp. 13-32.

P. H. Oosthuizen,David Naylor, An Introduction to Convective Heat Transfer Analysis ,WCB/McGraw Hill, 1999

Rayleigh-Benard Convection, UC San Diego, Department of Physics., http://web.archive.org/web/20090222182327/http://physics.ucsd.edu/was-daedalus/convection/rb.html, last accessed on May 2016

Sarp, S., Burçak, M., Y ıldırım, T., Y ıldırım, N., 1998. Biga yarımadas ın ın jeolojisi ve jeotermal enerji olanakları ile Balıkesir-Havran-Derman kapl ıca sahas ının detay jeotermal etüdü ve gradyan sondajları, *Gn. Directorate of Mineral Research and Exploration, Rep.No. 10537,* unpublished.

Seyitoglu, G. & Scott, B. C. 1992a. The age of the Buyuk Menderes graben (west) and its tectonic implications. Geological Magazine, 129, 239-242.

Seyitoglu, G., 1999. Discussion on evidence from the Gediz Graben for episodic two-stage extension in western Turkey. Journal of Geological Society, London, 156, 1240.

Seyitoglu, G.**,** Cemen, I. & Tekeli, O., 2000. Extensional folding in the Alasehir (Gediz) graben, western Turkey. Journal of the Geological Society, London, 157, 1097 -1100.

Seyitoglu, G.**,** Tekeli, O., Cemen, I., Sen, S. & Isik, V., 2002. The role of the flexural rotation / rolling hinge model in the tectonic evolution of the Alasehir graben, western Turkey. Geological Magazine, 139, 15-26.

Seyitoğlu, G.**,** Işık, V., 2009. Meaning of the Küçük Menderes graben in the tectonic framework of the central Menderes metamorphic core complex (western Turkey). Geologica Acta, 7(3), 323-331.

Şengör, A.M.C., Görür, N. and Şaroğlu, F., 1985; Strike-slip faulting and related basin formation in zones of tectonic escape:Turkey as a case study. The Society of Economic Paleontologists and Mineralogists, Special Publication, 37, 227-264.

Şengör, A.M.C. & Bozkurt, E. 2013. Layer-parallel shortening and related structures in zones undergoing active regional pure horizontal extension. International Journal of Earth Sciences 102, 101–119.

Şimşek Ş., Güleç, N., “Geothermal Fields of Western Anatolia”, International Volcanological Congress, Excursion Guide, IAVCEI, Ankara, s.7, 17-22 Eylül (1994).

Ural, T., 1978. Finite difference modelling of Edremit valley aquifers, M.S. thesis, Middle East Technical University, Ankara, p. 65.

Voss, C.I., 1984. SUTRA: A Finite-Element Simulation Model for Saturated Unsaturated Fluid-Density-Dependent Groundwater Flow with Energy Transport or Chemically Reactive Single Species Solute Transport, U.S. Geological Survey Water Resources Investigations Report 84-4369.

APPENDIX 1

BOREHOLE LOGS

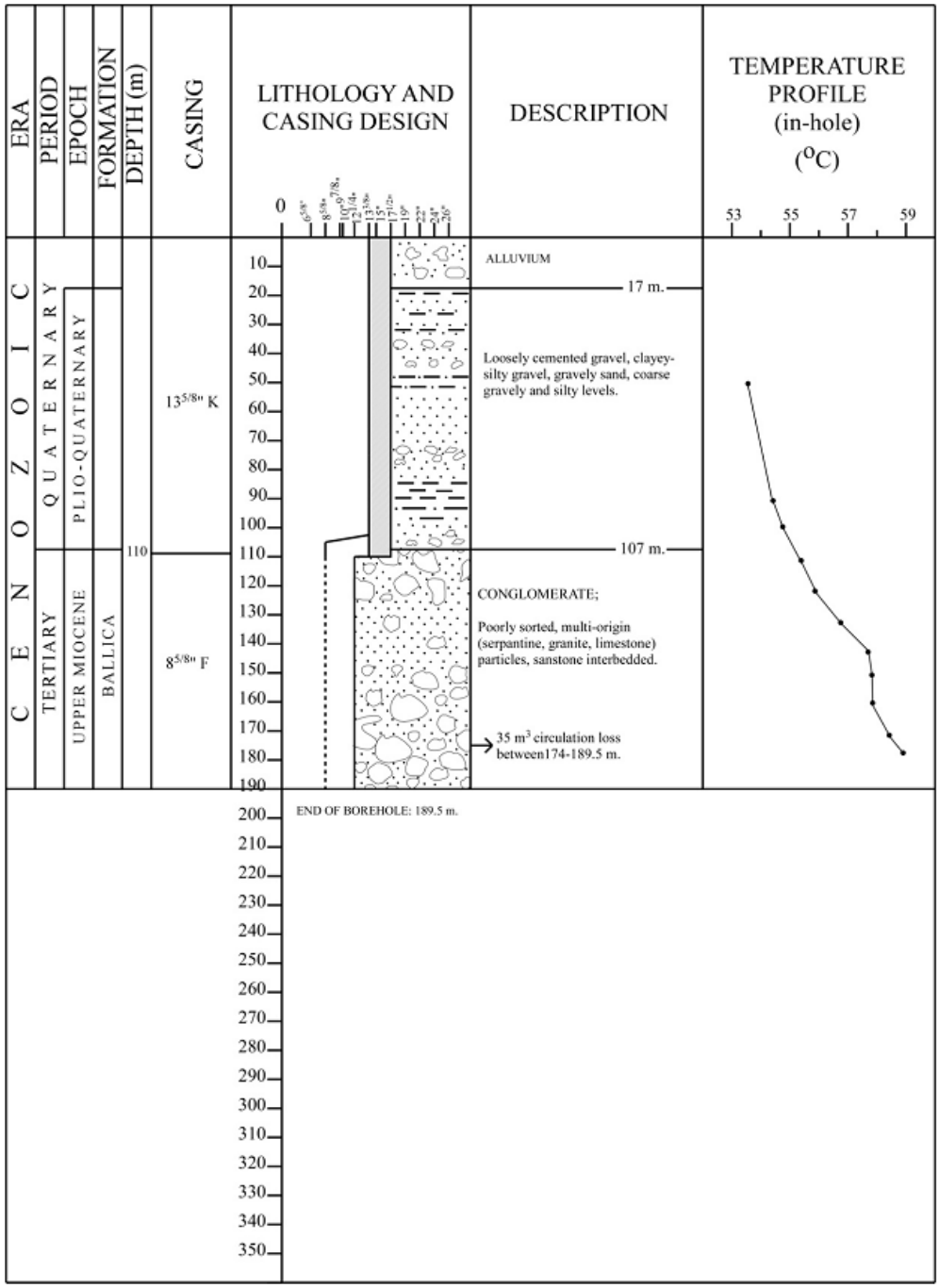

Figure A1.1: Borehole Log of ED-1 (MTA, 2001)

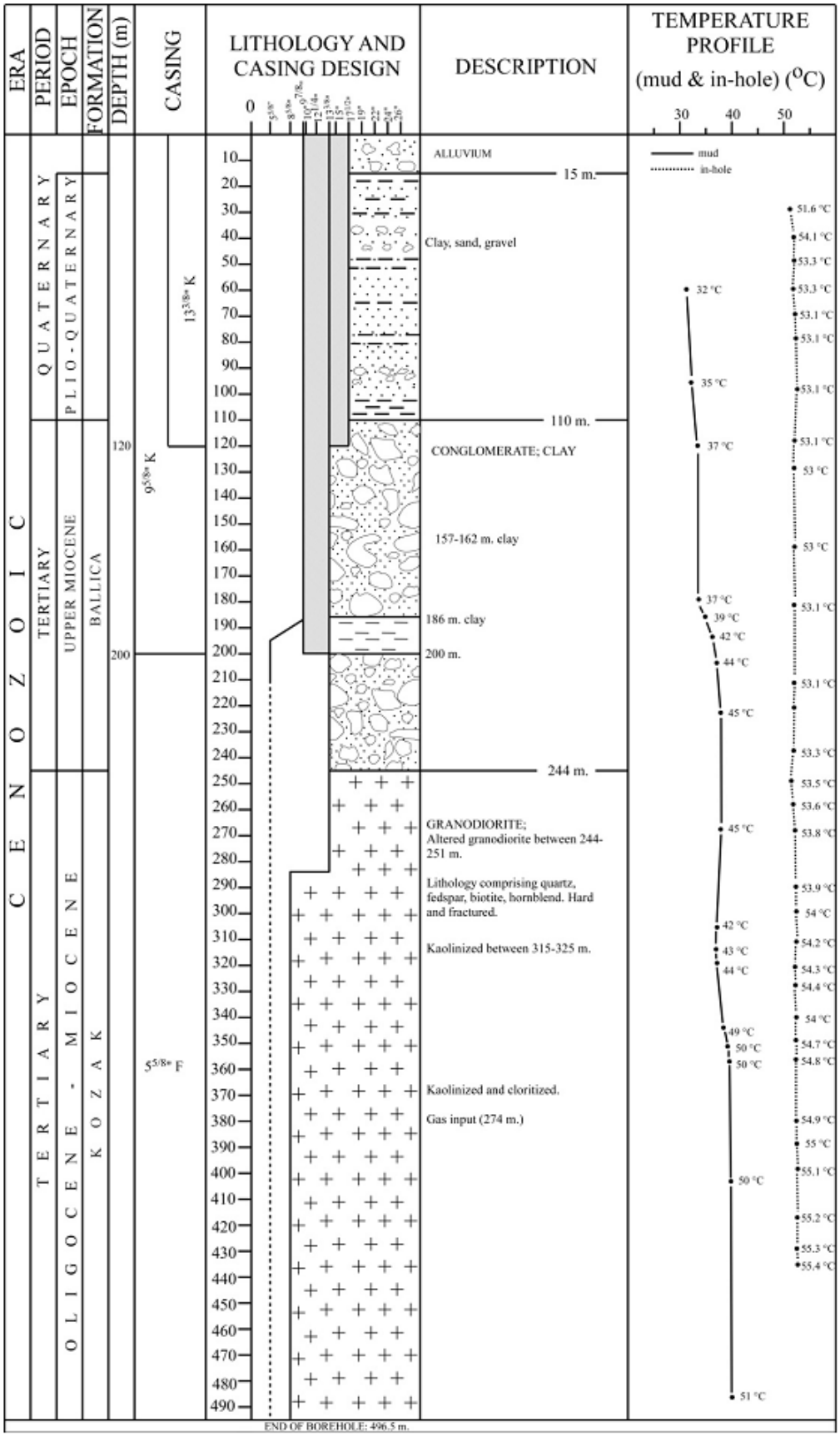

Figure A1.2: Borehole Log of ED-2 (MTA, 2001)

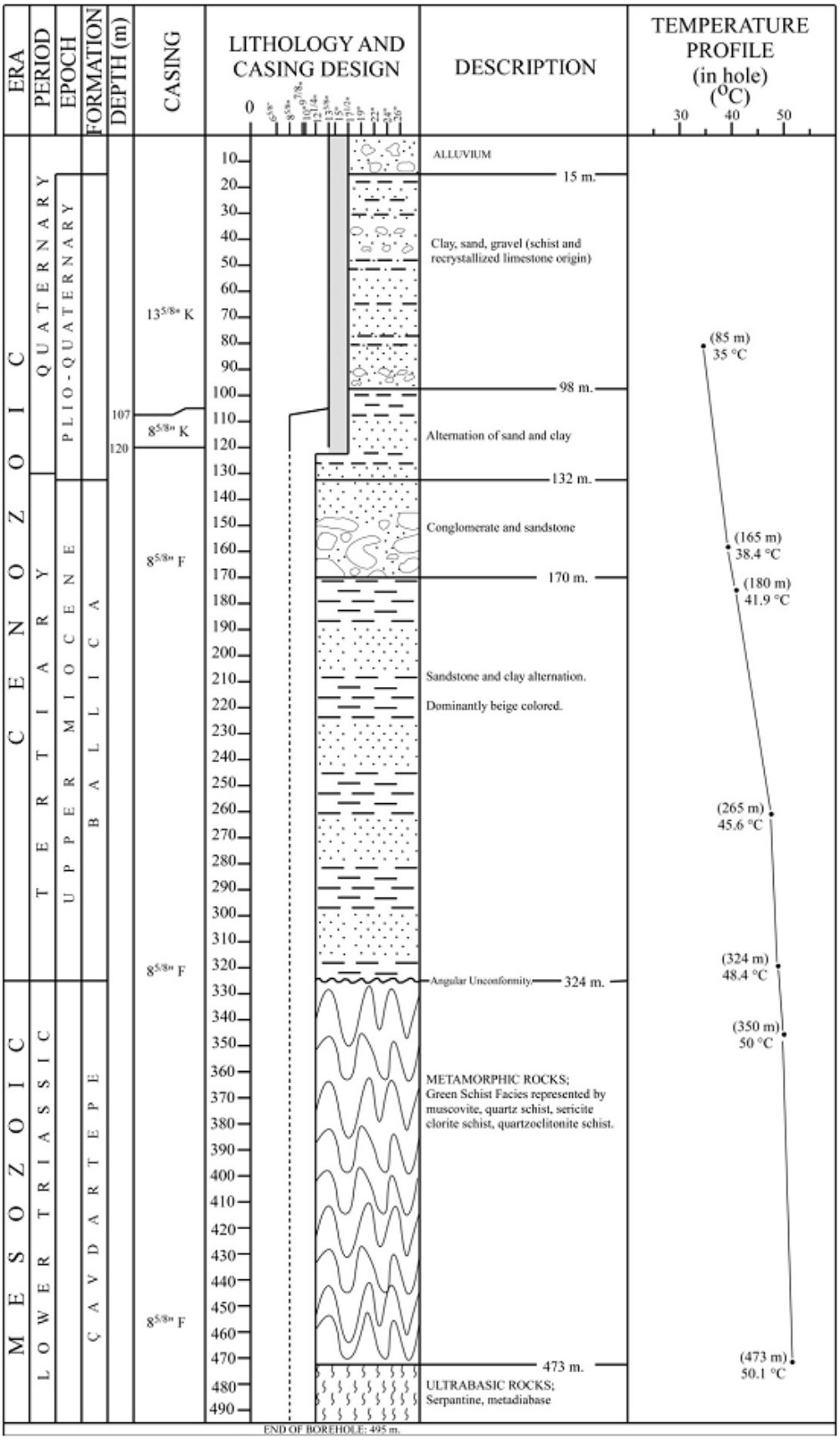

Figure A1.3: Borehole Log of ED-3 (MTA, 2001)

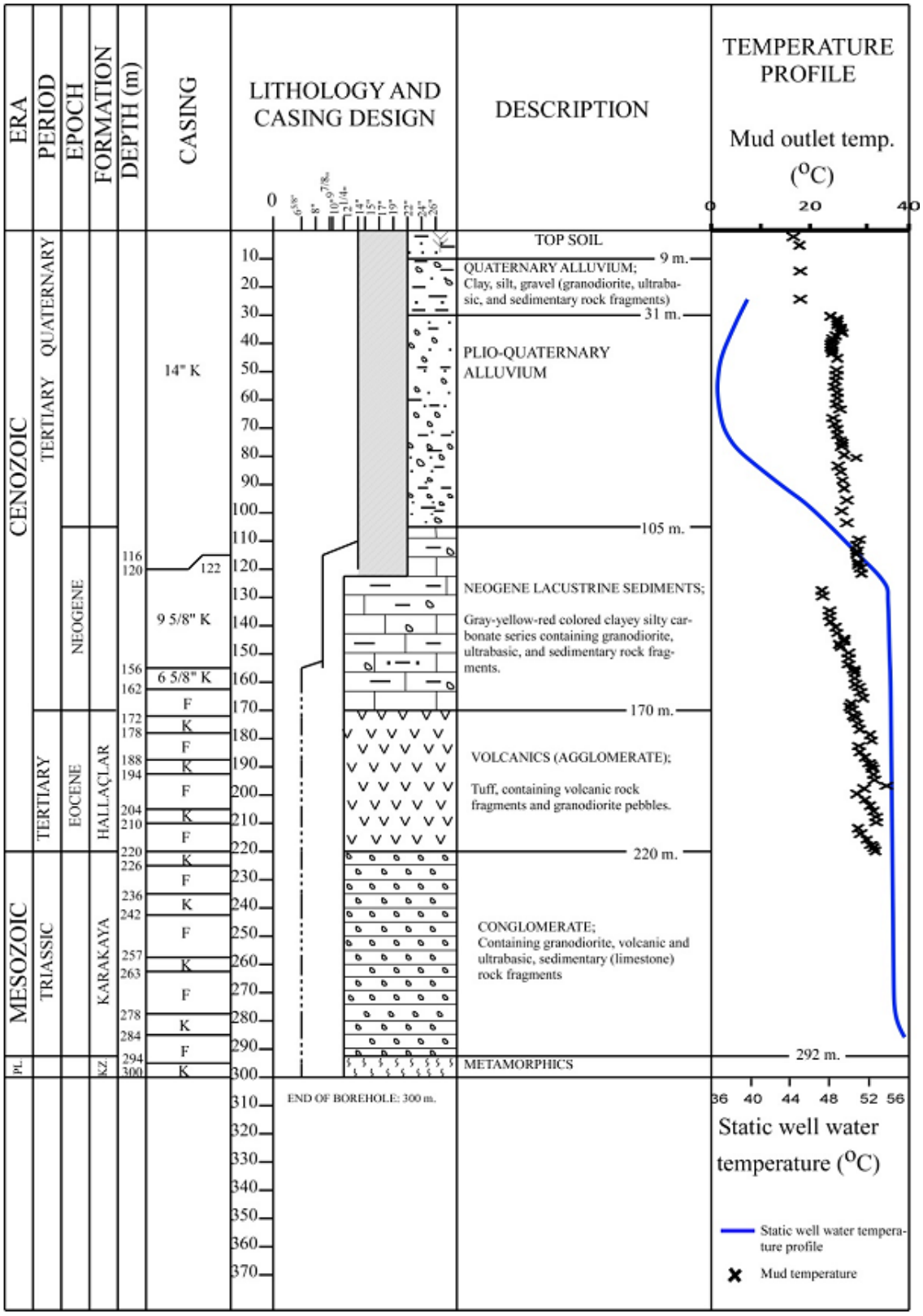

Figure A1.4: Borehole Log of EDJ-2 (İB, 2009)

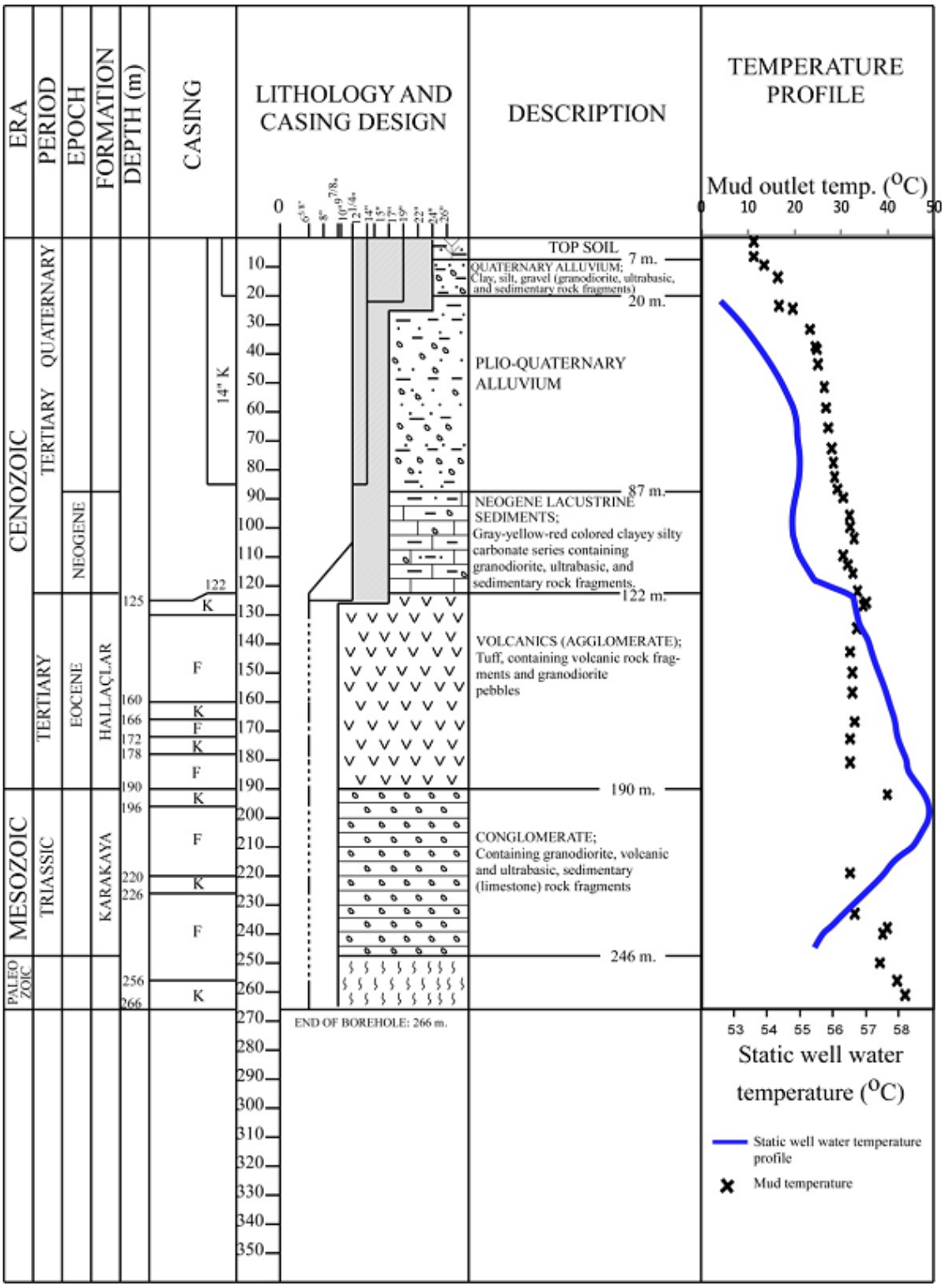

Figure A1.5: Borehole Log of EDJ-3. (İB, 2005)

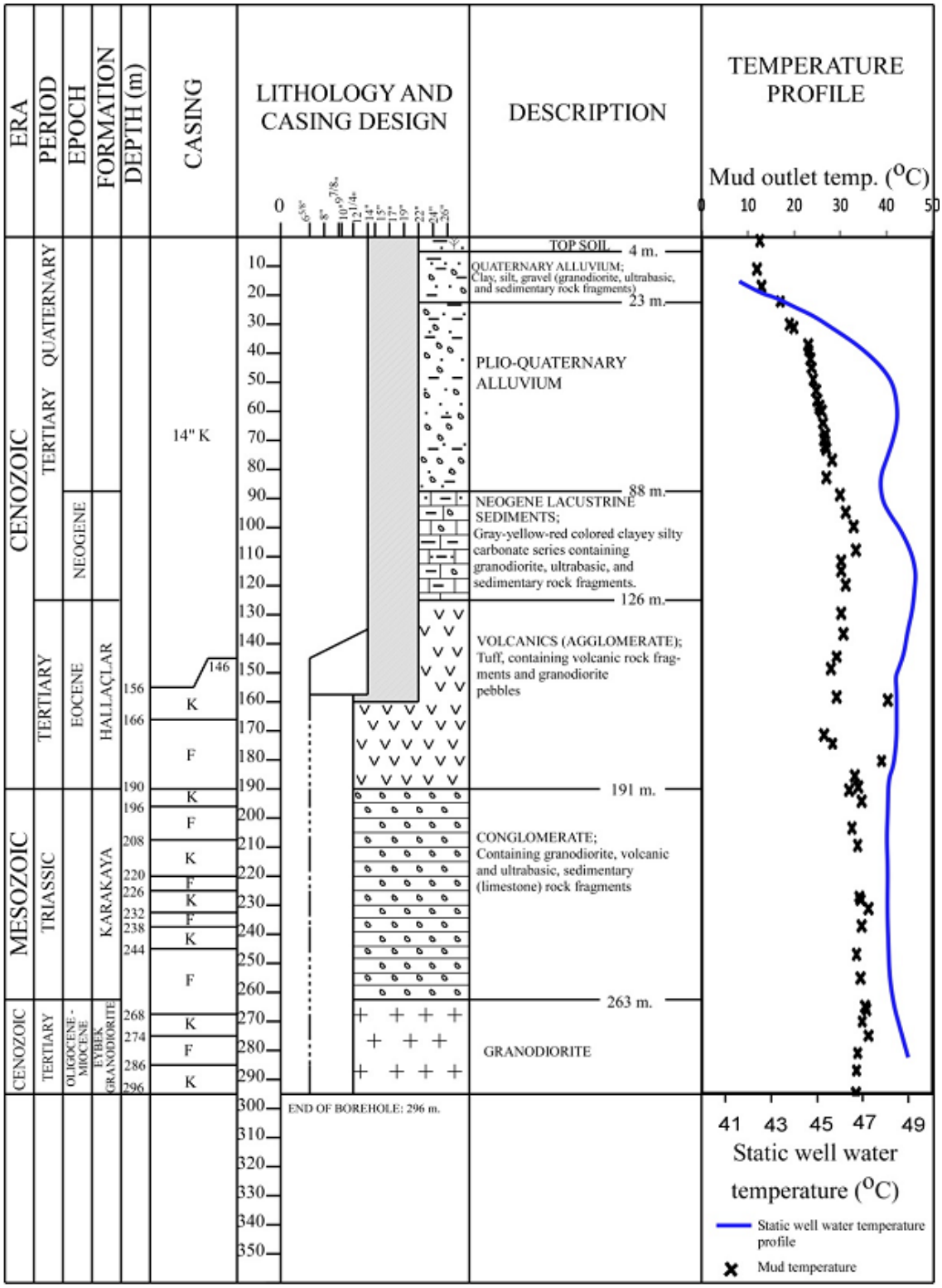

Figure A1.6: Borehole Log of EDJ-4 (İB, 2005)

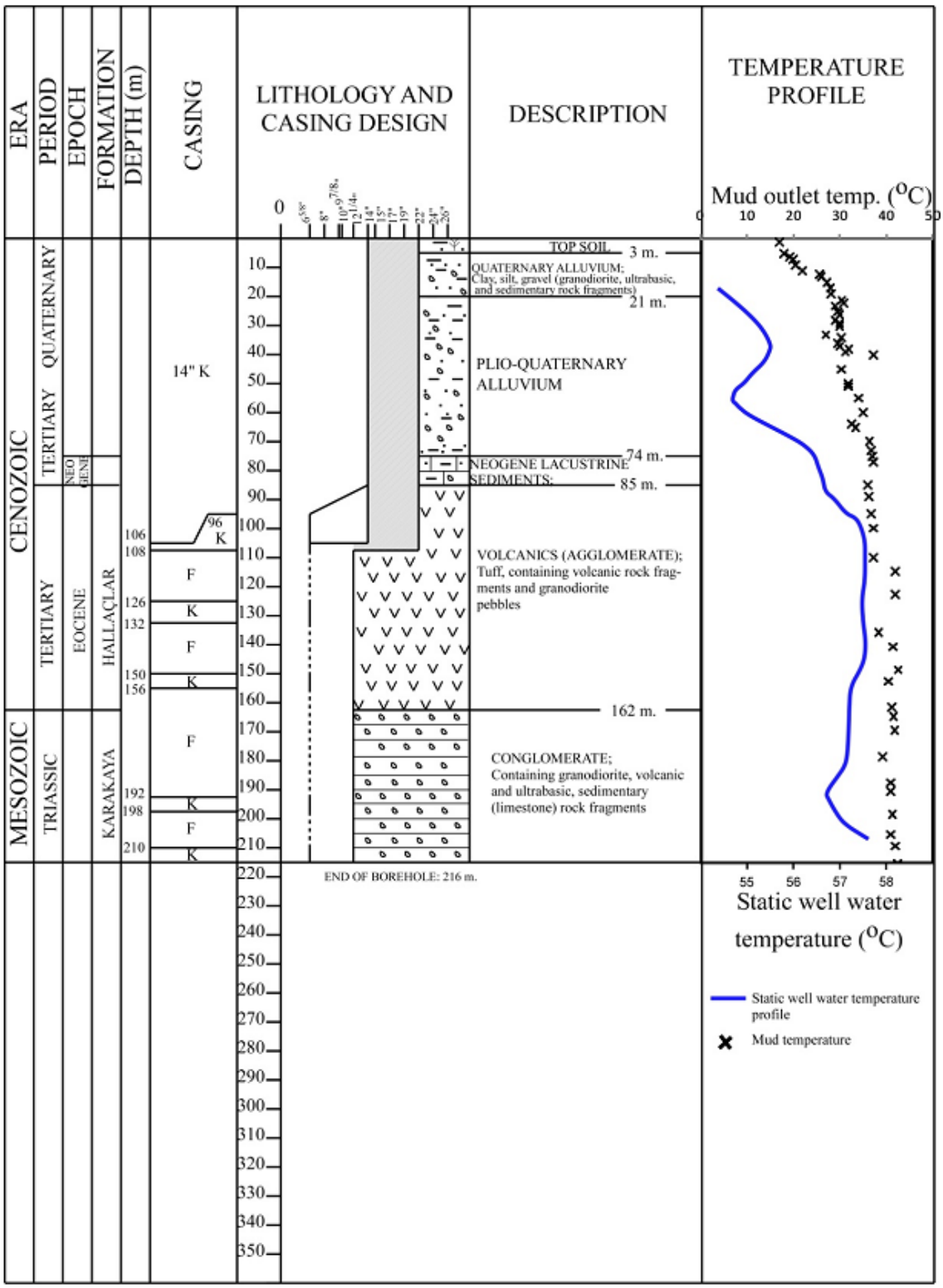

Figure A1.7: Borehole Log of EDJ-5 (İB, 2005)

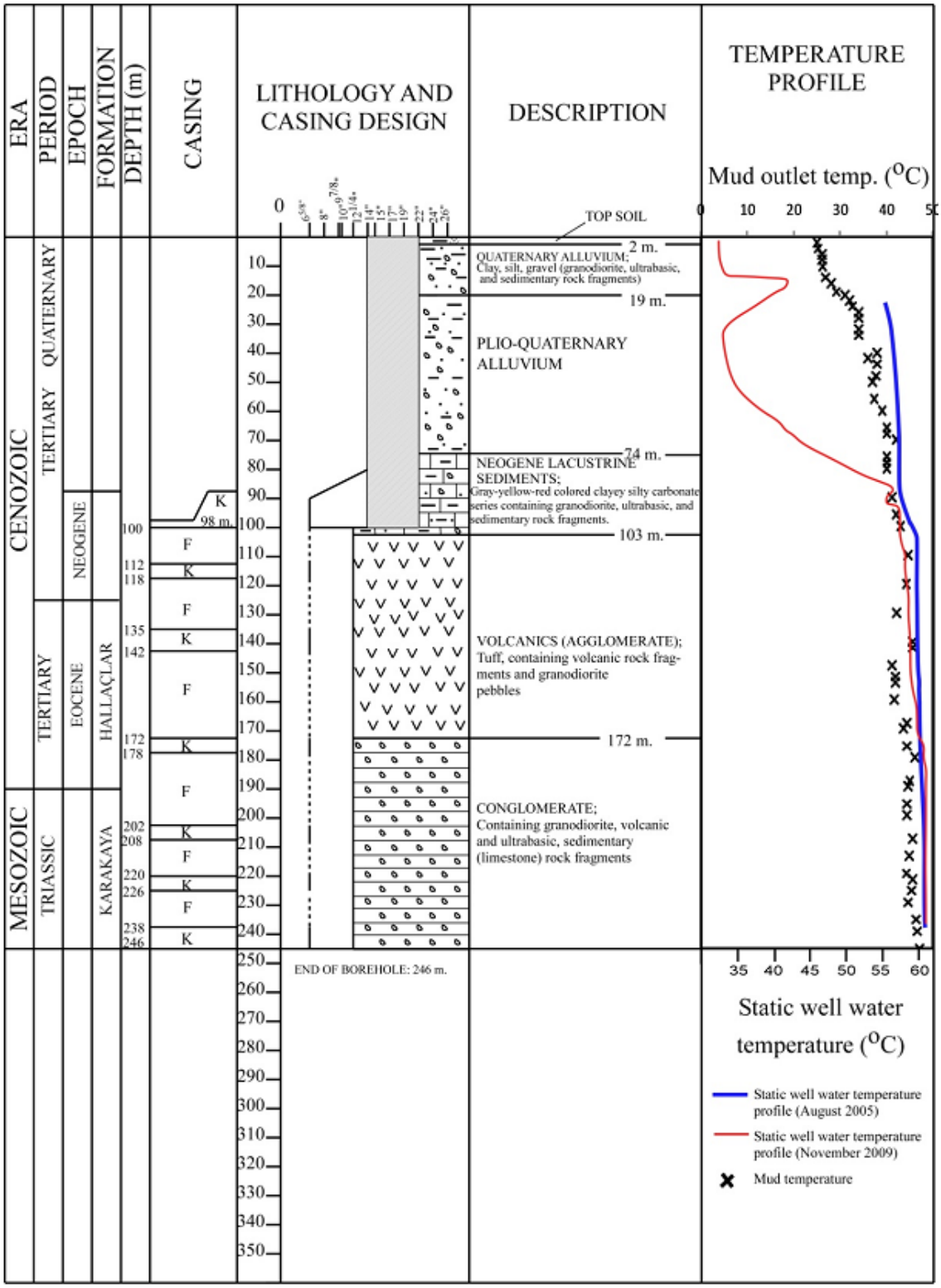

Figure A1.8: Borehole Log of EDJ-7 (İB, 2005; İB, 2010)

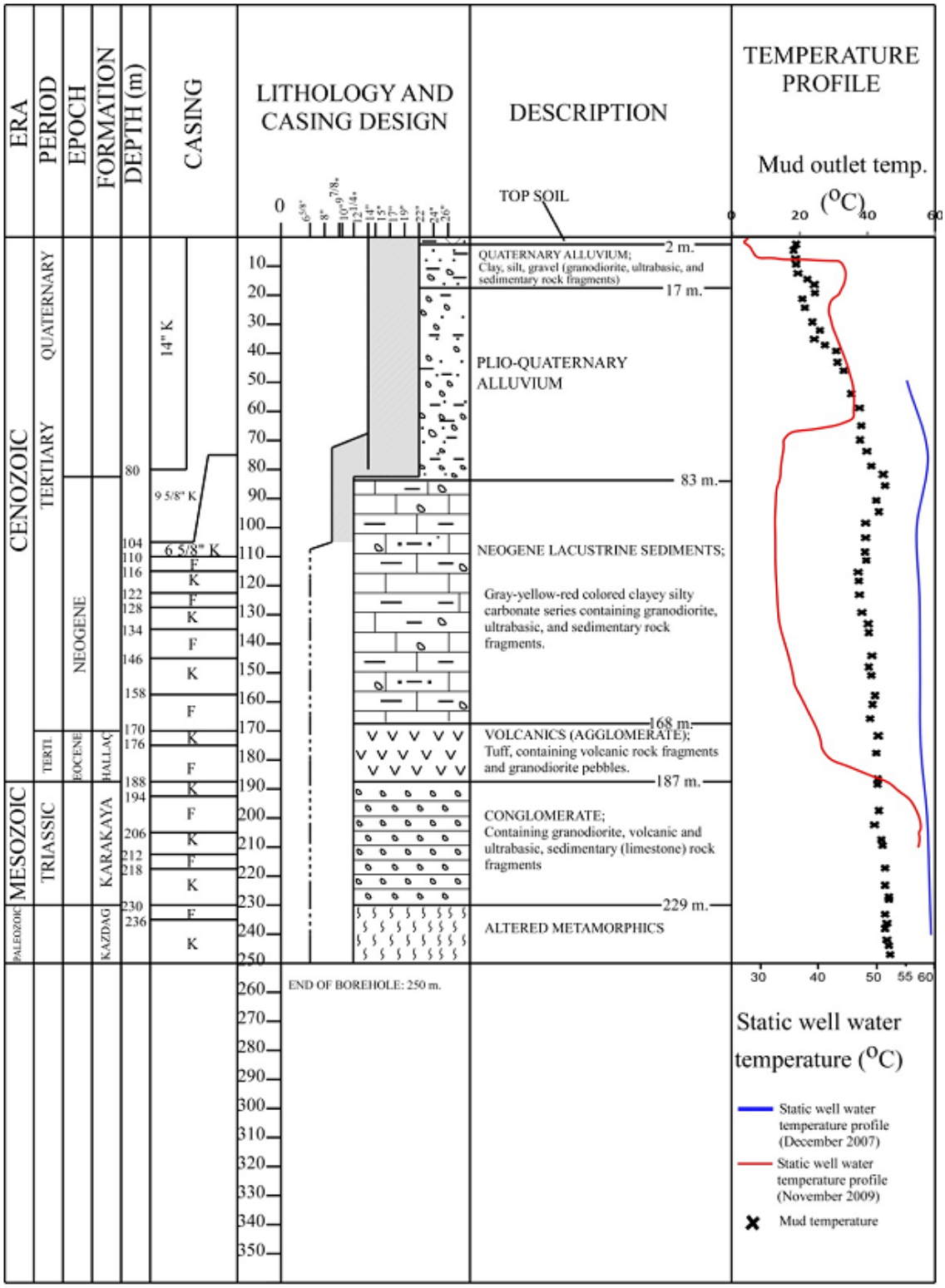

Figure A1.9: Borehole Log of EDJ-8 (İB, 2009; İB, 2010)

APPENDIX 2

CALIBRATION CALCULATIONS

Table A2.1: Calibration Results for Scenario 1 Part 1

Well	Depth (m)	T (ºC)	1 (ºC)	MSE	2 (ºC)	MSE	3 (ºC)	MSE	4 (ºC)	MSE	5 (ºC)	MSE	6 (ºC)	MSE	7 (ºC)	MSE
ED1_1	50	54	46.21	60.67	36.24	315.26	42.70	127.78	54.38	0.15	40.48	182.70	40.80	174.33	36.67	300.23
ED1_2	90	54.5	49.20	28.09	40.89	185.33	52.45	4.19	60.80	39.73	50.07	19.62	49.75	22.59	41.46	170.07
ED1_3	100	55	50.16	23.41	42.44	157.67	56.05	1.10	62.62	58.10	54.67	0.11	54.04	0.93	43.34	135.96
ED1_4	115	55.5	51.65	14.81	44.87	113.04	60.58	25.82	63.98	71.85	60.68	26.80	59.45	15.63	46.63	78.66
ED1_5	120	56	52.11	15.10	45.66	106.93	61.82	33.93	64.23	67.67	61.70	32.45	60.46	19.93	47.61	70.35
ED1_6	130	56.5	53.06	11.84	47.27	85.11	64.47	63.56	64.85	69.80	64.12	58.04	62.77	39.37	49.67	46.59
ED1_7	140	57	54.05	8.72	48.78	67.53	66.55	91.28	66.14	83.50	65.86	78.45	64.33	53.67	51.45	30.79
ED1_8	150	58	55.08	8.52	50.36	58.38	68.42	108.55	67.38	87.89	67.49	90.12	65.73	59.81	53.19	23.13
ED1_9	160	58	56.21	3.21	52.06	35.31	69.76	138.37	68.46	109.32	68.85	117.67	66.73	76.29	54.87	9.78
ED1_10	170	58.5	57.35	1.33	53.92	21.00	71.03	157.09	69.59	123.09	70.25	138.17	67.78	86.13	56.86	2.67
ED1_11	180	59	58.49	0.26	55.88	9.71	72.26	175.94	70.78	138.75	71.70	161.30	68.87	97.48	59.06	0.00
ED2_1	60	51.3	43.50	60.91	36.17	228.88	34.17	293.47	35.15	260.91	28.65	512.83	27.90	547.60	30.50	432.70
ED2_2	120	51.3	47.54	14.13	42.08	85.00	39.90	130.07	40.19	123.38	36.18	228.55	35.52	249.06	39.22	145.81
ED2_3	190	51.3	54.35	9.29	52.40	1.22	49.74	2.44	50.19	1.23	48.22	9.47	47.19	16.88	49.76	2.37
ED2_4	200	51.3	55.61	18.61	54.19	8.37	51.63	0.11	52.08	0.60	50.31	0.97	49.24	4.24	51.52	0.05
ED2_5	210	51.3	56.95	31.89	56.04	22.49	53.63	5.42	54.06	7.61	52.49	1.41	51.39	0.01	53.38	4.31
ED2_6	225	51.3	59.06	60.14	58.91	57.95	56.76	29.82	57.15	34.22	55.84	20.62	54.73	11.75	56.33	25.35
ED3_1	85	35	51.58	274.92	42.27	52.92	48.31	177.19	47.06	145.46	37.61	6.82	38.55	12.64	35.97	0.94
ED3_2	165	38.4	60.35	481.87	57.47	363.69	62.83	596.61	61.55	536.02	54.76	267.68	58.16	390.43	48.64	104.84
ED3_3	180	41.9	61.78	395.41	60.06	329.96	65.39	551.80	63.71	475.83	57.63	247.28	60.99	364.48	50.65	76.49
ED3_4	265	45.6	72.75	737.09	77.47	1015.99	77.81	1037.35	76.66	964.66	73.64	786.21	74.81	853.33	67.60	483.88
ED3_5	300	47.5	77.07	874.43	82.50	1225.12	80.99	1121.72	79.99	1055.82	77.41	894.85	78.87	984.34	74.96	754.10

Table A2.1 Continued

DERMAN	100	53	52.35	0.42	43.43	91.62	49.46	12.52	48.33	21.80	40.45	157.62	41.03	143.36	50.38	6.85
ENTUR	90	51	51.65	0.42	42.21	77.18	46.46	20.58	45.80	27.03	37.24	189.42	37.81	174.09	47.55	11.89
YAGCI	100	42	54.07	145.80	47.25	27.61	45.03	9.16	43.78	3.17	36.98	25.19	37.45	20.72	36.13	34.43
DSI6	95	39	53.86	220.91	43.69	22.04	40.91	3.65	40.10	1.21	32.74	39.13	34.95	16.42	40.92	3.67
DOGAN	30	32	50.51	342.49	38.40	40.95	38.13	37.56	39.99	63.80	29.71	5.24	31.03	0.95	34.79	7.80
DSI9	122	32	51.91	396.60	42.72	114.93	42.68	113.96	42.50	110.27	35.28	10.77	41.28	86.07	41.19	84.55
HASTANE	90	31	39.29	68.70	34.15	9.90	33.02	4.10	32.59	2.53	30.05	0.91	29.09	3.63	29.13	3.51
DSI5	91	30	51.00	440.79	41.37	129.27	38.88	78.92	36.37	40.59	30.99	0.98	31.68	2.82	39.65	93.05
DSI7	132	21	56.11	1232.54	45.85	617.54	44.01	529.57	42.73	472.26	38.23	296.99	42.11	445.64	48.22	741.09
DSI8	83	18	29.61	134.86	28.12	102.51	26.16	66.64	25.55	57.03	25.85	61.67	24.22	38.70	24.93	48.02
EDJ_2_1	105	48	52.56	20.81	43.09	24.16	40.62	54.51	38.16	96.84	32.88	228.52	33.65	205.95	41.72	39.46
EDJ_2_2	120	54	53.77	0.05	44.92	82.50	42.45	133.46	39.36	214.32	34.72	371.68	35.48	343.05	43.98	100.49
EDJ_2_3	170	55	58.63	13.18	52.50	6.23	49.71	27.94	45.27	94.68	42.45	157.50	42.84	147.87	51.62	11.40
EDJ_2_4	220	55	66.16	124.59	64.17	84.10	60.69	32.41	56.55	2.39	55.25	0.06	55.08	0.01	62.65	58.55
EDJ_2_5	292	56	75.69	387.89	78.27	495.76	74.93	358.18	72.34	267.13	72.45	270.46	71.38	236.65	76.48	419.24
EDJ_3_1	60	54.5	49.11	29.05	38.21	265.34	49.19	28.16	57.55	9.32	44.95	91.30	45.91	73.76	39.48	225.69
EDJ_3_2	122	56.5	54.89	2.58	47.43	82.33	61.66	26.63	63.28	46.03	58.90	5.75	62.69	38.31	60.10	12.99
EDJ_3_3	155	57.5	57.47	0.00	52.37	26.29	67.85	107.03	66.34	78.12	63.80	39.75	67.39	97.87	66.33	77.88
EDJ_3_4	190	58	60.87	8.23	57.98	0.00	72.36	206.16	69.02	121.40	66.53	72.70	69.47	131.57	68.20	104.00
EDJ_3_5	246	55.5	68.43	167.12	69.52	196.53	76.14	425.83	72.37	284.59	70.00	210.18	71.33	250.65	69.42	193.71
EDJ_4_1	23	43	52.36	87.69	41.84	1.36	46.79	14.39	52.48	89.96	39.49	12.31	42.41	0.35	39.77	10.46
EDJ_4_2	50	48	53.07	25.72	42.49	30.31	47.73	0.07	51.51	12.32	38.21	95.83	41.41	43.43	38.40	92.11
EDJ_4_3	88	48	55.18	51.62	45.05	8.70	49.85	3.42	50.92	8.53	37.96	100.74	42.55	29.69	40.59	54.88
EDJ_4_4	126	49	58.14	83.55	49.14	0.02	55.06	36.78	54.67	32.10	42.37	44.01	51.08	4.34	50.77	3.15
EDJ_4_5	191	48	63.34	235.35	55.41	54.88	63.18	230.38	62.33	205.35	50.73	7.45	62.45	208.82	57.62	92.57
EDJ_4_6	263	48	69.86	477.95	64.95	287.15	68.76	430.81	68.08	403.36	60.20	148.85	68.47	419.10	63.43	238.00

Table A2.1 Continued

EDJ_5_1	21	55	42.32	160.87	34.39	424.70	31.59	548.23	33.23	474.11	26.27	825.13	25.57	866.13	27.62	749.61
EDJ_5_2	74	56.5	44.35	147.55	37.27	369.87	34.78	471.70	34.74	473.53	29.56	725.93	29.07	752.39	31.46	627.16
EDJ_5_3	85	56.5	45.11	129.76	38.32	330.49	35.93	423.14	35.82	427.62	30.95	652.73	30.61	670.43	32.96	554.00
EDJ_5_4	162	57	51.38	31.59	47.96	81.70	45.33	136.21	45.32	136.52	42.57	208.13	42.53	209.26	43.98	169.55
EDJ_5_5	216	57.5	57.90	0.16	57.28	0.05	54.94	6.57	55.00	6.25	53.24	18.12	52.94	20.77	53.69	14.54
EDJ_7_1	30	56	41.68	205.01	33.58	502.77	35.39	424.82	40.20	249.71	31.19	615.67	30.54	648.35	29.71	691.12
EDJ_7_2	74	57	43.94	170.66	36.93	402.81	38.45	344.24	40.38	276.19	33.52	551.29	33.08	572.27	34.02	527.97
EDJ_7_3	103	59	46.34	160.19	40.68	335.67	43.03	255.02	43.66	235.30	38.54	418.56	38.71	411.66	39.50	380.18
EDJ_7_4	172	60	52.27	59.73	50.01	99.86	51.39	74.20	50.97	81.46	50.51	89.99	48.91	123.06	52.45	56.93
EDJ_7_5	246	60	61.45	2.11	62.88	8.28	62.66	7.08	62.87	8.23	64.17	17.42	61.55	2.39	62.66	7.07
EDJ_8_1	83	60	50.52	89.78	42.36	311.27	48.47	132.91	49.50	110.28	39.85	406.14	40.67	373.83	34.21	665.24
EDJ_8_2	168	60	60.69	0.48	59.45	0.31	62.54	6.46	60.23	0.05	57.19	7.90	58.80	1.44	47.02	168.38
EDJ_8_3	187	60	63.31	10.93	63.40	11.54	65.33	28.45	62.87	8.23	60.86	0.75	61.97	3.88	52.11	62.25
EDJ_8_4	229	60	67.90	62.44	69.93	98.63	70.03	100.70	67.97	63.58	66.71	44.99	67.15	51.16	61.44	2.06
RMSE				**12.09**		**12.95**		**13.21**		**12.55**		**13.39**		**13.88**		**12.92**

Table A2.2: Calibration Calculations for Scenario 1 Part 2

Well	Depth (m)	T (ºC)	1 (ºC)	MSE	2 (ºC)	MSE	3 (ºC)	MSE	4 (ºC)	MSE
ED1_1	50	54	36.78	296.44	39.22	218.39	48.80	27.03	49.49	20.37
ED1_2	90	54.5	40.88	185.63	46.37	66.10	54.35	0.02	54.45	0.00
ED1_3	100	55	42.26	162.38	49.09	34.89	55.97	0.94	55.91	0.82
ED1_4	115	55.5	44.35	124.42	52.72	7.75	57.32	3.33	57.12	2.64
ED1_5	120	56	45.00	120.99	53.76	5.00	57.58	2.50	57.36	1.84
ED1_6	130	56.5	46.34	103.18	55.97	0.28	58.23	2.98	57.92	2.01
ED1_7	140	57	47.64	87.52	57.84	0.71	59.36	5.55	58.86	3.46
ED1_8	150	58	49.01	80.90	59.59	2.53	60.46	6.04	59.79	3.22
ED1_9	160	58	50.47	56.71	61.02	9.14	61.45	11.88	60.67	7.13
ED1_10	170	58.5	52.05	41.56	62.40	15.19	62.52	16.17	61.67	10.07
ED1_11	180	59	53.72	27.90	63.74	22.42	63.66	21.74	62.77	14.19
ED2_1	60	51.3	36.49	282.45	33.07	409.21	33.06	409.65	32.69	424.64
ED2_2	120	51.3	42.01	123.03	38.53	212.35	37.79	234.47	35.75	300.88
ED2_3	190	51.3	50.74	5.59	47.34	33.22	46.63	41.91	44.11	80.80
ED2_4	200	51.3	52.22	0.78	48.95	17.26	48.27	23.29	45.82	52.99
ED2_5	210	51.3	53.75	0.42	50.63	6.09	50.00	9.59	47.64	29.83
ED2_6	225	51.3	56.12	9.10	53.27	0.03	52.70	0.16	50.51	6.73
ED3_1	85	35	41.00	36.00	44.71	94.38	43.47	71.69	43.83	78.05
ED3_2	165	38.4	54.42	256.67	57.62	369.38	56.25	318.45	55.05	277.37
ED3_3	180	41.9	56.59	215.74	59.88	323.19	58.33	270.03	56.89	224.65
ED3_4	265	45.6	70.83	636.68	72.05	699.38	70.38	614.22	69.24	558.87
ED3_5	300	47.5	75.54	786.47	75.61	790.36	73.72	687.61	72.48	624.07
DERMAN	100	53	43.68	86.87	45.70	53.35	44.58	70.93	45.18	61.23
ENTUR	90	51	42.62	70.15	43.34	58.64	42.33	75.15	42.87	66.14
YAGCI	100	42	44.74	7.49	42.32	0.10	40.84	1.35	40.49	2.27
DSI6	95	39	44.25	27.54	39.64	0.41	37.07	3.71	36.16	8.07
DOGAN	30	32	39.45	55.46	36.12	17.01	35.95	15.58	37.03	25.29
DSI9	122	32	42.47	109.65	41.35	87.49	39.50	56.20	39.02	49.24
HASTANE	90	31	32.68	2.84	31.76	0.58	31.34	0.12	31.09	0.01
DSI5	91	30	43.04	169.94	37.89	62.30	34.27	18.23	32.82	7.98
DSI7	132	21	47.82	719.14	42.92	480.28	35.52	210.83	39.69	349.32
DSI8	83	18	27.45	89.35	25.63	58.20	25.11	50.55	25.19	51.64
EDJ_2_1	105	48	44.54	12.00	39.48	72.60	35.82	148.40	34.21	190.30
EDJ_2_2	120	54	46.11	62.22	41.11	166.14	36.99	289.43	35.05	359.20
EDJ_2_3	170	55	52.37	6.90	47.43	57.24	42.45	157.51	39.34	245.38
EDJ_2_4	220	55	61.62	43.78	56.98	3.94	52.33	7.12	48.84	37.97
EDJ_2_5	292	56	72.78	281.65	69.29	176.68	66.10	102.06	63.05	49.69
EDJ_3_1	60	54.5	37.90	275.65	43.45	122.02	51.90	6.78	53.16	1.81
EDJ_3_2	122	56.5	46.37	102.59	55.30	1.45	57.25	0.56	58.22	2.96
EDJ_3_3	155	57.5	50.70	46.20	61.33	14.66	60.20	7.28	60.63	9.81
EDJ_3_4	190	58	55.58	5.87	66.42	70.94	63.14	26.40	62.92	24.24

Table A2.2 Continued

EDJ_3_5	246	55.5	65.12	92.52	71.37	251.72	67.38	141.21	66.58	122.74
EDJ_4_1	23	43	39.86	9.86	43.33	0.11	47.40	19.32	48.85	34.26
EDJ_4_2	50	48	40.81	51.71	44.52	12.09	46.79	1.46	48.17	0.03
EDJ_4_3	88	48	43.77	17.85	47.11	0.80	46.70	1.70	47.76	0.06
EDJ_4_4	126	49	47.95	1.09	52.10	9.61	50.11	1.22	50.74	3.02
EDJ_4_5	191	48	54.50	42.25	60.06	145.53	57.08	82.49	55.38	54.47
EDJ_4_6	263	48	63.76	248.46	65.61	310.13	62.93	223.02	59.08	122.85
EDJ_5_1	21	55	34.97	401.38	30.86	582.78	31.02	574.95	31.54	550.55
EDJ_5_2	74	56.5	37.58	358.05	33.81	514.86	32.87	558.39	31.53	623.55
EDJ_5_3	85	56.5	38.60	320.59	34.87	467.80	33.86	512.69	32.17	591.97
EDJ_5_4	162	57	47.05	98.93	43.38	185.49	42.33	215.26	39.53	305.33
EDJ_5_5	216	57.5	54.79	7.32	51.66	34.08	50.81	44.70	48.35	83.64
EDJ_7_1	30	56	33.55	503.91	33.18	520.63	37.21	352.95	38.38	310.50
EDJ_7_2	74	57	36.48	421.13	36.43	423.14	37.83	367.63	37.58	376.98
EDJ_7_3	103	59	39.85	366.62	40.65	336.74	40.85	329.29	39.75	370.65
EDJ_7_4	172	60	48.22	138.88	48.65	128.81	47.72	150.77	45.81	201.49
EDJ_7_5	246	60	58.93	1.14	58.40	2.57	58.12	3.54	56.64	11.30
EDJ_8_1	83	60	40.59	376.58	44.57	237.94	45.87	199.74	46.24	189.41
EDJ_8_2	168	60	55.69	18.58	57.74	5.12	55.71	18.38	54.90	25.97
EDJ_8_3	187	60	59.14	0.73	60.42	0.17	58.18	3.31	57.22	7.71
EDJ_8_4	229	60	64.79	22.98	64.74	22.44	62.73	7.43	61.84	3.39
RMSE				12.26		12.07		11.24		11.54

Table A2.3: Calibration Calculations for Scenario 2

Well	Depth (m)	T (ºC)	1 (ºC)	MSE	2 (ºC)	MSE	3 (ºC)	MSE	4 (ºC)	MSE
ED1_1	50	54	69.59	242.92	66.07	145.76	59.44	29.59	53.01	0.97
ED1_2	90	54.5	72.19	313.05	67.65	172.99	61.73	52.33	56.02	2.31
ED1_3	100	55	72.89	319.97	68.10	171.73	62.43	55.19	56.97	3.87
ED1_4	115	55.5	73.42	320.97	68.50	169.05	63.07	57.23	57.88	5.65
ED1_5	120	56	73.52	306.95	68.59	158.51	63.21	51.97	58.08	4.33
ED1_6	130	56.5	73.76	297.94	68.79	151.05	63.54	49.49	58.55	4.20
ED1_7	140	57	74.16	294.62	69.10	146.29	64.00	49.05	59.19	4.78
ED1_8	150	58	74.59	275.36	69.42	130.35	64.49	42.18	59.85	3.44
ED1_9	160	58	75.08	291.58	69.78	138.70	65.03	49.44	60.57	6.59
ED1_10	170	58.5	75.61	292.82	70.17	136.23	65.62	50.73	61.36	8.18
ED1_11	180	59	76.19	295.34	70.59	134.34	66.25	52.57	62.21	10.31
ED2_1	60	51.3	62.72	88.71	61.45	66.34	52.72	0.34	44.34	80.35
ED2_2	120	51.3	64.98	141.22	63.10	99.97	55.34	5.03	47.86	27.42
ED2_3	190	51.3	69.23	260.13	66.09	168.83	59.75	44.19	53.61	0.26
ED2_4	200	51.3	70.00	285.55	66.63	182.96	60.51	54.95	54.61	2.28
ED2_5	210	51.3	70.80	313.37	67.18	198.18	61.31	67.36	55.65	6.51
ED2_6	225	51.3	72.06	359.44	68.03	222.95	62.54	89.16	57.27	17.37
ED3_1	85	35	68.34	1111.83	65.42	925.20	58.18	537.15	51.16	261.01

Table A2.3 Continued

ED3_2	165	38.4	72.43	1158.25	68.13	883.63	62.97	603.45	58.27	394.70
ED3_3	180	41.9	73.13	975.12	68.61	713.44	63.77	478.23	59.44	307.53
ED3_4	265	45.6	79.91	1177.00	73.20	761.83	70.42	615.87	67.99	501.42
ED3_5	300	47.5	82.61	1232.46	75.02	757.16	72.95	647.76	71.11	557.40
DERMAN	100	53	68.53	241.18	65.55	157.55	58.55	30.76	51.82	1.39
ENTUR	90	51	67.37	267.97	64.77	189.73	57.43	41.40	50.40	0.36
YAGCI	100	42	66.44	597.23	64.01	484.23	56.46	209.23	49.27	52.83
DSI6	95	39	65.26	689.61	63.07	579.26	55.25	263.98	47.77	76.91
DOGAN	30	32	62.96	958.54	61.39	863.59	52.98	440.15	45.15	172.86
DSI9	122	32	64.63	1065.02	62.00	899.94	54.97	527.45	48.33	266.69
HASTANE	90	31	61.35	921.23	60.31	859.36	51.38	415.37	42.68	136.32
DSI5	91	30	64.45	1186.90	62.64	1065.27	54.40	595.47	46.29	265.50
DSI7	132	21	67.79	2189.67	64.52	1894.10	57.48	1330.96	50.56	873.78
DSI8	83	18	59.91	1756.41	59.56	1727.25	49.85	1014.70	40.20	493.02
EDJ_2_1	105	48	65.34	300.55	63.23	232.02	55.29	53.08	47.47	0.28
EDJ_2_2	120	54	66.19	148.52	63.83	96.55	56.13	4.53	48.51	30.09
EDJ_2_3	170	55	69.18	201.06	65.92	119.23	59.11	16.87	52.31	7.21
EDJ_2_4	220	55	73.03	325.05	68.57	184.23	63.11	65.78	57.74	7.53
EDJ_2_5	292	56	78.86	522.53	72.49	272.07	68.95	167.83	65.52	90.59
EDJ_3_1	60	54.5	71.86	301.33	67.21	161.57	61.11	43.70	55.12	0.38
EDJ_3_2	122	56.5	74.34	318.38	68.92	154.35	63.78	53.06	58.83	5.45
EDJ_3_3	155	57.5	75.76	333.42	69.95	154.92	65.41	62.59	61.05	12.58
EDJ_3_4	190	58	77.58	383.46	71.37	178.75	67.56	91.40	63.79	33.48
EDJ_3_5	246	55.5	80.32	616.15	73.55	325.68	70.83	234.93	68.08	158.22
EDJ_4_1	23	43	70.60	761.82	66.34	544.72	59.92	286.22	53.61	112.67
EDJ_4_2	50	48	70.82	520.76	66.67	348.61	60.20	148.83	53.78	33.43
EDJ_4_3	88	48	70.90	524.43	67.07	363.70	60.69	160.92	54.41	41.08
EDJ_4_4	126	49	72.31	543.32	67.94	358.90	62.56	183.76	57.25	68.00
EDJ_4_5	191	48	74.98	727.82	69.83	476.42	65.96	322.66	62.24	202.67
EDJ_4_6	263	48	77.36	861.75	71.63	558.20	68.43	417.54	65.55	307.95
EDJ_5_1	21	55	61.68	44.62	60.58	31.17	51.52	12.08	42.80	148.73
EDJ_5_2	74	56.5	62.60	37.16	61.35	23.50	52.73	14.18	44.44	145.47
EDJ_5_3	85	56.5	63.07	43.15	61.69	26.98	53.27	10.44	45.16	128.65
EDJ_5_4	162	57	67.07	101.35	64.55	56.95	57.58	0.33	50.87	37.54
EDJ_5_5	216	57.5	71.13	185.69	67.36	97.24	61.63	17.05	56.14	1.86
EDJ_7_1	30	56	64.77	76.90	62.88	47.38	54.67	1.76	46.72	86.19
EDJ_7_2	74	57	64.92	62.71	63.15	37.82	55.03	3.88	47.27	94.64
EDJ_7_3	103	59	65.95	48.36	63.88	23.85	56.31	7.25	49.14	97.14
EDJ_7_4	172	60	69.10	82.79	66.18	38.21	59.82	0.03	53.82	38.17
EDJ_7_5	246	60	74.35	205.95	69.65	93.19	64.93	24.27	60.44	0.20
EDJ_8_1	83	60	69.63	92.76	66.29	39.52	59.52	0.23	52.81	51.66
EDJ_8_2	168	60	72.81	164.00	68.55	73.11	63.46	11.96	58.70	1.69
EDJ_8_3	187	60	73.80	190.32	69.27	85.88	64.57	20.92	60.25	0.06

Table A2.3 Continued

EDJ_8_4	229	60	75.93	253.78	70.74	115.30	66.72	45.15	63.07	9.40
RMSE				**21.70**		**18.26**		**13.34**		**10.24**

APPENDIX 3

SUTRAPREP INPUT FILE CONTENTS

```
'sanki.prl'  'sanki.inp'  'sanki.ics'  'sanki.wrl'  'NONE'          # DATASET 1
3     20 5 20
3     20 5 20                                                                  # DATASET
2
3     11 2 17
'CORNER'  1. 1.     1.
0  0  0      0.    0.  -260.
0  1  0      0.   1490.  -320.
1  0  0      1531.    0.  -260.
1  1  0      1541.   1490.  -320.
0  0  1      0.    0.  -130.
0  1  1      0    1490     -130
1  0  1      1510.    0.  -130.
1  1  1      1510  1490 -130

0  0  2      0.    0.  -90.
0  1  2      0.   1490.  -98.
1  0  2      1505.    0.  -90.
1  1  2      1505.   1490.  -98.
0  0  3      0.    0.  0.
0  1  3      0    1490     0
1  0  3      1490.    0.  0.
1  1  3      1490  1490 0

0  2  0      0.    1510.  -220.
0  3  0      0.   3000.  -220.
1  2  0      1531.    1510.  -220.
1  3  0      1531.   3000.  -220.
0  2  1      0.    1510.  -160.
0  3  1      0    3000     -160
1  2  1      1510.    1510.  -160.
1  3  1      1510  3000 -160
```

0 2 2 0. 1510. -90.
0 3 2 0. 3000. -90.
1 2 2 1500. 1510. -90.
1 3 2 1500. 3000. -90.
0 2 3 0. 1510. 0.
0 3 3 0 3000 0
1 2 3 1490. 1510. 0.
1 3 3 1490 3000 0

2 0 0 1550. 0. -250.
2 1 0 1558. 1370. -300.
3 0 0 3000. 0. -250.
3 1 0 3000. 1370. -300.
2 0 1 1530. 0. -135.
2 1 1 1526 1436 -135
3 0 1 3000. 0. -135.
3 1 1 3000 1436 -135

2 0 2 1525. 0. -90.
2 1 2 1525. 1454. -90.
3 0 2 3000. 0. -90.
3 1 2 3000. 1454. -90.
2 0 3 1510. 0. 0.
2 1 3 1510 1490 0
3 0 3 3000. 0. 0.
3 1 3 3000 1490 0

2 2 0 1548. 1414. -240.
2 3 0 1548. 3000. -240.
3 2 0 3000. 1414. -240.
3 3 0 3000. 3000. -240.
2 2 1 1526. 1470. -100.
2 3 1 1526 3000 -100
3 2 1 3000. 1478. -100.
3 3 1 3000 3000 -100

```
2  2  2     1522.    1478.  -80.
2  3  2     1522.   3000.  -80.
3  2  2     3000.    1478.  -80.
3  3  2     3000.   3000.  -80.
2  2  3     1510.    1510.  0.
2  3  3     1510    3000     0
3  2  3     3000.    1510.  0.
3  3  3     3000  3000 0


'USER'    0  0  1    1   2                                          # DATASET 4
'BLOCK' 1.
 1.    1.    1.    1.   1.   1.   1.    1.    1.   1.   1.   1.
1  1  1    0     0.1
1e-12  1e-12  1e-12   0.    0.    0.   250.   250.   2.5   0.1   0.1   0.1
1  1  2    0     0.1
1e-15  1e-15  1e-15   0.    0.    0.   250.   250.   2.5   0.1   0.1   0.1
1  1  3    0     0.1
5e-12  5e-12  5e-12    0.    0.    0.   250.   250.   2.5   0.1   0.1   0.1
2  1  1    0     0.1
1e-14  1e-13  1e-12   0.    90.    0.   250.   250.   2.5   0.1   0.1   0.1
2  1  2    0     0.1
1e-14  1e-13  1e-12   0.    90.    0.   250.   250.   2.5   0.1   0.1   0.1
2  1  3    0     0.1
1e-14  1e-13  1e-12   0.    90.    0.   250.   250.   2.5   0.1   0.1   0.1
3  1  1    0     0.1
1e-12  1e-12  1e-12   0.    0.    0.   250.   250.   2.5   0.1   0.1   0.1
3  1  2    0     0.1
1e-15  1e-15  1e-15   0.    0.    0.   250.   250.   2.5   0.1   0.1   0.1
3  1  3    0     0.1
5e-12  5e-12  5e-12    0.    0.    0.   250.   250.   2.5   0.1   0.1   0.1

1  2  1    0     0.1
1e-12  1e-12  1e-12   0.    0.    0.   250.   250.   2.5   0.1   0.1   0.1
1  2  2    0     0.1
1e-15  1e-15  1e-15   0.    0.    0.   250.   250.   2.5   0.1   0.1   0.1
1  2  3    0     0.1
5e-12  5e-12  5e-12    0.    0.    0.   250.   250.   2.5   0.1   0.1   0.1
2  2  1    0     0.1
```

1e-14 1e-13 1e-12 0. 90. 0. 250. 250. 2.5 0.1 0.1 0.1
2 2 2 0 0.1
1e-14 1e-13 1e-12 0. 90. 0. 250. 250. 2.5 0.1 0.1 0.1
2 2 3 0 0.1
1e-14 1e-13 1e-12 0. 90. 0. 250. 250. 2.5 0.1 0.1 0.1
3 2 1 0 0.1
1e-14 1e-13 1e-12 0. 90. 0. 250. 250. 2.5 0.1 0.1 0.1
3 2 2 0 0.1
1e-14 1e-13 1e-12 0. 90. 0. 250. 250. 2.5 0.1 0.1 0.1
3 2 3 0 0.1
1e-14 1e-13 1e-12 0. 90. 0. 250. 250. 2.5 0.1 0.1 0.1

1 3 1 0 0.1
1e-12 1e-12 1e-12 0. 0. 0. 250. 250. 2.5 0.1 0.1 0.1
1 3 2 0 0.1
1e-15 1e-15 1e-15 0. 0. 0. 250. 250. 2.5 0.1 0.1 0.1
1 3 3 0 0.1
5e-12 5e-12 5e-12 0. 0. 0. 250. 250. 2.5 0.1 0.1 0.1
2 3 1 0 0.1
1e-14 1e-13 1e-12 0. 90. 0. 250. 250. 2.5 0.1 0.1 0.1
2 3 2 0 0.1
1e-14 1e-13 1e-12 0. 90. 0. 250. 250. 2.5 0.1 0.1 0.1
2 3 3 0 0.1
1e-14 1e-13 1e-12 0. 90. 0. 250. 250. 2.5 0.1 0.1 0.1
3 3 1 0 0.1
1e-12 1e-12 1e-12 0. 0. 0. 250. 250. 2.5 0.1 0.1 0.1
3 3 2 0 0.1
1e-15 1e-15 1e-15 0. 0. 0. 250. 250. 2.5 0.1 0.1 0.1
3 3 3 0 0.1
5e-12 5e-12 5e-12 0. 0. 0. 250. 250. 2.5 0.1 0.1 0.1
'TEMPERATURE' 5 'UNIFORM' 100
'TEMPERATURE' 2 'UNIFORM' 18
'TEMPERATURE' 1 'UNIFORM' 21
'PRESSURE' 3 'LINEAR' 0 0. 0. 0. 0. 0. -9810. 20.
'PRESSURE' 4 'LINEAR' 63765 0. 0. 0. 0. 0. -9810. 20.
'INITIAL' 0.
'LINEAR' 0. 0. 0. 0. 0. 0. -9810. # DATASET 7
18.
'ELEMENTS' 1. 1. 1. # DATASET 8